Zeynep Şenel

Ph.D. Thesis

AGU 2024

DESIGN AND IMPLEMENTATION OF NANOPHOTONIC ARCHITECTURES USING SMART-SELF ASSSEMBLY OF COLLOIDAL NANOMATERIALS

Ph.D. THESIS
SUBMITTED TO THE DEPARTMENT OF
ELECTRICAL AND COMPUTER ENGINEERING
AND THE GRADUATE SCHOOL OF ENGINEERING AND SCIENCE
OF ABDULLAH GUL UNIVERSITY
IN PARTIAL FULFILLMENT OF THE REQUIREMENTS
FOR THE DEGREE OF
Ph.D.

By
Zeynep Şenel
August 2024

DESIGN AND IMPLEMENTATION OF NANOPHOTONIC ARCHITECTURES USING SMART-SELF ASSSEMBLY OF COLLOIDAL NANOMATERIALS

A THESIS
SUBMITTED TO THE DEPARTMENT OF ELECTRICAL AND COMPUTER ENGINEERING
AND THE GRADUATE SCHOOL OF ENGINEERING AND SCIENCE OF ABDULLAH GUL UNIVERSITY
IN PARTIAL FULFILLMENT OF THE REQUIREMENTS
FOR THE DEGREE OF
Ph.D.

By
Zeynep Şenel
August 2024

SCIENTIFIC ETHICS COMPLIANCE

I hereby declare that all information in this document has been obtained in accordance with academic rules and ethical conduct. I also declare that, as required by these rules and conduct, I have fully cited and referenced all materials and results that are not original to this work.

Name-Surname: Zeynep Şenel
Signature :

REGULATORY COMPLIANCE

Ph.D. thesis titled Design and Implementation of Nanophotonic Architectures Using Smart-Self Asssembly of Colloidal Nanomaterials has been prepared in accordance with the Thesis Writing Guidelines of the Abdullah Gül University, Graduate School of Engineering & Science.

Prepared By	Advisor
Zeynep Şenel	Dr. Öğretim Üyesi Talha Erdem
Signature	Signature

Head of the Electrical and Computer Engineering Program

Doç. Dr. Samet Güler

Signature

ACCEPTANCE AND APPROVAL

Ph.D. thesis titled Design and Implementation of Nanophotonic Architectures Using Smart-Self Asssembly of Colloidal Nanomaterials and prepared by Zeynep Şenel has been accepted by the jury in the Electric & Computer Engineering Graduate Program at Abdullah Gül University, Graduate School of Engineering & Science.

…….. /…….. / ……..

(Thesis Defense Exam Date)

JURY:

Advisor : (Assist.Prof. Talha Erdem)…….....

Member : (Assist. Prof. Zeliha Soran Erdem)……. .....

Member : (Assist. Prof. Şerife Ayaz Güner)…….....

Member : (Assoc. Prof. Ömer Aydın)…….....

Member : (Prof. Evren Mutlugün)…….....

APPROVAL:

The acceptance of this Ph.D. thesis has been approved by the decision of the Abdullah Gül University, Graduate School of Engineering & Science, Executive Board dated ….. /….. / …….. and numbered ……..……. .

…….. /…….. / ……..

(Date)

Graduate School Dean

Prof. İrfan ALAN

ABSTRACT

DESIGN AND IMPLEMENTATION OF NANOPHOTONIC ARCHITECTURES USING SMART-SELF ASSSEMBLY OF COLLOIDAL NANOMATERIALS

Zeynep Şenel

Ph.D. in Electrical and Computer Engineering

Advisor: Assist.Prof. Talha Erdem

August 2024

DNA-driven self-assembly techniques offer precise control over the positioning of colloidal nanoparticles through specific Watson–Crick interactions, and its reversibility via controlling the temperature of medium. This thesis explores an alternative strategy to control DNA-functionalized nanoparticles' binding/unbinding process by leveraging laser radiation, inducing localized heating within the nanoparticles to facilitate disassociation. First, we demonstrate the active manipulation of the optical properties of DNA-assembled gold nanoparticle networks via external optical excitation. Specifically, irradiation with a green hand-held laser yields a substantial ∼30% increase in total transmittance, accompanied by a transition from opaque to transparent states observable in optical microscopy images. The reversibility of this process is demonstrated by the restoration of the nanoparticle network post-irradiation cessation, underscoring the efficacy of optical excitation in tailoring both the structure and optical characteristics of DNA-mediated nanoparticle assemblies. Second, we introduce a method to tailor DNA-driven self-assembly of semiconductor nanoparticles on glass by applying an external optical field. A green laser directs the assembly of DNA-functionalized red-emitting quantum dots (QDs) on DNA-functionalized glass, leaving uncoated spots owing to localized heating. This effect becomes prominent after three hours of radiation using a laser with an irradiance of 57.1 W/cm^2. Experiments with different lasers and nanoparticle types confirm the role of laser-induced heating in preventing QD-glass bonding via DNA-DNA interaction. Secondary coating of previously uncoated spots with DNA-functionalized green-emitting QDs and dye-functionalized DNAs indicates a successful hierarchical self-assembly. Our findings highlight the potential of light-assisted DNA-driven self-assembly for diverse nanoparticle architectures, promising applications in optoelectronics and nanophotonics.

Keywords: Programmable self-assembly, DNA-driven self-assembly, localized heating, colloidal nanoparticles, DNA conjugation.

ÖZET

KOLOİDAL NANOMALZEMELERİN AKILLI KENDİNDEN DİZİLİMİ İLE NANOFOTONİK MİMARİLERİN TASARIMI VE UYGULAMASI

Zeynep Şenel

Elektrik ve Bilgisayar Mühendisliği Anabilim Dalı Doktora

Tez Danışmanı: Dr. Öğr. Üyesi Talha Erdem

Ağustos-2024

DNA tabanlı kendiliğinden dizilim teknikleri, özgül Watson-Crick etkileşimleri aracılığıyla kolloidal nanoparçacıkların yerleşimini hassas bir şekilde kontrol etmeyi ve ortamın sıcaklığını kontrol ederek bu sürecin geri dönüştürülebilirliğini sağlamayı mümkün kılar. Bu tez, lazer ışınımı kullanarak DNA ile işlevselleştirilmiş nanoparçacıkların bağlanma/ayrılma sürecini kontrol etmek için alternatif bir strateji araştırmaktadır. Bu tezde, ilk olarak, DNA ile birleştirilmiş altın nanopartikül ağlarının optik özelliklerinin, dış optik uyarım yoluyla aktif olarak nasıl manipüle edilebileceği gösterilmiştir. Özellikle, yeşil bir el lazeri ile ışınlandığında, toplam geçirgenlikte yaklaşık %30'luk önemli bir artış gözlemlenmiş, buna optik mikroskop görüntülerinde gözlemlenebilen opak durumdan şeffaf duruma geçiş eşlik etmiştir. Bu sürecin tersine çevrilebilirliği, ışınlamanın kesilmesinden sonra nanoparçacık ağının restorasyonu ile kanıtlanmıştır. Bu gözlem, DNA-takılı nanoparçacık ağlarının hem yapısını hem de optik özelliklerini uyarlamada optik uyarmanın etkinliğinin altını çizer. İkinci olarak, harici bir optik alan uygulayarak, DNA-takılı yarı iletken nanoparçacıkların eşlenik DNA-takılı cam yüzeyler üzerinde birleşmesini kontrol etmek için bir yöntem sunulmuştur. Çalışmalarımızda, yeşil bir lazer, DNA-takılı cam üzerinde kırmızı ışık yayan DNA-takılı kuantum noktalarının birleşmesini yönlendirmiş ve lokal ısıtma nedeniyle kaplanmamış noktalar bırakmıştır. Bu etki, 57.1 W/cm² ışınım yoğunluğuna sahip bir lazer kullanılarak üç saatlik ışınım sonrasında belirgin hale gelmiştir. Farklı lazerler ve nanoparçacık türleri ile yapılan deneyler, lazer kaynaklı ısıtmanın DNA-DNA etkileşimi ile kuantum nokta-cam bağlanmasını önlemedeki rolünü doğrulamıştır. Önceden kaplanmamış noktaların DNA takılı yeşil ışık yayan kuantum noktalar ve boya takılı DNA'lar ile ikincil kaplanması, hiyerarşik birleşmeyi göstermiştir. Bulgularımız, çeşitli nanoparçacık mimarileri için ışık destekli DNA tabanlı kendiliğinden birleşmenin potansiyelini vurgulamakta, optoelektronik ve nanofotonik alanlarında yenilikçi uygulamalar vaat etmektedir.

Anahtar kelimeler: Programlanabilir kendinden dizilim, DNA-tabanlı kendinden dizilim, yerel ısıtma, koloidal nanoparçacıklar, DNA bağlama.

Acknowledgements

First and foremost, I would like to express my deepest gratitude to Allah, the Almighty, for His endless blessings, guidance, and strength throughout this journey. Without His mercy and grace, none of this would have been possible. All praise is due to Allah for granting me the perseverance, patience, and wisdom to overcome the challenges I faced along the way.

I would also like to extend my sincere thanks to my advisor Dr. Talha Erdem and for his unwavering support, mentorship, and encouragement throughout my doctoral studies. Your expertise, patience, and dedication have been invaluable, and I am profoundly thankful for the countless hours you spent helping me navigate the complexities of this research. I have learned so much from you, not only academically but also professionally and personally.

I am also immensely grateful to the members of my thesis jury, Dr. Kutay İçöz, Dr. Şerife Ayaz Güner, Dr. Zeliha Soran Erdem and Prof. Evren Mutlugün. Your insightful feedback, constructive criticism, and valuable suggestions have greatly enhanced the quality of my work. Thank you for taking the time to review my research and for your thoughtful contributions. I would like to thank Dr. Ömer Aydın for accepting to be in my thesis committee for my PhD defence.

To my beloved family, I cannot thank you enough for your love, patience, and unwavering belief in me. To my parents, Nuray Şenel and M. Sami Şenel, your constant encouragement and sacrifices have been the foundation upon which I have built my aspirations. To my siblings, A. Cihat Şenel and Mitat Şenel, and extended family, thank you for being a source of inspiration and for always cheering me on, no matter the distance.

To my best friends, Dr. Kevser Şahin Tıraş, Pınar Kubaşık, Dr. Merve Taş, Dr. Hilal Hacılar, Dr. Sena Büşra Yengeç Taşdemir, Ece Sultan Karacık, Müzeyyen Savaş thank you for being my pillars of strength, offering your humor, understanding, and support whenever I needed it most. Your friendship has been a source of great comfort and joy during this journey.

I would also like to thank past and present members of Smart Nanophotonics Group for creating a collaborative and encouraging environment.

I would like to thank YÖK and TÜBİTAK for the financial support that are the Higher Education Council (HEC) of Turkey YÖK-100/2000 Ph.D. Scholarship Program, Tübitak 2211-A National Ph.D. Scholarship Program, Tübitak 2247-A Program (Grant no. 120C124).

Finally, I extend my appreciation to everyone who has contributed to this work, whether directly or indirectly. Your support, encouragement, and guidance have been instrumental in helping me reach this milestone.

Thank you all.

TABLE OF CONTENTS

LIST OF FIGURES

LIST OF ABBREVIATIONS

AuNPs	Gold Nanoparticles
AgNWs	Silver Nanowires
CAC	Charge-Assisted Coating
CDs	Carbon Dots
DNA	Deoxyribo Nucleic Acid
NPs	Nanoparticles
SiO_2	Silica \ Silicon Dioxide
SDG	Sustainable Development Goal
QDs	Quantum Dots

To my beloved family

Chapter 1

Introduction

1.1 The Proposal of Thesis

In this thesis, we propose developing a new technology that enables controlling the self-assembly of colloidal nanoparticles using light. We believe that this technology has the potential to revolutionize the fabrication of optoelectronic devices and nanophotonic structures. At the end of the thesis, the development of a low-cost, environmentally friendly and easy-to-apply micro/nanofabrication technique will be an alternative to existing micro and nano fabrication techniques. Furthermore, the use of colloidal materials along with the ability of recycling unbound nanoparticles will significantly decrease the amount of produced waste. In addition, this method may enable to produce structures that are not possible or very difficult and expensive to manufacture with classical fabrication techniques. Through this method, the cost of equipment and the cost of operating the equipment will be significantly reduced and the way to cheaper production compared to standard methods will be opened. Thus, the widespread use of our results will drastically decrease the negative impact of nano/microfabrication processes to the environment. Moreover, the novelty of our proposed technique has an economic potential as it may attract the industry's attention.

1.2 Fabrication Methods of Micro- and Nano-sized Structures

The prefix 'nano' is referred to a Greek prefix meaning 'dwarf' or something very small and it represents one thousand millionth of a meter (10^{-9} m). Nanoscience is the study of structures and molecules on the nanometer scales, ranging between 1 and 100 nm, while nanotechnology is the practical application of nanoscience in devices and other uses [1]. As one of the most promising technologies of the 21st century, nanotechnology involves the transformation of nanoscience theories into practical applications by observing, measuring, manipulating, assembling, controlling, and manufacturing matter at the nanometer scale. This field enables novel applications across a diverse range of

disciplines, including chemistry, physics, biology, medicine, engineering, and electronics [2]. There are two main approaches to the synthesis of nanostructures: top-down and bottom-up, each differing in quality, speed, and cost. The top-down approach involves breaking down bulk material into nano-sized particles using advanced techniques like precision engineering and lithography, which have been developed and optimized over recent decades [3]. Lithography specifically involves the patterning of surfaces through exposure to light, ions, or electrons, followed by the deposition of material onto that surface to produce the desired material [3].

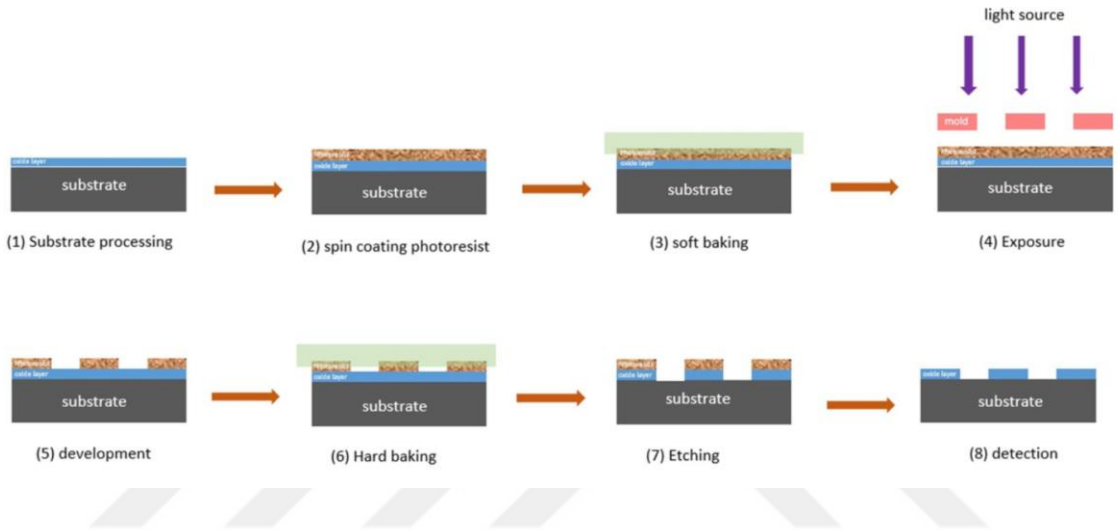

Figure 1. 1: Schematic diagram of lithography process steps [4].

Conversely, the bottom-up approach involves building nanostructures atom-by-atom or molecule-by-molecule using physical and chemical methods within the nanoscale range (1 nm to 100 nm). This method utilizes the controlled manipulation of self-assembly of atoms and molecules [3]. Self-assembly, the spontaneous organization of components into structured formations using noncovalent interactions such as ionic, hydrogen bonds, dipole-dipole, π–π stacking, and van der Waals forces, is a primary method used by nature to create complex structures [5]. However, designing and fabricating small-sized structures presents various challenges [6]. The nano size of these structures makes it difficult to orient them toward each other and the larger macroscopic world.

An important challenge in materials science and nanotechnology is to develop novel strategies to fabricate functional materials and devices with potentially nm-scale precision over large areas**.** Traditional "top-down" technologies encounter several issues, including high cost, complexity, and energy consumption, in addition to the physical limitations related to the miniaturisation of classical materials [7], [8]. Incompatibility in the lattice

parameters or chemical interactions of the coated materials is among the critical obstacles to coating hybrid materials. While forming shaped structures, lithography systems should be used [9]. Due to the nature of this method, some parts of the coated material are unusable, and the complexity of production increases by additional steps in the process. In addition, the increase in waste production during the removal of undesirable parts [10] increases the negative impact of this traditional method on the environment. Although solution processing is especially beneficial for cost reduction, using lithography remains inevitable to obtain shaped structures [11].

1.2.1 Bottom-up Fabrication Techniques

A few bottom-up strategies that potentially remedy the abovementioned problems have been investigated [12],[13]. Currently, various molecules such as DNA [14], RNA [15], protein [16], and lipid [17] etc. have emerged as primary units of self-assembly.

RNA, protein, and lipid self-assembly are fundamental processes in biology, where molecules spontaneously organize into functional structures driven by non-covalent interactions. RNA self-assembles into complex secondary structures, playing roles in catalysis and genetic information storage, which are vital for early life evolution theories (Jaeger & Chworos, 2006). Protein self-assembly forms diverse structures like enzymes, cytoskeletal filaments, and pathological aggregates, such as amyloid plaques in Alzheimer's disease, through hydrogen bonding, hydrophobic effects, and electrostatic interactions (Whitesides & Grzybowski, 2002). Lipids, due to their amphipathic nature, self-assemble into bilayers and vesicles, forming the basis of cell membranes and enabling compartmentalization and cellular functions (Alberts et al., 2002). These processes are central to biomaterial fabrication and have significant applications in biotechnology (Zhang, 2003).

Since DNA molecules have unique properties, including biocompatibility, high specificity, and Watson-Crick base pairing, DNA is a suitable material for the self-assembly of well-defined nanostructures [18], [19]. Among the bottom-up fabrication technologies, DNA-driven smart self-assembly stands out as a promising tool because it enables programming the assembly of nanomaterials in complex architectures owing to the selectivity of DNA molecules, which is not feasible by any other state-of-the-art technique [20]. In this technique, usually synthetic DNAs are employed. These synthetic DNA sequences generally do not code for proteins but carry information that dictates the strength and specificity of the interactions guiding self-assembly [21].

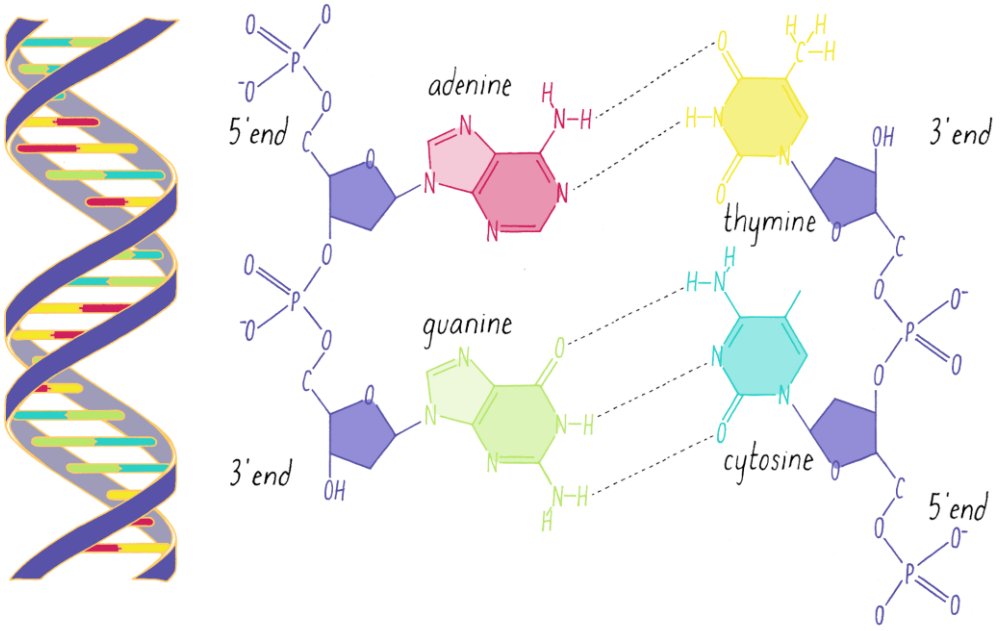

Figure 1. 2: The base pairs of adenine with thymine and guanine with cytosine hold the double helix together. The dashed lines represent hydrogen bonds that form between these bases. The phosphate-sugar backbone is colored in purple [22]. (https://explorebiology.org/collections/genetics/the-structure-of-dnaHHMI)

DNA is a macromolecular polymer whose backbone consists of deoxyribose sugar and phosphate groups, while the four bases containing the genetic information are either purine (adenine (A) and guanine (G)) or pyrimidine (thymine (T) and cytosine (C)) derivatives. A cooperative interplay of hydrogen-bonding, p-stacking, electrostatic, and hydrophobic interactions drives one DNA strand to assemble with its complement into a double helix according to extremely precise base-pairing rules. According to the Watson-Crick base pairing principle, A binds to T with two hydrogen bonds while G binds to C with three hydrogen bonds. The number and order of bases in the polynucleotide chain determine the coding information and structural function of DNA [23]. This specific and highly predictable pairing allows for the well-programmed interaction between DNA oligonucleotides.

Additional attributes, such as rigidity on the nanoscale, a diameter of approximately 2 nm, and a nearly infinite number of potential sequences, extend DNA's utility beyond a genetic blueprint for life. DNA's exceptional molecular recognition properties and structural features make it one of the most promising templates for patterning materials with nanoscale precision. The growth of rationally designed crystals and materials, first envisioned and later realized by Nadrian Seeman, has opened the door to applications of DNA in materials science such as photonics, biosensing, biocatalysis, biomedicine,

molecular electronics, biocompatible materials, gene delivery systems, DNA-based computing, functionalized surfaces [14] [24]. DNA is also emerging as a powerful tool in nanoscience; it is a promising template for organizing nanomaterials in a programmable manner. DNA-based self-assembly offers significant opportunities for synthesizing functional materials that exhibit special properties [25]. Ongoing research in nanotechnology promises to use DNA to dictate the precise positioning of materials and molecules into deliberately designed nanostructures in one, two, and three dimensions. These structures have been used to precisely position proteins, nanoparticles, transition metals, and other functional components into deliberately designed patterns. They also serve as templates for the growth of nanowires, assist in the structural determination of proteins, and provide new platforms for genomics applications. The field of DNA nanotechnology is expanding in multiple directions, promising significant impacts on materials science [26]. The fabrication of new generation complex, self-assembled structures in one, two, or three dimensions [27] using DNA-functionalised colloids [27] gives endless opportunities in various fields such as biology [28], photonics [29], [30] and nanodevices [31].

The integration of DNA with colloids to promote colloidal assembly has sparked great interest within the soft matter community [32], [33], [21], [34], [35], [36]. Colloidal particles made from various compositions such as metals, semiconductors, polymers, and oxides, range in size from several nanometers to several micrometers. Colloidal self-assembly refers to a solution-processed assembly of nanometer-/micrometer-sized, well-dispersed particles into secondary structures, with collective properties controlled by both the properties of the nanoparticles and the symmetry, orientation, phase, and dimensionality of the superstructure [37]. The initial instance of chemically modifying CdSe quantum dots with DNA involved a technique combining ligand exchange with particle surface engineering [38]. More recent research has used quantum dots as labels embedded within polymeric structures. Building on this approach, Nie and colleagues demonstrated a proof-of-concept showing the potential of quantum dots as markers for multiplexed DNA detection [39]. By carefully designing these colloidal assemblies, it may be possible in the future to harness novel properties of nanoparticles not yet exploited in devices [40]. The self-assembly of colloidal particles into superstructures holds significant potential in applications including plasmonic [41], photonics [42], catalysis [43], and sensing [44]. Coating colloids with DNA introduces an additional method for controlling the interaction potentials between particles, and DNA-coated nanoparticles

are used as a model system for studying colloidal self-assembly [45], [46], [27]. A striking example involves using tetrahedral origami cages to guide spherical gold nanoparticles into forming a diamond-like lattice [47]. In the case of colloids, the Chaikin and Seeman group has successfully designed a cross-shaped DNA origami that precisely assembles chiral colloidal clusters. The integration of spherical or patchy colloids with DNA tiles or origami structures is anticipated to open new and exciting possibilities for creating highly complex ordered assemblies. Furthermore, it is worth exploring whether the strategies developed with DNA can be extended to other biomolecules or their analogs, such as peptides, for even broader applications [48].

The introduction of DNA oligonucleotides attached to colloidal nanoparticles and the formation of lattices of nanoparticles in this way was first demonstrated in 1996 by Alivisatos et al. [46] and Mirkin et al. [45] These essential articles reported the crystal structures formed by the self-assembly of the gold nanoparticles mediated by the synthetic and short, single-stranded DNAs (ssDNA). They utilized the hydrogen bonds between the complementary ssDNA molecules attached to the nanoparticles. These nanoparticles were shown to stick to each other when the temperature decreases while they separate from each other at elevated temperatures.

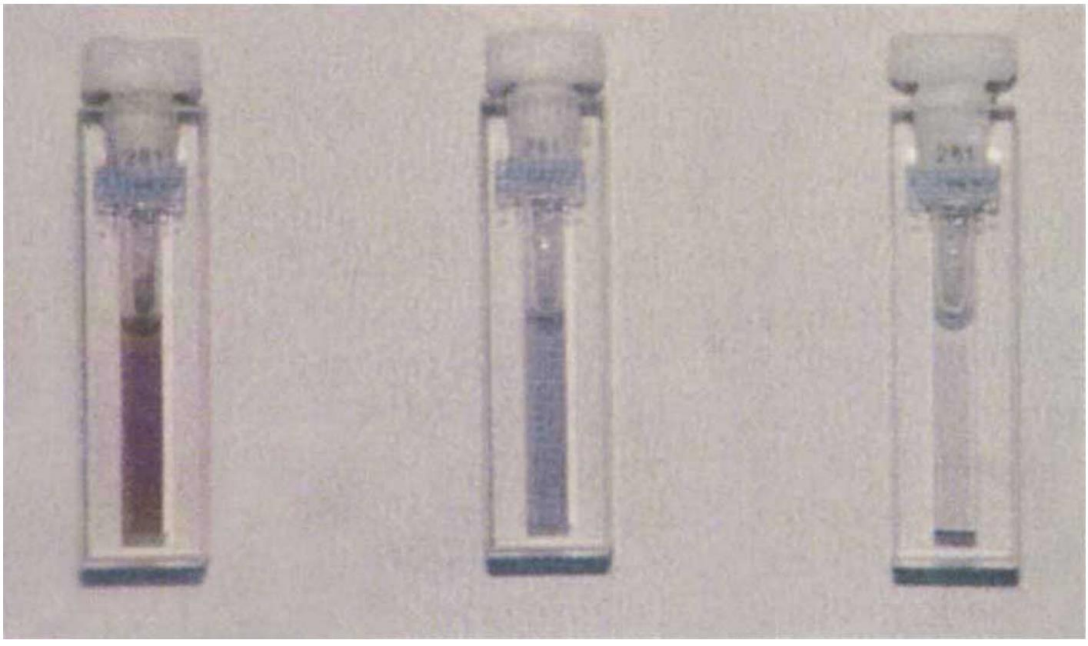

Figure 1. 3: Cuvettes with the Au colloids and the four DNA strands responsible for the assembly process. Left cuvette, at 80 °C with DNA-modified colloids in the unhybridized state; centre, after cooling to room temperature but before the precipitate settles; and right, after the polymeric precipitate settles to the bottom of the cuvette. Heating either of these cool solutions results in the reformation of the DNA-modified colloids in the unhybridized state (shown in the left cuvette) [45].

In the following years, several DNA-functionalisation methods were studied, and including the conditions of forming crystals of NPs [49], the effect of the length of the DNA molecules or cooling rate on the crystal formation dynamics [30], the self-assembly and crystal structures of DNA-functionalised magnetic, dielectric, metal, and semiconductor NPs , have appeared in the literature [50]. Over the years, many one- and two-dimensional (2D) structures have been fabricated for applications including nanoelectronics, sensing, and computation [14],[51],[52],[26],[53]. For example, Mirkin et al. demonstrated the formation of DNA-modified gold nanoparticle crystals by varying DNA strand length and salt concentration [45]. Further research explored how the length of DNA molecules and cooling rate influence crystal formation dynamics, revealing that longer DNA strands produce larger and more stable crystals, while slower cooling rates result in better-ordered structures [30]. This provided the environment to achieve crystalline morphologies of nanoparticle assemblies via the thermal pathway (Figure 1.4). DNA-coated magnetic nanoparticles have been employed to create responsive materials controllable by external magnetic fields [54]. DNA-guided self-assembly has been utilized to create 2D nanoparticle arrays for highly sensitive biosensors [29].

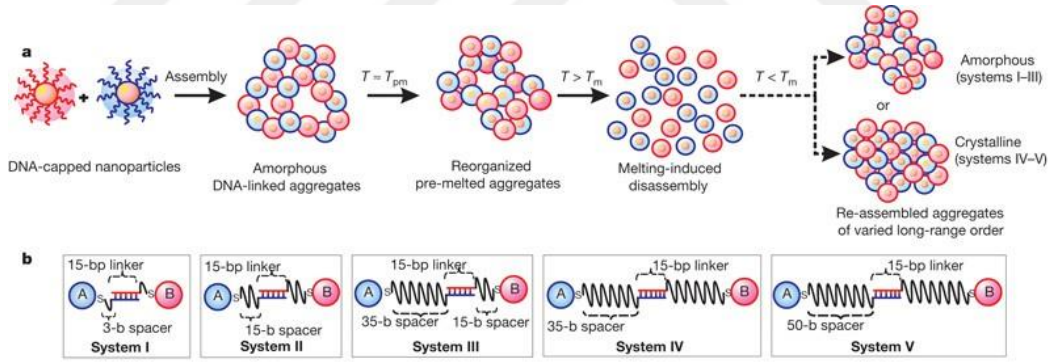

Figure 1. 4: (a) The assembly system of DNA-capped nanoparticles, the aggregates of which show a series of structural changes under a variety of thermal conditions. (b) DNA linkages between nanoparticles (one interparticle linkage is shown for clarity, not to scale) with recognition sequences for the A (blue) and B (red) sets of DNA capping. bp, base pairs. b, bases. s, thiol termination of DNA [30]**.**

In the long-term maturation process of this subject, the research efforts first focused on DNA-driven smart self- assembly of different nanoparticles to prepare crystal structures of nanomaterials in solution. Later, the successful production of crystal structures have been followed by the investigation of the photonic effects of DNA-functionalized nanomaterials [55]. In recent years, research efforts have focused on utilising DNA-driven self-assembly in nanofabrication to form metamaterials [56] and nanoparticle superlattices [57]. In these studies, the nanostructures were first defined

using electron-beam lithography followed by the DNA-functionalization of these specific regions. Subsequently, DNA-functionalised nanoparticles were attached to these regions and metamaterials [56], and nanoparticle superlattices [57] were obtained. These studies demonstrated a method for assembling plasmonic nanoparticle superlattices using DNA and lithography, allowing precise control over nanoparticle placement and enabling the dynamic tuning of optical properties. Furthermore, a hybrid lithography technique was proposed by Alivisatos et al. [56], where the DNA-functionalised regions were determined using lithography to eventually control the light scattering. This research combined lithography with DNA-directed self-assembly to create dynamic plasmonic metamaterials capable of shifting their optical properties in response to chemical changes, particularly by exhibiting electromagnetically induced transparency. This work opens avenues for advanced sensing technologies and next-generation dynamic materials.

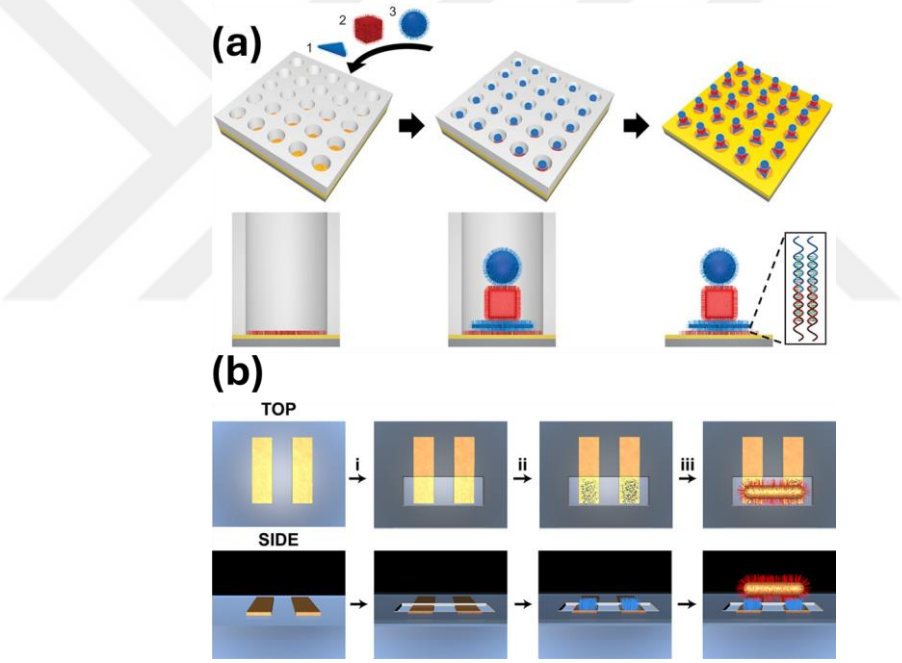

Figure 1. 5: (a) Programmable assembly of reconfigurable nanoparticle (NP) architectures. 1D pores are fabricated in a PMMA-coated gold substrate using top-down lithography, and the gold surface at the bottom of each pore is densely functionalized with DNA. DNA-functionalized colloidal NPs are then assembled in a layer-by-layer manner to have a terminal DNA sequence complementary to that of the previous layer. The porous PMMA template is removed to generate NP superlattices with 2D periodicity that are composed of oriented NP architectures. Bottom images depict cross-sectional views of a single pore [57]. (b) Schematic illustration of the lithography and assembly process of hybrid inorganic–organic structures. Parallel rods are first written on the indium tin oxide coated glass surface using e-beam lithography followed by gold evaporation. (i) A second layer exposure is done to open a trench over a specific position of the parallel rods, and a brief O2 plasma etch is used to remove residual PMMA in the trench. (ii) Thiolated DNA (blue) is then added to the exposed portion of the parallel rods. (iii) Finally, the orthogonal rod functionalized with complementary DNA (red) is incubated on the glass slide, falls into the PMMA trench and hybridizes on the parallel rods [56].

The main drawback of these works was the use of complicated, energy-hungry, and expensive tools to form desired structures. Therefore, alternative routes that especially involve the use of light have attracted the interest of the research community. For example, Simoncelli et al. [58] controllably cleaved DNAs on the surface of the gold nanorods by polarization-dependent plasmonic heating using a femtosecond laser. Using this method, they managed to achieve nanoscale control on the molecular self-assembly. Moreover, the effect of the exposed light on the DNA-attached gold NPs was studied by Goodman et al. [59]. They found out that the DNA molecules were released from the surface of the metal NPs when the particles were treated with a femtosecond laser. In contrast, continuous-wave lasers keep the DNA molecules on the NP's surface (Figure 1.6b). In another work, Zornberg et al. employed thermophoresis to trigger a motion of DNA-functionalised gold NPs to create a pattern [60]. A different strategy to control the nanoparticle self-assembly with light was followed by de Fazio et al. They showed the reversible photoligation of NPs using light-responsive cyanovinylcarbazole-modified DNA molecules which enabled the formation of superlattices when excited at 365 nm and resolving the structure when excited at 312 nm (Figure 1.6c) [61]. A similar strategy was followed using azobenzene-modified DNA to control the self-assembly of gold NPs using light [62], [63]. In these studies, Kanayama et al. employed photo-isomerization of an azobenzene moiety placed in close proximity of DNAs on gold nanoparticles to control their binding/unbinding process using light leading to a controlled color transition of the sample between violet and pink [62]. Using azobenzene-modified DNAs to functionalize the nanoparticles, Zhu et al. modified the nanoparticle superlattice type between body-centered cubic and face-centered cubic owing to photoisomerization of azobenzene (Figure 1.6a) [63]. Also, plasmonic heating of the nanoparticles has also been extensively employed in ultrafast photonic PCRs where efficient energy conversion from light to heat enables reduced nucleic acid amplification time [64], [65]. Another study is about the local heating with plasmonic particles also found applications in controlled drug release as shown by Song et al.[66].

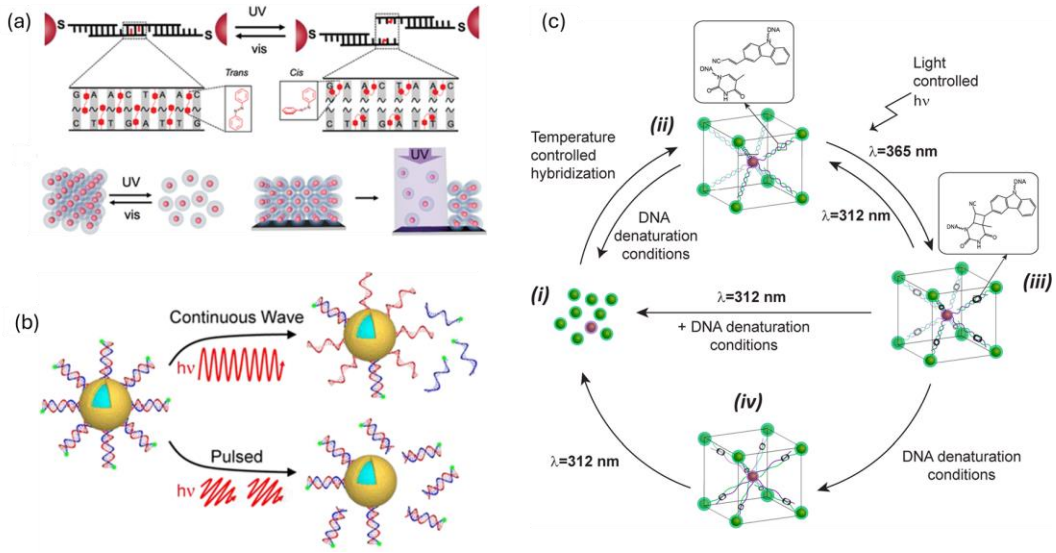

Figure 1. 6: (a) Schematic showing how azobenzene moieties are incorporated in the DNA sticky end, such that the *trans* (left) and *cis* (right) states of the azobenzene molecules can be toggled via visible or UV light, respectively. Under visible light (*trans*-form), the DNA sticky ends remain hybridized, but under UV light, the *cis*-form azobenzene molecules induce dehybridization of the DNA sticky ends. (b) NIR-Light-Induced DNA Release. CW irradiation results in dehybridization and release of fluorescently tagged ssDNA, while pulsed irradiation results in Au–S bond breakage and release of dsDNA. (c) Reversible photochemical ligation of nanoparticle superlattices. Nanoparticles conjugated with oligonucleotides are hybridized under the appropriate conditions to form superlattices.

1.2.2 Photothermal Control of DNA-Driven Self Assembly

This thesis followed an alternative route and demonstrated that the laser light absorbed by the gold NPs is enough to control the binding and unbinding of the DNAs attached to gold NPs in the solution without adding any chemical molecules [67]. We showed that by controlling the formation and disassociation of the nanoparticle network optical transmission of the nanoparticle network can be reversibly tailored using light as an external manipulator. Since the light emitted by the green laser is absorbed by the gold nanoparticles forming a network via DNA–DNA interactions, the nanoparticles heat their surroundings. Using optical microscopy, we showed that the applied laser light causes a reversible disassociation of the network owing to this optical heating effect. Furthermore, we examined the changes in the optical properties of the nanoparticle network in account of this optical excitation causing structural changes in the network. In this context, we observed that laser excitation increased the transmittance of the nanoparticle network by ~30% in the visible regime.

Similar to the photothermal effect of the gold nanoparticles, the QDs also experience local heating when optically excited due to the nonradiative recombination of the excitons. In literature, this photothermal effect was extensively studied [68]. For

example, del Rosal et al. demonstrated that PbS/CdS/ZnS QDs experience temperature increase upon exposure to infrared radiation and they used this phenomenon for photothermal therapy [69]. Similarly, Chu et al. employed visible laser radiation exciting CdSe and CdTe QDs for photothermal therapy [70]. Hanifi et al. approached the photothermal effect from a different angle. They tracked the heating of the QDs upon excitation to optimize a synthesis procedure so that super-efficient QDs can be obtained. They demonstrated that quantum yields of the QDs being >99.6% nearly suppress nonradiative decay channels and eliminate the photothermal effects [71]. These studies clearly show that unless the QDs have a quantum yield close to unity, they experience temperature increases upon photoexcitation.

Being inspired with these earlier works, here, we explore the possibility of tailoring the DNA-driven self-assembly of the QDs on two-dimensional surfaces using light. Another idea of this thesis relies on the local heating of the DNA-functionalised QDs upon optical excitation, which breaks the hydrogen bonds connecting the DNA-functionalised QDs to the DNA-functionalised surfaces. This eventually should lead the QDs not getting coated on the illuminated regions of the sample.

To test this idea, we added the DNA-functionalised red-emitting nanocrystal QDs on the DNA-functionalised glass surface. During the coating process, we irradiated a certain region on the sample with the laser light that is absorbed by the QDs. We observed that the QDs did not connect to the illuminated regions of the sample. Next, to prove that the coating control requires the absorption of light by the QDs, we employed a red laser whose light cannot be absorbed by our QDs. Results proved that irradiation at a wavelength not coinciding with the QD absorption does not allow for any control on the self-assembly of the QDs. To further support our hypothesis, we studied the self-assembly of DNA-functionalised silica NPs on 2D surfaces using the same laser that we used to control the QD self-assembly. We demonstrated that their self-assembly was not affected by the laser light since the silica NPs do not absorb the light. After showing that the obtained dark spots in the microscopy images are not due to photobleaching of QDs, we concluded that the photothermal effect is responsible for controlling the DNA-driven self-assembly of the QDs. Finally, we successfully covered the uncoated spot using DNA-functionalised green emitting QDs and DNA-functionalised dye molecules. These proved the feasibility of our method for two-dimensional structure formation without the need of expensive, complicated, and energy-hungry fabrication tools. The method we present here

can be employed in sustainably fabricating nanophotonic and nanoelectronic structures [72].

In summary, being inspired with these recent works, this thesis focuses on to explore the ability to control the binding/unbinding process of DNA-functionalised colloidal nanoparticles (gold nanoparticles, quantum dots, silver nanowires, carbon dots and silica nanoparticles) by irradiating them with a hand-held low-cost laser and employ the photothermal effect to tailor the optical features of the DNA-self-assembled nanoparticle networks in aqueous solutions without needing any other light-responsive chemical groups. We believe that our results will pave the way for novel applications of a DNA-driven self-assembly especially in actively controlling near-field interactions between different types of nanomaterials and all-solution-processed and sustainable nanofabrication technologies.

Chapter 2

MATERIALS AND METHODS

Nanoparticles are increasingly utilized in DNA functionalization due to their large surface area, which allows a significant number of DNA molecules to be attached, enabling highly precise and stable assemblies. This is particularly beneficial in fields like biosensing and drug delivery, where the ability to target specific sequences and ensure stability is crucial. Nanoparticles also protect DNA from degradation, enhancing its functionality in various applications. In the realm of photonics, nanoparticles are invaluable because they can manipulate light at the nanoscale. Their size, shape, and composition can be engineered to fine-tune their optical properties, such as light absorption, emission, and scattering. This tunability is essential for developing advanced technologies, including sensors, lasers, and other optoelectronic devices. Metallic nanoparticles can exhibit localized surface plasmon resonances, which amplify electromagnetic fields at their surfaces, leading to enhanced light-matter interactions. The ability to combine these unique properties of nanoparticles with DNA functionalization opens new avenues for creating materials and devices with unprecedented precision and efficiency. Whether in medicine, where targeted drug delivery and diagnostics are critical, or in technology, where the manipulation of light is key, nanoparticles serve as a foundational tool, bridging the gap between biological and optical systems, and driving innovation across multiple scientific fields.

2.1 NANOPARTICLES SYNTHESIS

2.1.1 Gold Nanoparticle (AuNP) Synthesis

All the chemicals used are purchased from Sigma Aldrich unless otherwise stated. The gold nanoparticles (Au NPs) were synthesized by reducing hydrogen tetrachloroaurate ($HAuCl_4$) and using a trisodium citrate solution following Ref. [73]. According to this procedure 47.5 ml water mixed with 2.5 ml gold three chloride solution (0.2 % w/v) until boil to them at 150 °C. After 15 min of boiling 2 ml tri sodium citrate

dehydrate solution (1% w/v) and boil the solution until see red color. After that solution left until cool down.

Figure 2. 1: Photograph of the AuNPs Synthesized in Our Laboratory.

2.1.2 Silver Nanowire (AgNW) Synthesis

AgNWs were synthesized through the polyol process which is a solution processing method developed by Kim et al. [74]. First, 200 mL of ethylene glycol (EG) and 6.68 g of Polyvinylpyrrolidone (PVP) were mixed in a two-necked flat-bottom flask and stirred at 350 rpm with a magnetic stirrer until PVP was completely dissolved in EG. The mixture was heated to 170°C and 0.2 g NaCl, 0.1 g KBr and 2.793 g $AgNO_3$ were added to the solution when it reached 170°C and stirring was continued. Afterwards, the solution was held at 170°C for 4 h to allow the AgNW growth process to occur. Subsequently, it was cooled to room temperature by placing the flask in a water bath. To get rid of impurities, the nanowire solution was centrifuged with methanol and acetone at a 3:1 ratio twice at 5000 rpm for 10 min. Collected AgNWs were finally dispersed in ethanol [75].

Figure 2. 2: Photograph of the AgNWs Synthesized in Our Laboratory.

2.1.3 Silica Nanoparticle (SiO_2 NP) Synthesis

Briefly, 2.79 mL of tetraethylorthosilicate (TEOS) was added to 22.2 mL of ethanol. A solution containing 0.638 mL of ammonium hydroxide, 6.8 mL of deionised water, and 17.6 mL of ethanol was prepared in a separate container. Next, two solutions were mixed while stirring at 300 rpm for 5 h at room temperature [76].

Figure 2. 3: Photograph of the SiO_2 NPs synthesized in our laboratory.

2.1.4 Red-emitting CdSe/ZnS Nanocrystal QDs (CdSe/ZnS) Quantum Dot

Red-emitting QDs synthesized according to Refs. [77], [78]. In a typical procedure, 1 mmol of CdO, 1.68 mmol of $Zn(Ac)_2$, and 5 mL OA were mixed in a three-necked round bottom (50 mL), the contents were heated at 140 °C for 30 min under the vacuum

(vacuum level reaching ca. 10^{-3} Torr). Then, the mixture's temperature was reduced to 50 °C and 25 mL of ODE was added to the reaction mixture. After that, the reaction mixture was first heated to 100 °C under the vacuum, later the temperature was increased to 300 °C under the continuous flow of Argon (Ar) gas. The Se precursor (1M TOP-Se) was prepared separately in the glove box by mixing the Se pellet in 1 mL TOP, the solution was stirred overnight at 800 rpm at 100 °C. Then, 0.2 mL of TOP-Se solution was injected rapidly into the reaction mixture at 300 °C and kept for 80 s. Afterward, 0.3 mL of DDT/ 1 mL ODE was injected into the reaction flask. After 20 min 1 mL of TOP-S (2M) was injected very slowly (in 10 min) into the reaction mixture at 300 °C. Later, the solution was allowed cool at room temperature. The crude solution was centrifuged at 5000 rpm for 15 mins with absolute acetone and a small amount of methanol. The cleaning process was repeated 2 times and finally, the CdSe/ZnS QDs pellet was redispersed in hexane.

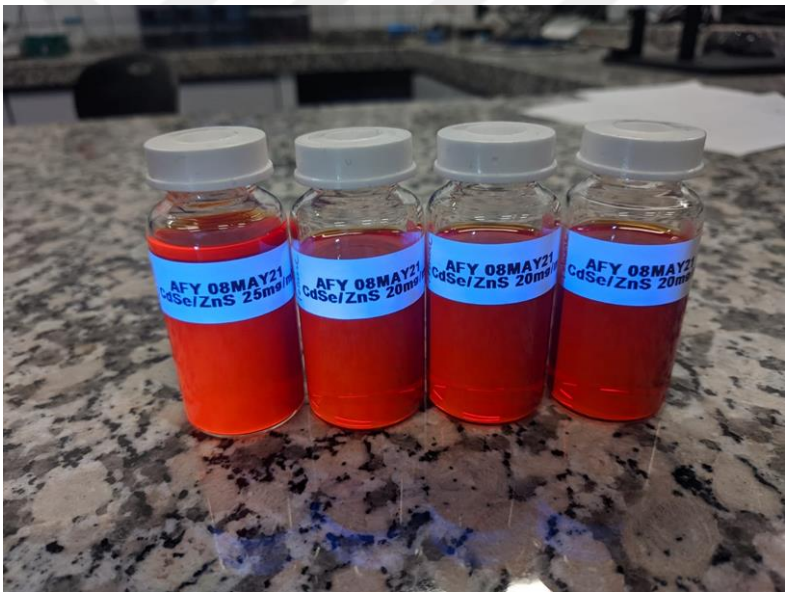

Figure 2. 4: Photograph of the QDs Synthesized in Our Laboratory.

2.1.5 Surface Modification of Silver Nanowires

345 µl of the AgNW-ethanol solution (9mg/ml) were centrifuged at 2000 rpm to remove ethanol. 20.7 mg 3-Mercaptopropionic acid (MPA) was added into 10 ml Dimethylformamide (DMF), then AgNWs were added into the solution and stirred using a magnetic stirrer for 24 hours at room temperature. Subsequently, the solution was centrifuged and precipitated AgNWs were dispersed in 10 ml ultra-pure water [75] that

shows in Figure 2.5. At the end of this thesis, carboxylic acid functionalized AgNWs were obtained.

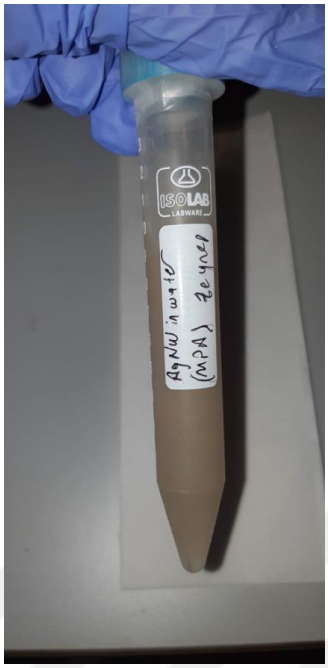

Figure 2. 5: Surface Modification of Silver Nanowires (AgNWs) with carboxylic groups.

2.2 Glass Coating with AgNWs Using Charge-Assisted Coating (CAC)

The glass substrate was washed with Hellmanex (%1) followed by double-distilled water (ddH_2O), acetone and isopropanol in sequence in ultrasonicator for 20 min at room temperature. Residual solvents were removed using air gun. All processes were applied to increase the negative polarity of the surface (mainly through hydroxyl groups). A precursor layer of strong polyelectrolytes was used to further increase the surface polarity of the glass substrate. The polyelectrolytes used in this study were 2mg/ml poly (diallyldimethylammonium chloride) (PDDA; avg. Mw ≈ 200,000–350,000) and 2mg/ml poly (sodium 4-styrene sulfonate) (PSS; avg. Mw ≈ 70,000) with 0.1 M sodium chloride (NaCl) as the polycation and polyanion, respectively. The glass substrate was alternately dipped in each polyelectrolyte solution for 5 min with intermediate rinsing and drying. Thus, 3 layers of PDDA and 2 layers of PSS were alternately stacked. The PDDA-terminated glass was dipped in the functionalized AgNWs solution (with -COOH) for 5 min or 1,5 hours at room temperature for trial, followed by rinsing with flowing DI water as seen in Figure 2.6. It is noted that non-treated AgNWs were removed in rinsing process whereas strongly bonded AgNWs remained on the substrate [79] [80] [81].

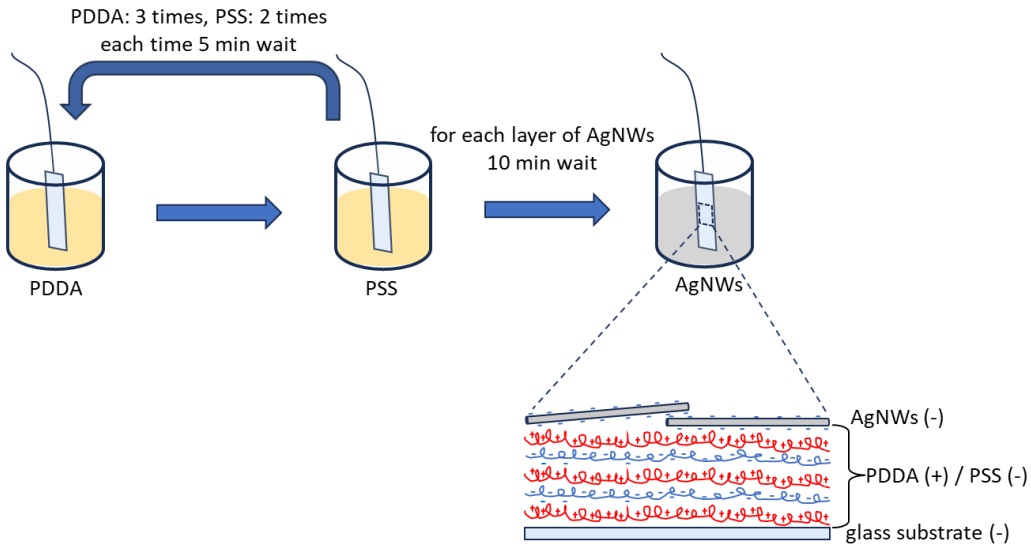

Figure 2. 6: Schematics of Charge-Assisted Coating (CAC) of Glass Surface

2.3 DNA FUNCTIONALIZATION OF NANOPARTICLES & GLASS

We used different types of DNA such as single-stranded and thiolated DNA, single-stranded and amine-functionalized DNA, single-stranded Cy-5 dye-attached DNA for functionalizing nanoparticles. The choice of DNA depends on the desired binding specificity, stability, structural properties.

2.3.1 Gold Nanoparticle

2.3.1.1 Breaking the Disulfide Bond of Dithiol DNA by using DTT

DTT is a valuable tool for reducing disulfide bonds to free thiol groups. The reaction proceeds via a nucleophilic attack where one of DTT's thiol groups attacks the disulfide bond, leading to the formation of two S-H groups. To prevent oxidation, maintaining the disulfide (S-S) form is more stable and secure. Before use, the disulfide functionality on the oligonucleotides was removed by adding DTT to ssDNA, and the resulting mixture was kept at -20 °C for 1 h (0.1M DTT, 10 mM phosphate buffer (PB)). Cleaved oligonucleotides were purified using a NAP-25 column as shown in Figure 2.7. The process begins with the preparation of the column, excess storage buffer is allowed to drain by gravity flow through the column. Subsequently, the column is equilibrated with a user-selected buffer, such as PBS. Following equilibration, the sample is applied to the column. The final step is elution, the purified sample is eluted from the column using the

same user-selected buffer (PBS buffer). Freshly cleaned oligonucleotides were added to the gold nanoparticles as mentioned below [82].

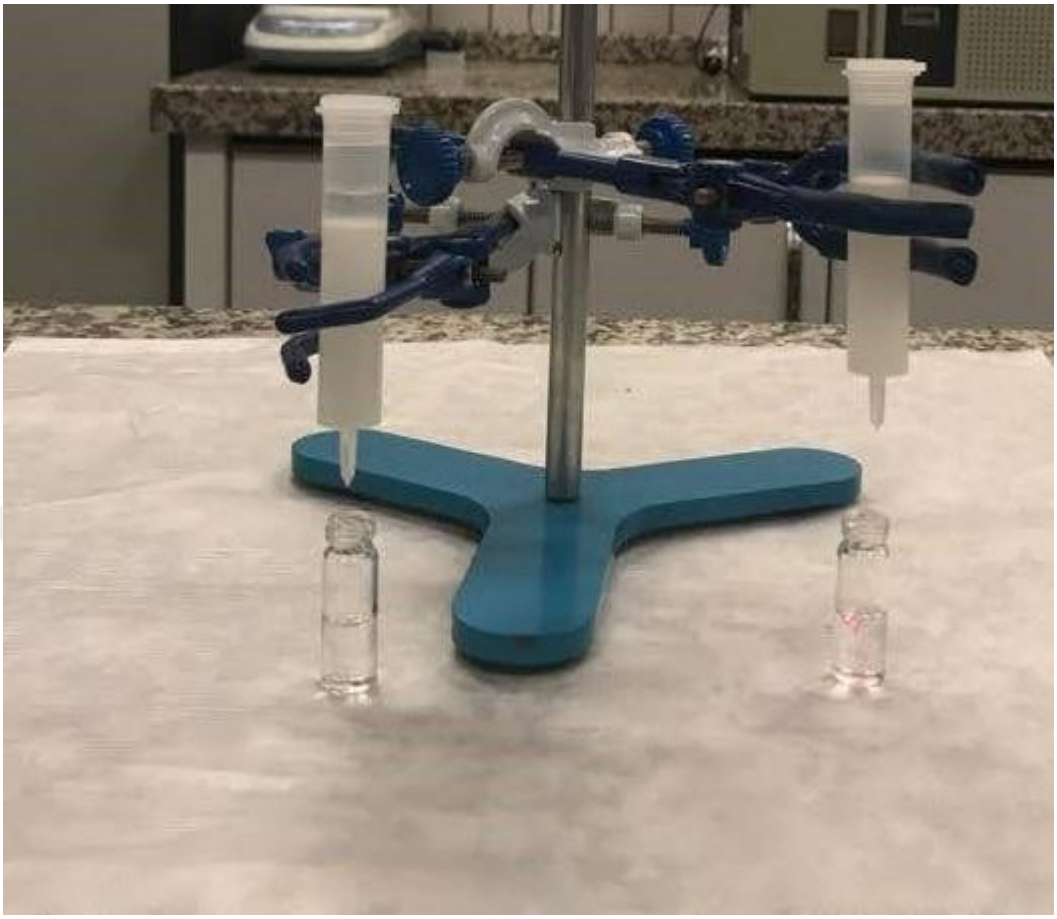

Figure 2. 7: Purification of DNAs with thiol groups attached using NAP-25 column

2.3.1.2 DNA Functionalization of AuNPs

The synthesized Au NPs were functionalized with thiol-modified, single-stranded DNAs following the methods developed by Mirkin and co-workers [45],[83],[84][85],[82]. In a typical experiment, the Au NPs are centrifuged for 1 h at 30 000 rcf to remove any residues left from the synthesis. Subsequently, the precipitated Au NPs are taken into a mixture of phosphate buffer (10 mM, pH = 7.4) and sodium dodecyl sulfate (SDS, 0.015 wt. %) solution. Here, SDS molecules avoid the aggregation of gold nanoparticles. Next, two complementary thiol-functionalized DNA chains were separately added to gold nanoparticles. The single-stranded DNAs that we used have the following bases: (1) 5'-HS-TTTTTTTTTTTTTTTGGTGCTGCG-3' and (2) 5'-HS-TTTT TTTTTTTTTTCGCAGCACC-3'. To increase the number of DNAs connected to each gold nanoparticle, NaCl solution in 0.015 wt. % SDS and 10 mM PB mixture is added stepwise such that the total salt concentration reaches 0.7M within 3 h. Following

the final salting step, the tubes are shaken overnight. The DNA-coated nanoparticles are then cleaned by centrifugation three times to remove unconnected single-stranded DNAs and salt from the solution. The precipitated gold nanoparticles are redispersed in 0.015 wt. % SDS-containing PB solution in the first two centrifuges. After the third centrifugation process, no SDS was added to the DNA-coated nanoparticles. Next, about 50 μl of the nanoparticles that have complementary DNAs surrounding them is taken from each tube and mixed, and NaCl solution in PB is added to increase the final salt concentration to 100 mM. After hybridization, the color of the solution varies from red-pink to violet-black indicating the self-assembly of the nanoparticles and the formation of the nanoparticle networks, whereas heating the mixture turned the color to its initial case.

2.3.1.3 Sample Preparation for Optical Characterizations

Prior to optical characterizations, the hybridized and heated samples are then loaded between two microscope slides, sealed with epoxy, and left for cooling. An Ocean Optics halogen light source connected to a fiber is used to illuminate the microscope slides at a normal angle (spot size: 0.2 cm^2). The transmitted light is collected using a fiber equipped Ocean Optics spectrometer. The transmission measurements are carried out first by recording the spectrum of the transmitted light through the microscope slides loaded with PB and then measuring the spectrum of the light transmitted through the same type of microscope slides filled with the DNA-functionalized Au NPs. The reported transmittance indicates the ratio of the measurement taken with Au NPs to the measurement taken with only PB. The effect of the external light is evaluated by continuously illuminating the sample with a green hand-held laser pointer (Yopigo ESO-2000, spot size: 0.35 cm^2) whose optical intensity variation was presented in Fig. 2.15. The transmission spectra are recorded before laser illumination and every 10 min after the laser radiation is applied. Microscopy images of the samples are recorded using a Nikon transmission optical microscope prior to laser irradiation and every 30 min after laser irradiation started. The electron microscope images are taken using a Zeiss Gemini scanning transmission electron microscope.

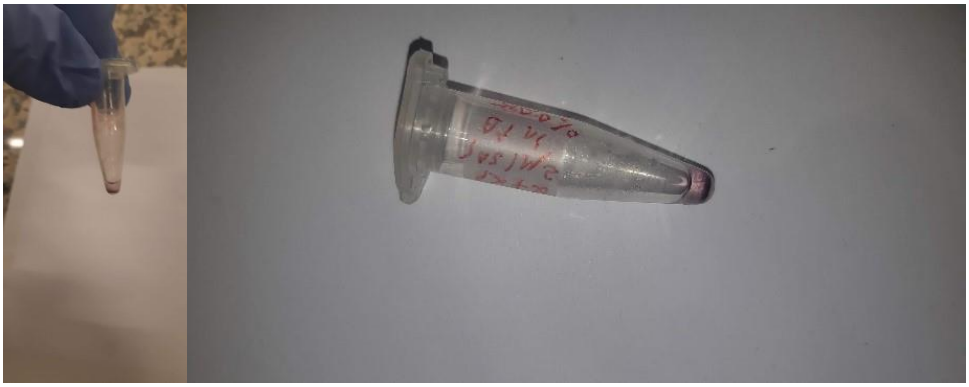

Figure 2. 8: Photograph of DNA-functionalized AuNPS that possess complementary DNA chains. The formed after hybridization can be clearly seen.

2.3.2 Silver Nanoparticles DNA Functionalization

The synthesized Ag NWs were functionalized with thiol-modified single-stranded DNAs following the method developed by Han et al. [86]. In a typical experiment, Ag NWs which were dispersed in ethanol was precipitated and redispersed in ultra-pure water such that the final concentration was fixed at 1 mg/mL. The single-stranded DNAs utilized in the experiment have the following sequences: (1) Thiol 5'-HS-TTTTTTTTTTTTTTGGTGCTGCG-3', and (2) 5'-HS-TTTTTTTTTTTTTTCGCAGCACC3'. The monothiol DNA sequences were subjected to deprotection using a 0.10 M Dithiothreitol (DTT) solution and then purified using a NAP-25 column. Afterward, two monothiol-functionalized DNA chains that are complementary to each other were added separately to the silver nanowires solution, resulting in a final DNA concentration of approximately ~5 μM. The mixed solution was then salted with 0.15 M NaCl and 0.01 w% sodium dodecyl sulfate (SDS), buffered to 10 mM phosphate at pH 7.4, and incubated overnight at 25°C. Subsequently, the DNA-coated Ag NWs were cleaned using centrifugation for three times. After the first two centrifugation steps, the precipitated silver nanowires were redispersed in a solution containing 0.015 w% SDS in phosphate buffered saline (PB). After the third centrifugation process, the solution was dispersed in 10 mM PB solution for further analysis in subsequent experiments.

2.3.3 Silica Nanoparticle DNA Functionalization

The silica NPs were functionalised with ssDNA molecules in following steps as illustrated in Figure 2.9 [76], [87]: 50 ml colloidal dispersion of silica NPs (19.5 mg/mL)

was mixed with 0.3 mL of 3-aminopropyltriethoxysilane (APTES) and stirred vigorously overnight [76], followed by centrifugation at 7000 rpm for 5 min, and the collected pellet was redispersed in phosphate buffered saline (PBS). In the next step, 1 ml of APTES-coated silica NPs solution was mixed with 1 ml of 8% glutaraldehyde (in PBS), and solution was kept shaking for 5 h. Subsequently, the mixture was centrifuged and washed with water at 7000 rpm for 5 min [87]. Then, the APTES and glutaraldehyde coated silica NPs were functionalised with NH_2-ssDNA. First, two different NH_2-ssDNA chains (Oligomer Biotechnology) were added to the two vials containing silica NPs separately. The ss-DNAs that we use have the following bases: 5'-NH_2-TTTTTTTTTTTTTTTCGCAGCACC-3'. The NPs and DNA solution were kept in a shaker overnight at room temperature to allow the NH_2-ssDNA to interact with the glutaraldehyde-modified silica NPs. Later, the fluorophore-modified DNA (Cy5-DNA), complementary to the NH_2-ssDNA, was added to the DNA functionalised silica NPs (NH_2-ssDNA-coated silica NPs) for Cy5-DNA functionalization. Cy5-DNA is used to confirm the attachment of DNA chains to silica nanoparticles (see section 3.2.2) Cy5-functionalized DNA chain was as follows: 5'-Cy5-TTTTTTTTTTTTTTGGTGCTGCG-3'. Further, 100 µM NaCl solution in 10 mM PBS was added to the solution to maximize the DNA coverage on each silica particle, and the solution was shaken overnight. Next, the NH_2-ssDNA-coated silica NPs (with or without Cy-5 DNA functionalization) was centrifuged and washed for three times with PBS at 7000 rpm for 5 min. Finally, the collected pellet was redispersed in PBS [72].

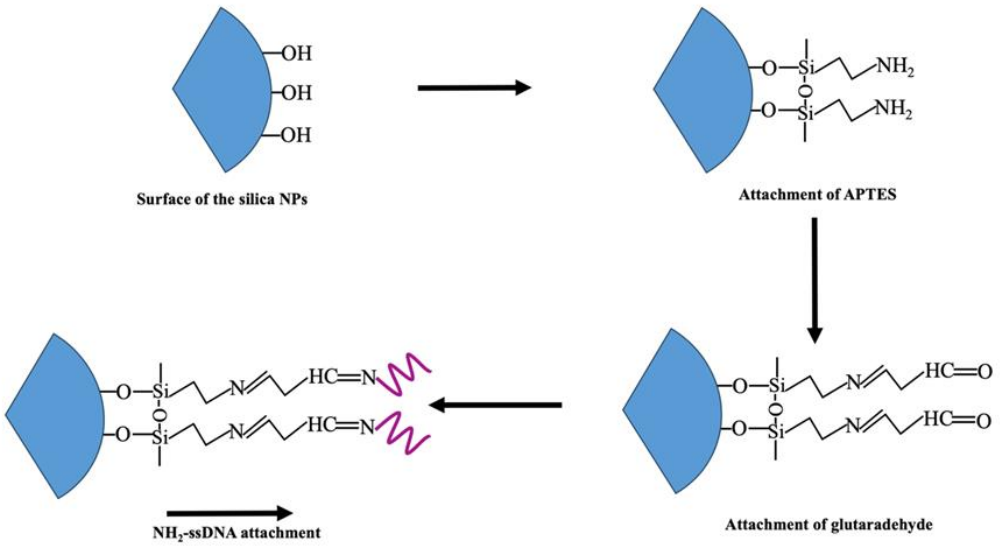

Figure 2.9: Illustration of DNA-functionalization procedure of silica NPs.

2.3.4 Quantum Dot DNA Functionalization

2.3.4.1 Phase Transfer of QDs to Aqueous Phase

Prior to DNA functionalization, the QDs need to be transferred to aqueous medium. The phase change procedure for oleophilic CdSe/ZnS QDs to hydrophilic CdSe/ZnS with mercaptopropionic acid (MPA) was carried out as reported elsewhere with slight modifications [88]. In a typical experiment, 0.5 mL (10 mg/mL) of QDs solution in hexane was precipitated by centrifugation with absolute acetone at 8000 rpm for 15 min. The pellet was redispersed in 1 mL chloroform and transferred into a 4 mL glass vial. Then, 0.5 mL ethylenediamine (EDA) was added to the above solution with vigorous stirring. The solution was stirred for 30 min, and then 0.15 M aqueous MPA solution (1 mL) was added to the mixture and stirred for 1 h. Afterwards, stirring was stopped, and a coloured aqueous layer containing water, EDA, ligand exchanged QDs, and an organic layer containing hydrophobic materials formed. The aqueous layer was collected using a pipette, followed by centrifugation using an excess amount of methanol to precipitate the QDs from the crude solution. The pellet was redispersed in ultrapure water and stored in a refrigerator for further studies.

Figure 2.10: QDs in Aqueous Phase. These QDs possess MPA as their ligands with COO^- facing the aqueous medium.

2.3.4.2 DNA Functionalization of QDs

We followed a previously reported protocol with minor modifications to functionalise the QDs with single-stranded DNA (ssDNA) [89], which we illustrate in Figure 2.11. The aqueous QDs were conjugated with amine-functionalized ssDNA (NH_2-ssDNA; Oligomer Biotechnology) having the following bases: 5'-NH_2-TTTTTTTTTTTTTTTCGCAGCACC-3'. Briefly, 25 µL QD solution (8 µM) was diluted with 200 µL borate buffer (50 mM, pH=6.1) in a glass vial. In the above QDs solution, 8 µL aqueous solution (50 mM) of N-Ethyl-N′-(3- dimethylaminopropyl) carbodiimide hydrochloride (EDC, Aldrich) and 8 µL aqueous solution of (50 mM) N-Hydroxysuccinimide sodium salt (NHS, Aldrich) were added. Next, 400 µL of NH_2-ssDNA (100 nM) solution was immediately added to the mixture. During the conjugation, the salt concentration was increased with a time interval of 1 hour such that the final NaCl concentration reached 0.1M. The QDs and DNA solutions were stirred overnight after the final salting step. Subsequently, the QD-DNA conjugates were centrifuged via an ultrafiltration unit with 50kDa weight cutoff at 6000 rpm for 5 min to remove unattached/excess DNAs, followed by 4-5 times washing with borate buffer (50 mM, pH = 6.1). The purified QD-DNA conjugates were redispersed in borate buffer (50 mM, pH = 6.1, [NaCl] = 0.1M) for further characterisation and assembly.

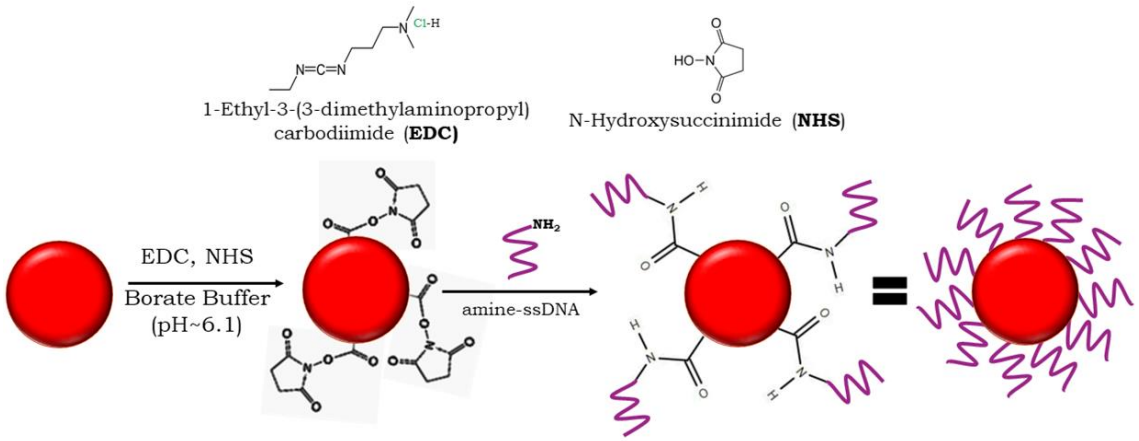

Figure 2.11: Schematic illustration of DNA conjugation reaction of QDs.

2.3.5 DNA Functionalization of Glass

To optimise the silanisation process, the glass substrates (high quality microscopy slides) were cleaned thoroughly to remove contamination. The glass substrates (2 cm x 2 cm) were first ultrasonicated in 1% Hellmanex solution, followed by ultra-pure water

(UPW), acetone, and isopropanol in sequence for 20 min each at room temperature, and then dried with the nitrogen. After drying, the substrates were placed in a plasma cleaner (PE-50, Plasma Etch, Inc, Harrick Plasma) for 5 min. Next, the substrates were immediately immersed in 2% APTES (v/v) solution in 90% methanol for 30 min. After 30 mins, the glass substrate was washed 3 times with 90% methanol and pure water, dried in an oven at 120 °C for 45 min in ambient atmosphere, and allowed to cool at room temperature [90],[91]. To functionalise the amine (NH_2) group of APTES with an aldehyde group of glutaraldehyde, 100 µL of 5% glutaraldehyde was spin-coated (VTC-100, Vacuum Spin Coater, MTI Corporation) at each substrate for 1 min at 500 rpm. The amines were allowed to react with glutaraldehyde at room temperature for 30 min and washed thoroughly with UPW [92]. The DNA immobilisation on glass substrates was done by spotting 60 µL of NH_2-ssDNA (100mM) on the amino-silanised and aldehyde-functionalized glass substrate. The single-stranded DNAs that we use have the following bases: 5'-NH_2-TTTTTTTTTTTTTTGGTGCTGCG-3'. After that, the substrates were incubated overnight at 37 °C and washed with 0.1% Triton X-100, 0.1M HCl (pH=4), 0.1M KCl and UPW [93]. The DNA-functionalisation of the substrate is schematically represented in Figure 2.12. To confirm the DNA-functionalisation of the glass substrate, we added Cy5-DNA on the functionalized glass substrate (DNA chain: 5'-Cy5-TTTTTTTTTTTTTTCGCAGCACC-3'). The fluoescence microscopy image (Figure 2.13) affirmed the successful coating of ssDNA over the glass substrates[72].

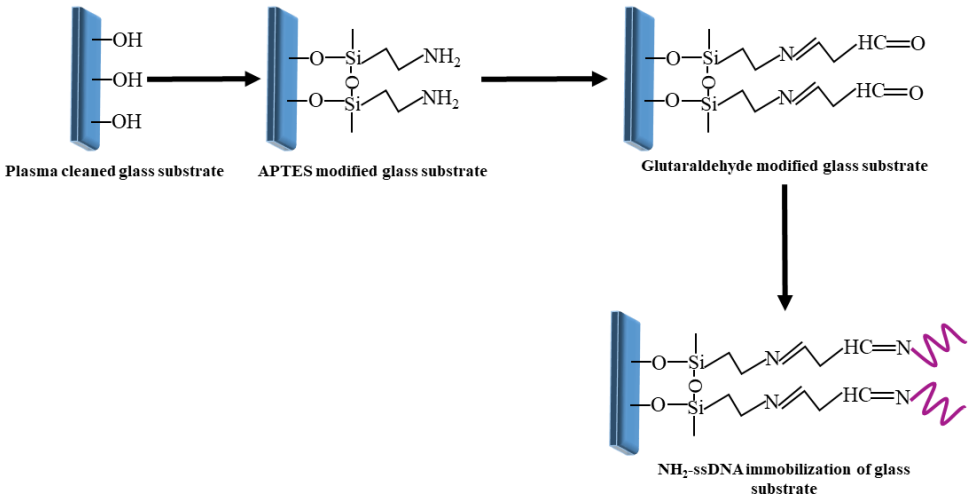

Figure 2. 12: Coupling of amine-functionalized ssDNA on glass surface.

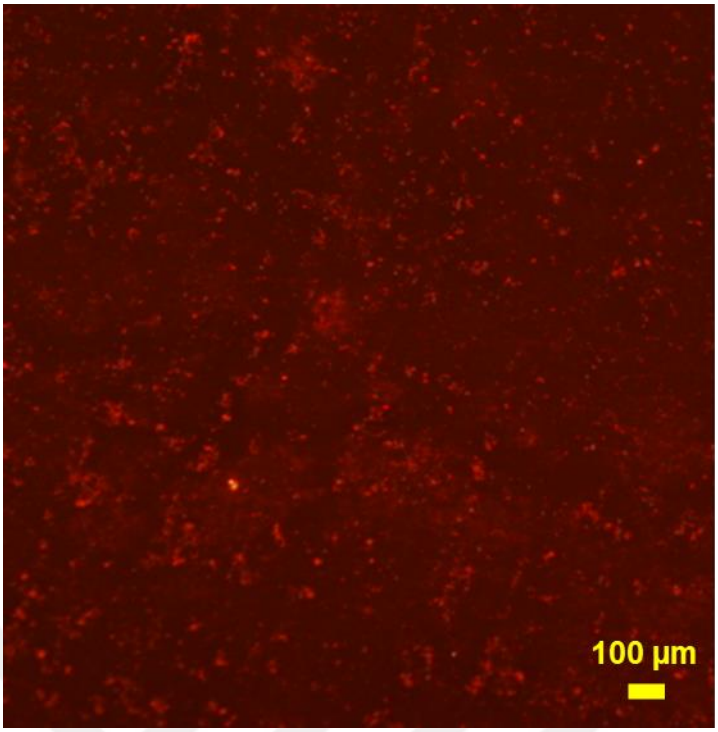

Figure 2. 13: Fluorescence microscopy image of DNA-functionalized glass surface and Cy5-DNA under the green fluorescence light.

2.4 Light-Assisted Control of Self-Assembly

2.4.1 Experimental Set-Up for Monitoring Transmission During Laser Irradiation

To measure the transmission, during laser irradiation, the heated samples that are including complementary DNA-functionalized AuNPs then loaded between two microscope slides, sealed with epoxy, and left for cooling. An Ocean Optics halogen light source connected to a fiber is used to illuminate the microscope slides at a normal angle (spot size: 0.2 cm^2). The transmitted light is collected using a fiber equipped Ocean Optics spectrometer. The transmission measurements are carried out first by recording the spectrum of the transmitted light through the microscope slides loaded with PB and then measuring the spectrum of the light transmitted through the same type of microscope slides filled with the DNA-functionalized Au NPs. The reported transmittance indicates the ratio of the measurement taken with Au NPs to the measurement taken with only PB. The effect of the external light is evaluated by continuously illuminating the sample with a green hand-held laser pointer (Yopigo ESO-2000, spot size: 0.35 cm^2, 20mW) whose optical intensity variation was presented in Fig. 2.15. The transmission spectra are recorded before laser illumination and every 10 min after the laser radiation is applied.

Microscopy images of the samples are recorded using a Nikon transmission optical microscope prior to laser irradiation and every 30 min after laser irradiation started. The electron microscope images are taken using a Zeiss Gemini scanning transmission electron microscope.

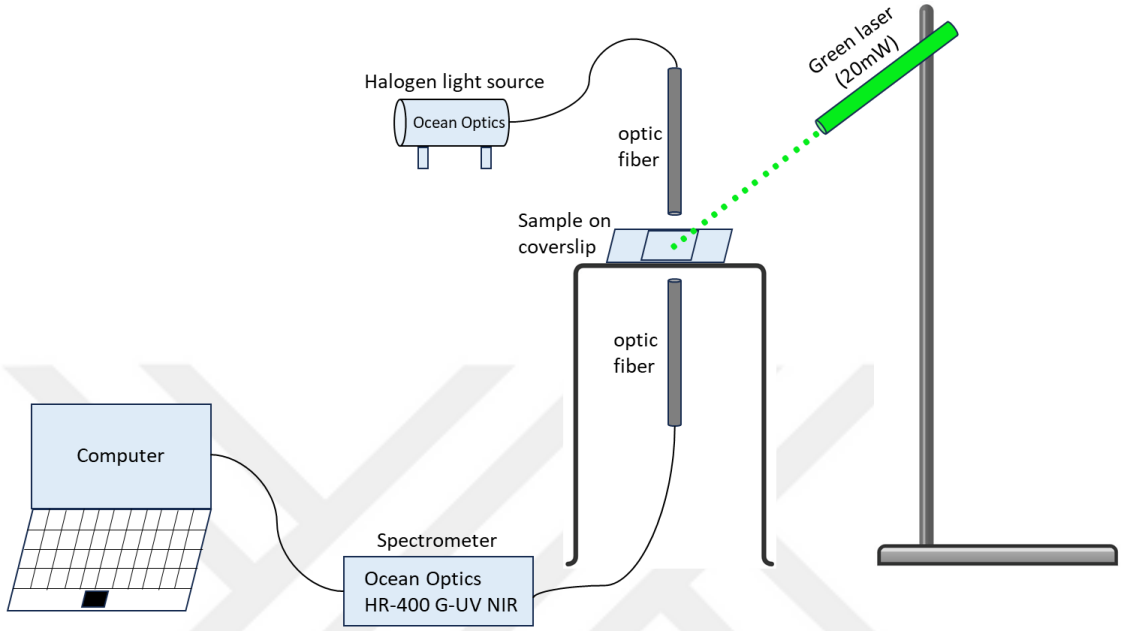

Figure 2. 14: Illustration of the transmittance measurement setup [67]

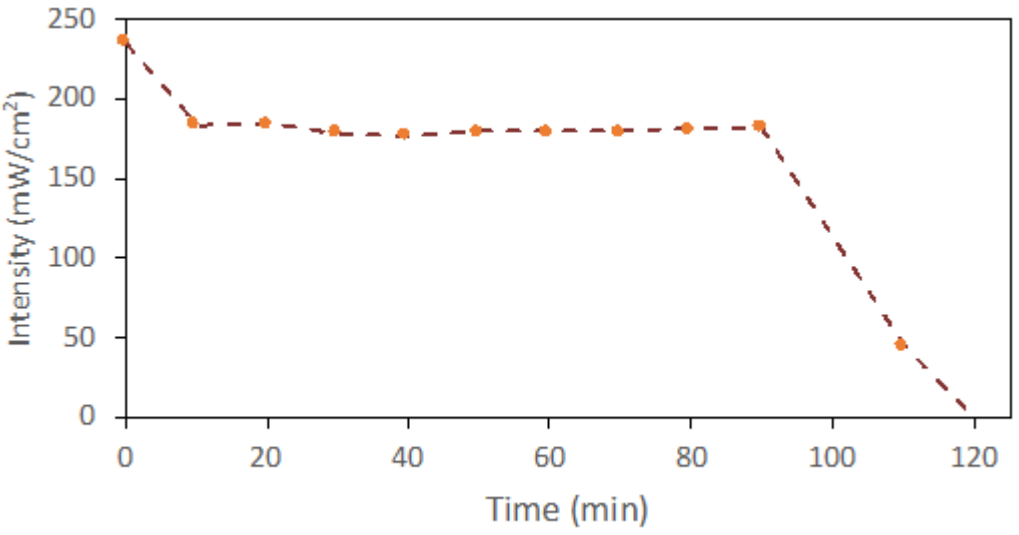

Figure 2. 15: Time evolution of the optical intensity of the hand-held battery-powered green laser used in this work.

2.4.2 Experimental Set-Up for Light Assisted Pattern Formation

A green-emitting hand-held laser (20 mW) was used as a light source to control the self-assembly of QDs (and to analyse the coating of silica NPs) on the glass substrate. Briefly, 60 µL of QD-ssDNA conjugates were dropped over the complementary immobilized NH_2-ssDNA glass substrate in the presence of salt solution, and the substrate was illuminated with laser light for 4 h. During this time, the ssDNAs, conjugated with QDs, were allowed to hybridise with the ssDNAs present on the glass substrates forming a double helical structure and hence achieving the utmost attachment to the substrate. While the area of the substrate under the laser spot was remained uncovered or intact from the QDs, forming a spherical structure over the glass substrate. Once the targeted coating duration is achieved, we washed the sample with PBS buffer three times using a pipette while the laser irradiation continues. It is also worth emphasizing that the time-dependent analyses of the coatings were carried out under the same conditions but by employing different samples for each time duration we tested.

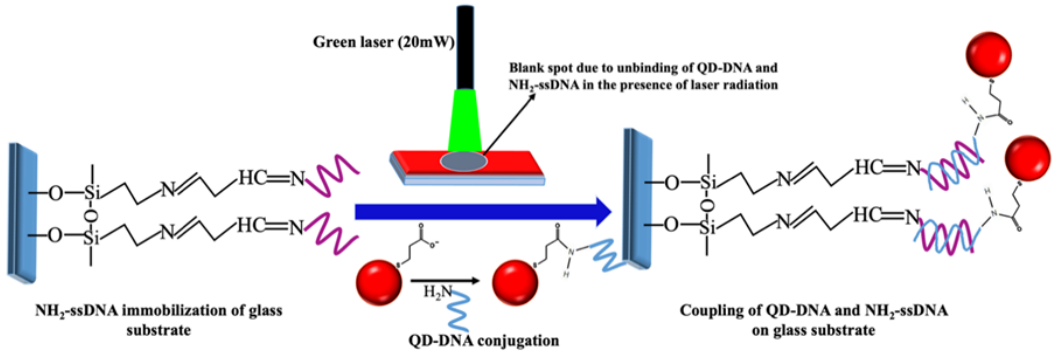

Figure 2. 16: Illustration of the system used to control the self-assembly of DNA-functionalized QDs on DNA-functionalized glass surface using laser irradiation.

2.4.3 Experimental Set-Up for Light Assisted Glass Coating with AgNWs

To create a conductive, patterned shape, we wanted to control the electrostatic coating of AgNWs was on glass using laser light. For this purpose, we applied blue laser on the glass substrate that dipped inside AgNWs solution after the polyelectrolytes coating.

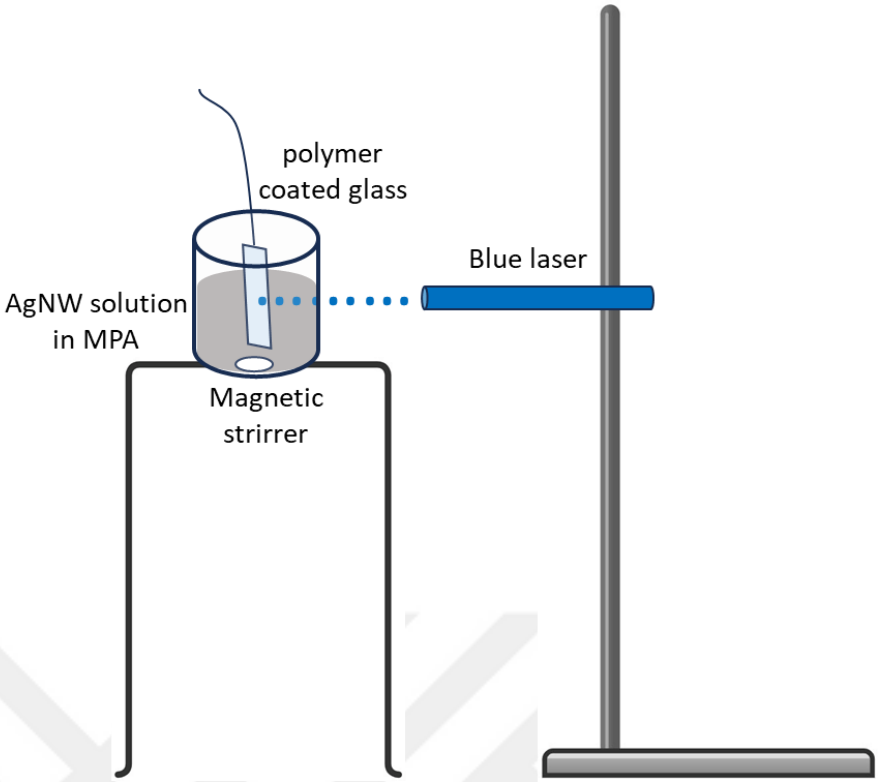

Figure 2. 17: Blue Laser Experimental Set-Up for Glass Coating with AgNWs

We tried some further steps to increase conductivity of AgNWs coated glass surface. First, increasing the number of coating layer AgNWs and then the duration of staying glass inside the AgNWs solution, Additionally, we increased the concentration of AgNWs solution. Finally, the coated AgNW layer on glass were mid-processed to improve their conductivity by heating at 100°C in between each layer of coating AgNWs.

2.5 Measurements & Characterizations

The absorption and photoluminescence spectra of synthesised materials were recorded on Genesys 10S UV-Vis spectrophotometer (Thermo Scientific) or Shimadzu UV1800 UV-vis spectrometer and Cary Eclipse Fluorometer (Agilent Technologies), respectively. To determine the size (hydrodynamic) and surface charge on the synthesized AuNPs, QDs, AgNWs and SiO_2 NPs dynamic light scattering (DLS) and zeta potential measurements were done on ZetaSizer Nano-ZS (Malvern Instruments, U.K.) at room temperature. A scanning electron microscope (SEM, Zeiss Gemini-SEM300) was used to analyse the morphological features of the NPs, and the morphology of AuNPs and QDs was determined by scanning tunnelling electron microscope (STEM, Zeiss Gemini-SEM300). The sample for STEM was prepared by sonicating 1 mL of AuNPs and QDs

in 10 mL ultrapure water, and this solution was deposited on to carbon-coated copper grid by the fishing method. The optical images were collected by using Nikon transmission optical microscope to verify the QD coating on the glass substrates and to measure transparency of AuNPs network. An Ocean Optics halogen light source connected to a fiber is used to illuminate the microscope slides at a normal angle (spot size: 0.2 cm^2). The reflection and transmission spectra is collected from prepared films including AuNPs and SiO_2 NPs by using a fiber equipped Ocean Optics spectrometer. The power of the lasers light was measured using a Newport (Model 843-R) power meter, and the average intensity was calculated at irradiated surfaces. Sheet resistance is measured by four-probe instrument Keithley2400 (Source Meter) to observe conductivity of AgNWs coated glass surfaces.

Chapter 3

RESULTS AND DISCUSSION

3.1 Nanoparticle Synthesis

In this thesis, we have synthesized metal, semiconductor, and dielectric nanoparticles. Below we present our results of characterizations belonging to these syntheses.

3.1.1. Gold Nanoparticle Synthesis

Gold nanoparticles (AuNPs) are preferred materials for studies involving DNA functionalization owing to easiness in attaching thiol groups to the gold surface. In our thesis, with this motivation but also to study optical feature control, we synthesized AuNPs. The absorption spectra of synthesized AuNPs in water possess a plasmon peak around 525 nm (Figure 3.1.). This absorption region is especially important because light emitted by the commercially available, low-cost green lasers can be absorbed by our nanoparticles.

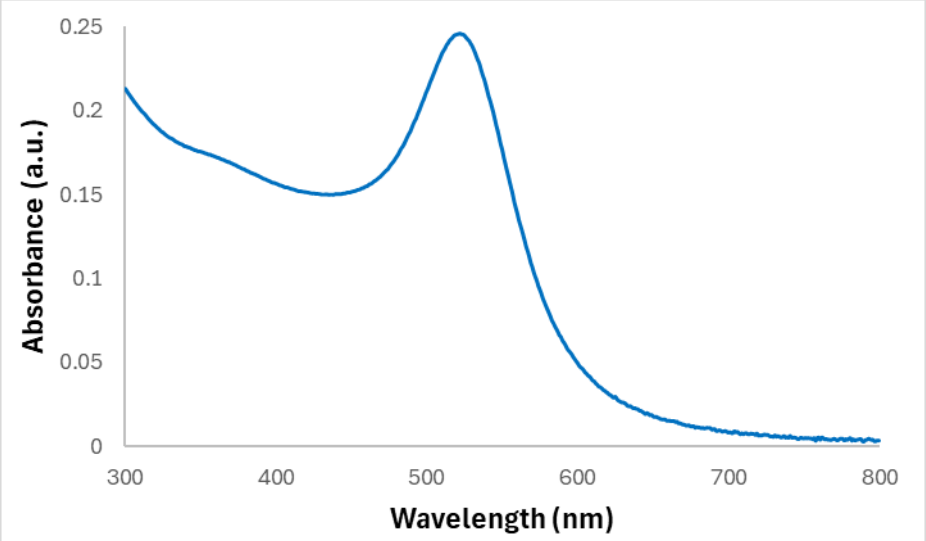

Figure 3. 1: UV-visible absorption spectra of the AuNP colloidal solution

3.1.2. Silver Nanoparticle Synthesis

To obtain conductive patterned surfaces, we aimed at using silver nanowires that will be coated on 2D surfaces using charge assisted coating method. For this purpose, we synthesized AgNWs following the polyol method as described in Chapter 2. The absorption spectra of AgNWs in water are shown in Figure 3.2. These NWs have a strong plasmon peak of around ~380 nm and a shoulder at ~360 nm that are attributed to longitudinal and vertical modes of electron oscillations [94] [95]. The zeta potential measurements revealed that the surface charge on silver nanowires was -19 mV (Figure 3.3) and indicate that the NWs are relatively stable. To analyse the dimension of AgNWs we took their SEM images indicating straight wires with an average diameter of 50 nm and average length of 4 μm (Figure 3.4).

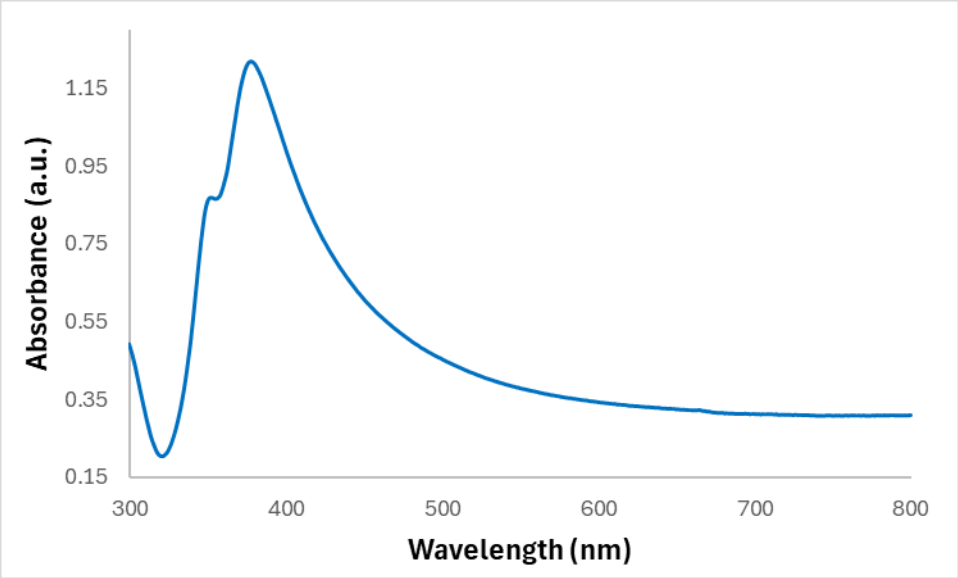

Figure 3. 2: UV-visible absorption spectrum of the AgNW colloidal solution

Results

		Mean (mV)	Area (%)	St Dev (mV)
Zeta Potential (mV):	-19,6	**Peak 1:** -19,6	100,0	7,68
Zeta Deviation (mV):	7,68	**Peak 2:** 0,00	0,0	0,00
Conductivity (mS/cm):	0,0267	**Peak 3:** 0,00	0,0	0,00
Result quality	Good			

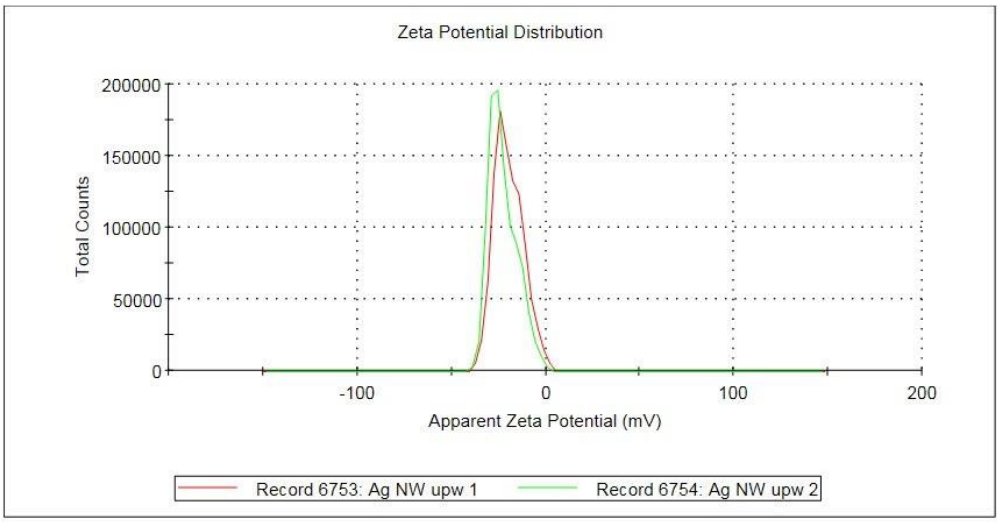

Figure 3. 3: Zeta potential measurements of AgNW colloidal solution

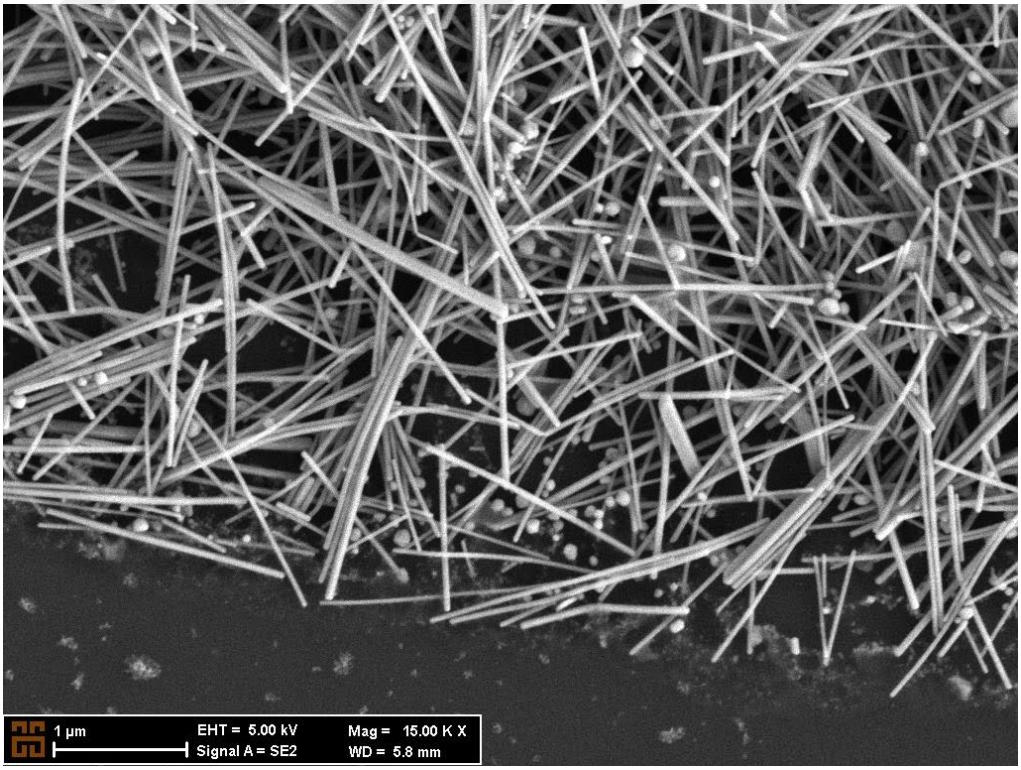

Figure 3. 4: SEM image of AgNWs.

3.1.3. Silica Nanoparticle Synthesis

To test the effectiveness of light on tailoring the self-assembly, we needed a material that would not absorb the light and would not experience local heating. Silicon dioxide (also called silica) nanoparticles are great fit for this purpose. With this motivation, we synthesized silica NPs as described in Chapter 2. The surface morphology and average size of silica NPs were measured by DLS and SEM, showing an average size of 140-200 nm (Figure 3.5 and 3.6, respectively). The zeta potential measurements revealed that the surface charge on bare silica NPs was -29 mV (Figure 3.7) indicating colloidal stability.

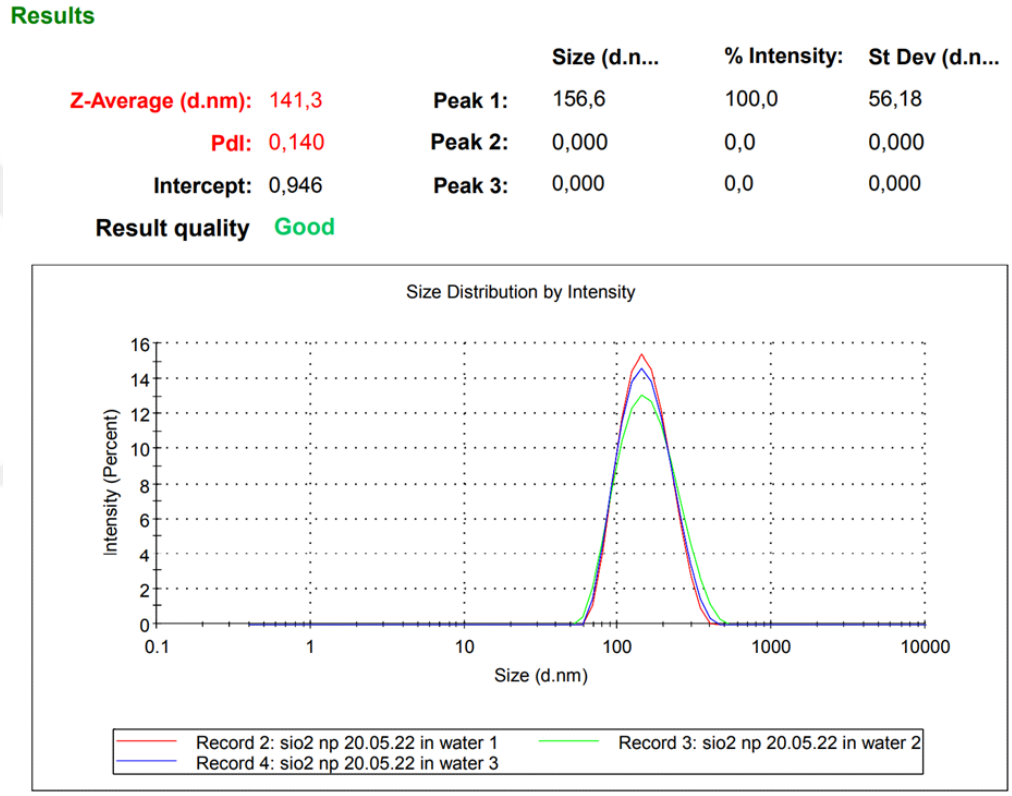

Figure 3. 5: DLS measurement results of silica NPs

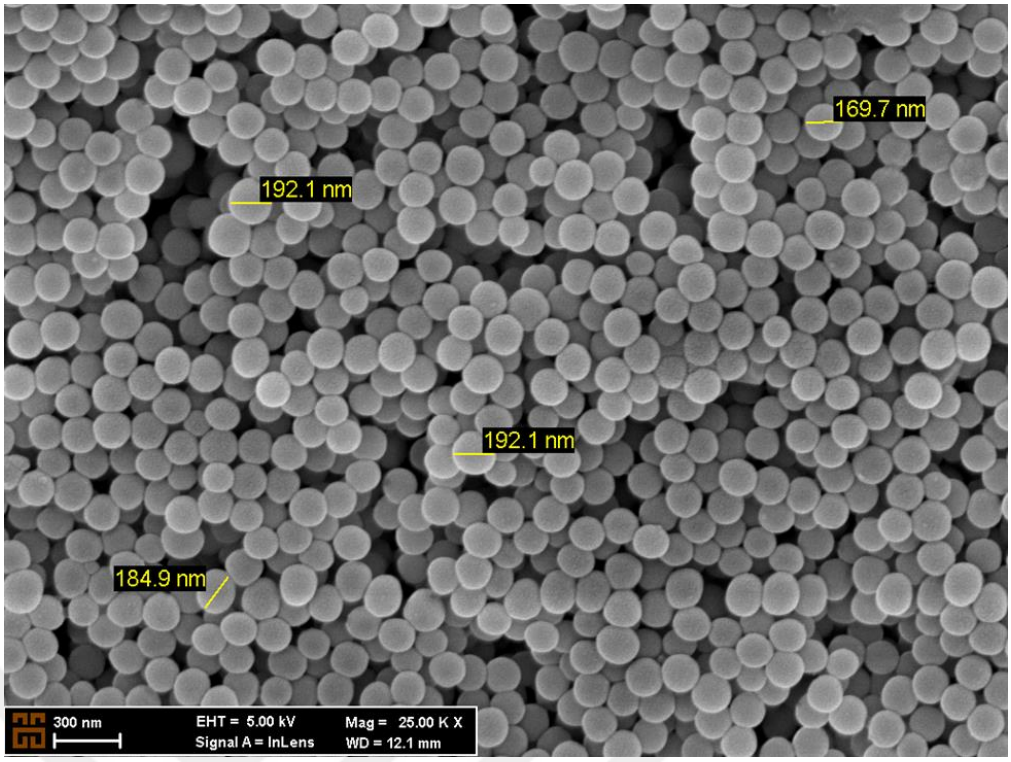

Figure 3. 6: SEM image of Silica NPs.

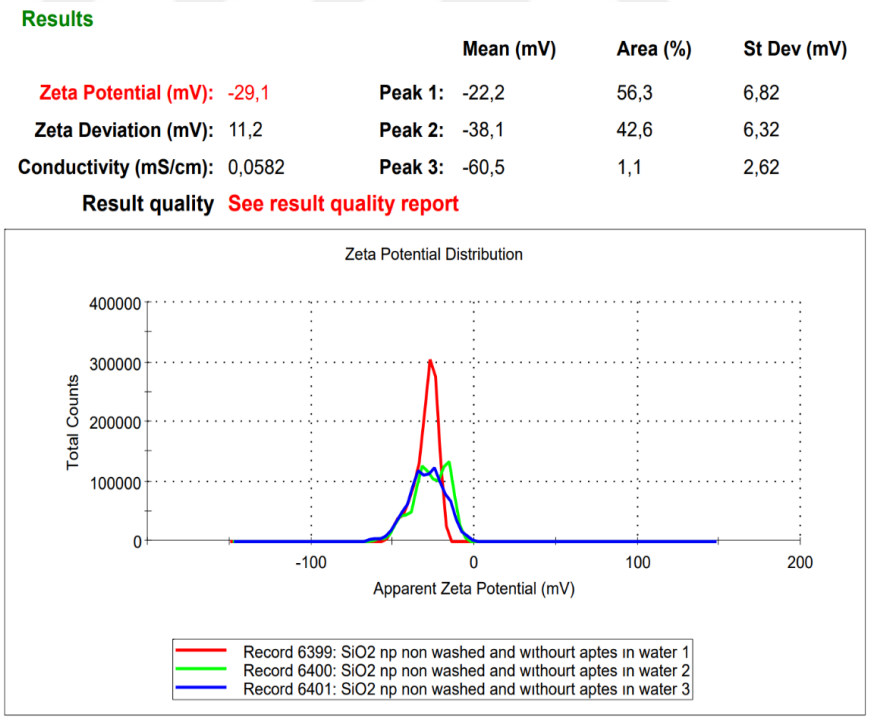

Figure 3. 7: Zeta potential measurements of silica NPs.

3.1.4. Quantum Dot Synthesis

The complete establishment of our purposed technique on light-controlled self-assembly entails the inclusion of semiconductor nanoparticles to the list of materials that

can be employed. For this purpose, in this thesis, we synthesized red-emitting CdSe/ZnS QDs. The oleophilic red-emitting CdSe/ZnS QDs were synthesized by the hot-injection method. The photoluminescence and absorption spectra of the QDs is presented in Figure 3.9. indicate a clear first-exciton peak at ~610 nm while the photoluminescence peak is located at ~630 nm. Furthermore, the STEM images in Figure 3.11. show a diameter of ~9 nm.

These QDs were then transferred to the aqueous phase via the ligand exchange process in the presence of EDA. The EDA helps to detach the original ligands from the QDs surface, allowing MPA to attach more firmly to the QDs and make them water-soluble. The MPA molecule attaches to the QDs surface via its thiol group (-SH), whereas the carboxyl group (-COOH) remains available for interaction with NH_2-ssDNAs. The zeta potential measurements were performed to observe the surface charge of the carboxyl-functionalized CdSe/ZnS QDs. As shown in Figure 3.8, the QDs were negatively charged with the zeta potential value of -37.7 mV, attributed to the presence of terminal carboxyl groups. The colloidal solutions with a zeta potential value above +30 mV or below -30 Mv [96] are considered stable, hence carboxyl-functionalized CdSe/ZnS QDs solution was ascribed to be stable. The quantum efficiency was calculated using the Eq. (3.1):

$$QE_{QD} = QE_{dye} \times (I_{QD}/I_{dye}) \times (h_{QD}/h_{dye})^2 \qquad \textbf{Eq. (3.1)}$$

where QE is the quantum efficiency of the standard dye (Sulphorhodamine 101), I is the integrated fluorescence spectra of quantum dot or the standard (at the excitation wavelength corresponding to the same absorbance value); and η is the refractive index of QDs solvent (hexane and water) and standard dye solvent (ethanol). After the calculations, the QE of the CdSe/ZnS (in hexane) and CdSe/ZnS/MPA (in water) QDs were found to be 51%, and 30%, respectively.

Results

		Mean (mV)	Area (%)	St Dev (mV)
Zeta Potential (mV):	-37,7	**Peak 1:** -34,3	67,4	4,94
Zeta Deviation (mV):	7,49	**Peak 2:** -46,0	32,6	3,98
Conductivity (mS/cm):	0,0363	**Peak 3:** 0,00	0,0	0,00
Result quality	Good			

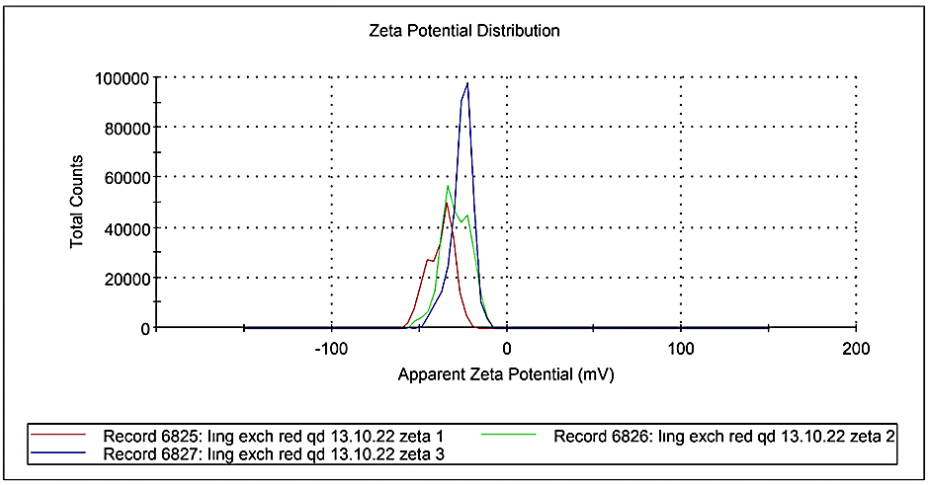

Figure 3. 8: Zeta potential measurement results of CdSe/ZnS (red-emitting) QDs in water.

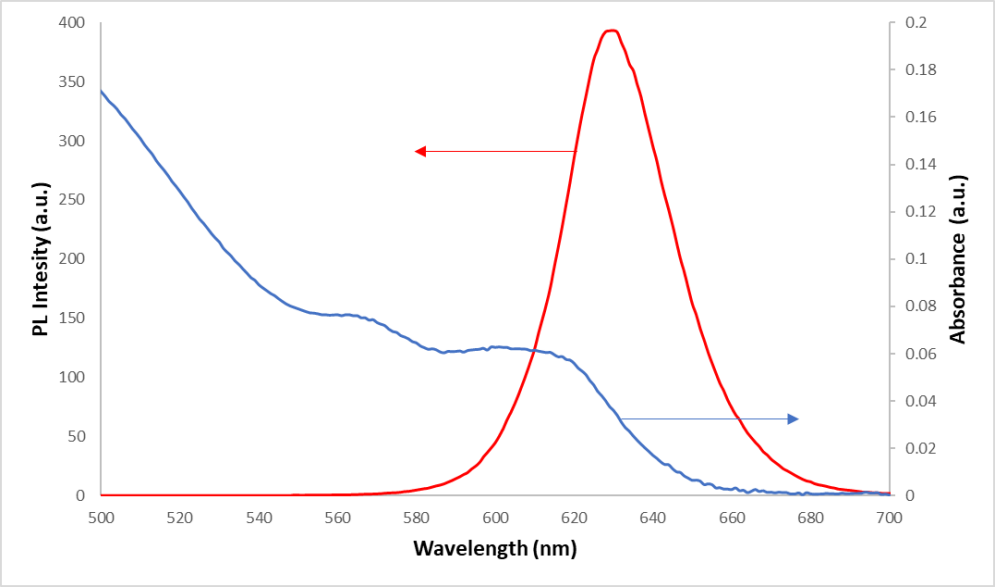

Figure 3. 9: Photoluminescence and absorption spectra of red-emitting CdSe/ZnS QDs in hexane.

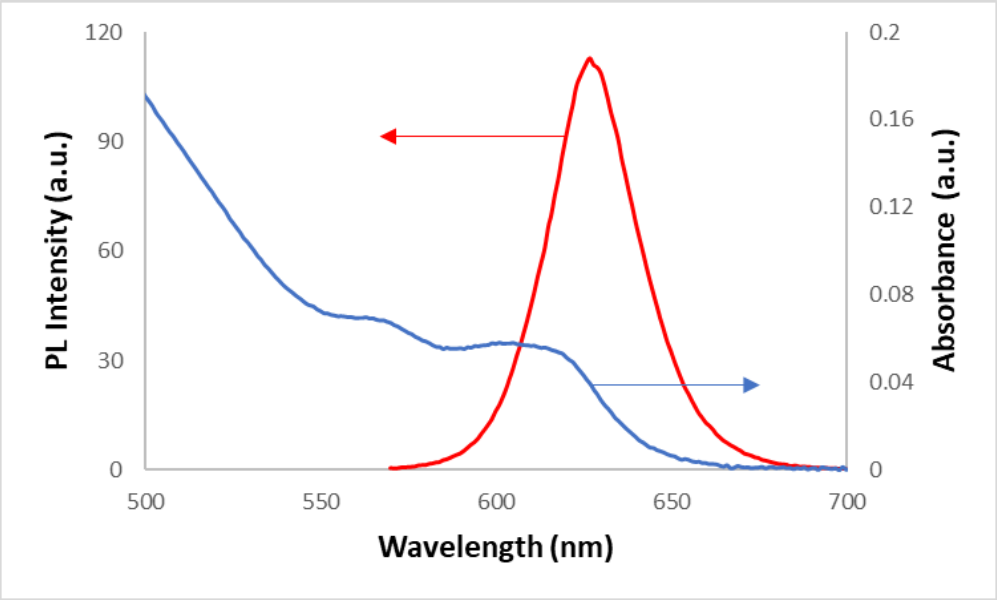

Figure 3. 10: Photoluminescence spectra and absorption spectra of MPA-functionalized CdSe/ZnS QDs in water.

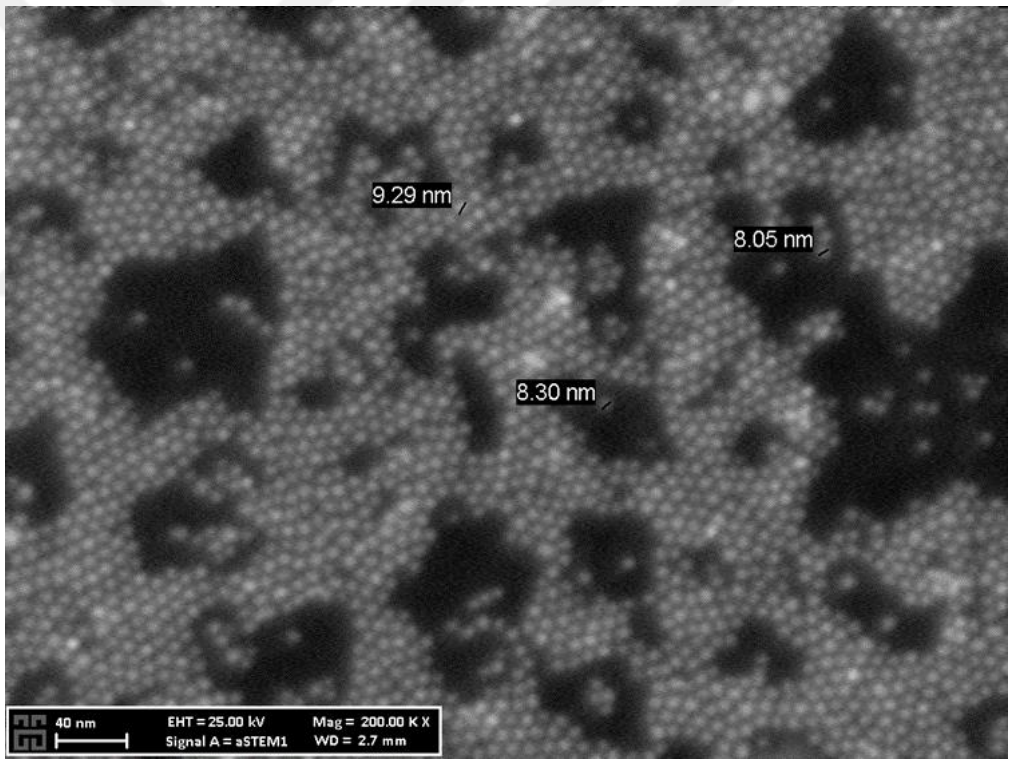

Figure 3. 11: STEM Image of CdSe/ZnS QDs.

3.2. DNA Functionalization of Nanoparticles

3.2.1. DNA Functionalization of Gold Nanoparticles

As described in Chapter 2, AuNPs were coated with single-stranded DNAs. The success of the coating was imminent when we observed precipitation of nanoparticles

network upon hybridization with AuNPs possessing complimentary DNAs. We furthermore, measured the melting temperature to be 51 °C (Figure 3.14)

3.2.2. DNA Functionalization of Silica Nanoparticles

Silica NPs were functionalized with ssDNA. The surface morphology and average size of DNA-functionalized silica NPs. Figures 3.12 and 3.13 show the zeta potential values of -2.92 and 21.7 mV for the APTES and glutaraldehyde-functionalized NPs, respectively. The change in zeta potential values confirms the successful functionalization of silica NPs with APTES and glutaraldehyde. However, upon further functionalization of glutaraldehyde coated silica NPs with ssDNA, the zeta potential again turned out to be negative (-33.2 mV) owing to the negative charge on the DNA molecules (Figure 3.14).

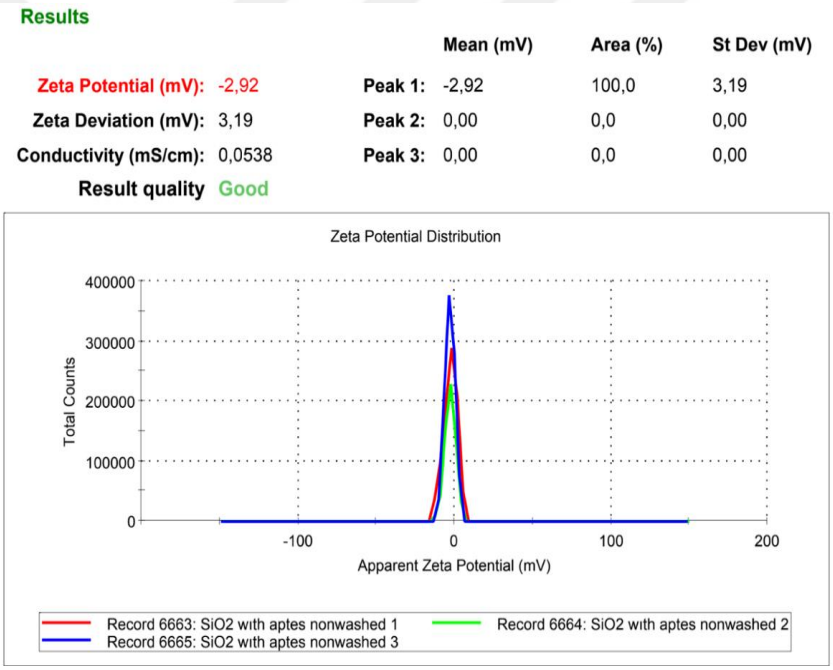

Figure 3. 12: Zeta potential measurements of the silica NPs whose surface is functionalized with APTES.

Results

		Mean (mV)	Area (%)	St Dev (mV)
Zeta Potential (mV): 21,7	Peak 1:	21,7	100,0	3,12
Zeta Deviation (mV): 3,12	Peak 2:	0,00	0,0	0,00
Conductivity (mS/cm): 0,597	Peak 3:	0,00	0,0	0,00
Result quality Good				

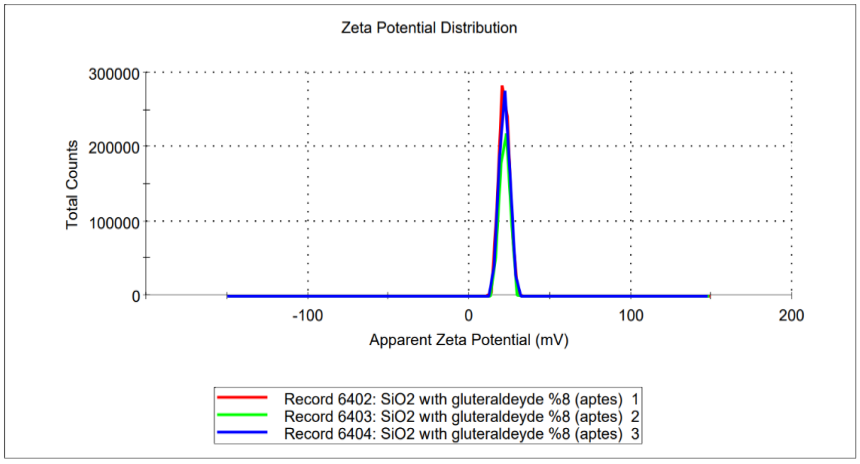

Figure 3. 13: Zeta potential measurements of the silica NPs whose surface is functionalized with glutaraldehyde.

Results

		Mean (mV)	Area (%)	St Dev (mV)
Zeta Potential (mV): -33,2	Peak 1:	-33,2	100,0	3,23
Zeta Deviation (mV): 3,23	Peak 2:	0,00	0,0	0,00
Conductivity (mS/cm): 0,820	Peak 3:	0,00	0,0	0,00
Result quality Good				

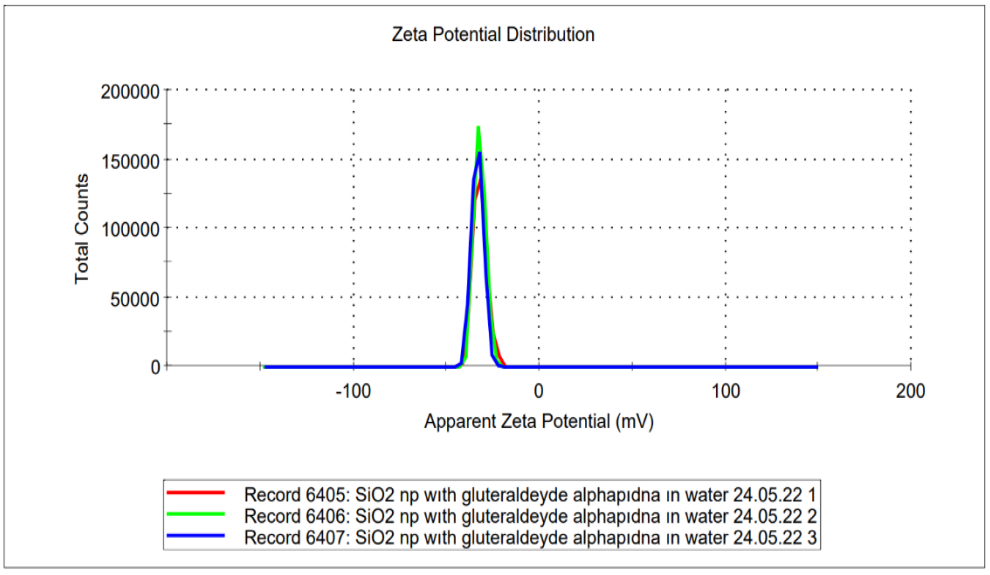

Figure 3. 14: Zeta potential measurements of the silica NPs after DNA functionalization.

To test the presence of DNA on the NP surface, we mixed DNA-coated SiO_2 NPs with Cy5-DNA possessing complimentary DNA chains. In Figure 3.15, the absorbance

peak at 633 nm shows the presence of Cy5 [97]. In this experiment, Cy5 was used to understand whether ssDNA links to SiO_2 nanoparticles or not. When we measure the UV-VIS spectrum of ssDNA-functionalized SiO_2 nanoparticles with Cy5-DNA, it gives a peak around 633-650 nm. It confirms the hybridization between DNA-functionalized SiO_2 nanoparticles and Cy5-DNA.

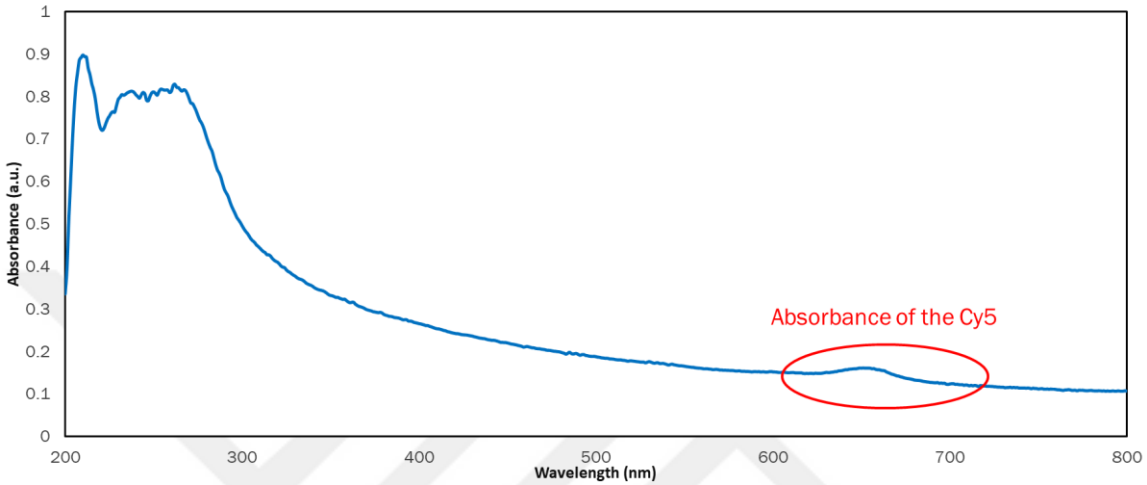

Figure 3. 15: Absorbance spectrum of Hybridized alphapi-DNA-functionalized-SiO_2 Nanoparticles and Cy5-DNA

From the absorbance measurements we selected excitation wavelength to be 633 nm. Cy5 gives a peak around 680-700 nm when excited at 633 nm [97]. Results of PL measurements that Figure 3.16 and Figure 3.17 point out that hybridization occurred between ssDNA-functionalized SiO_2 nanoparticles and Cy5-DNA.

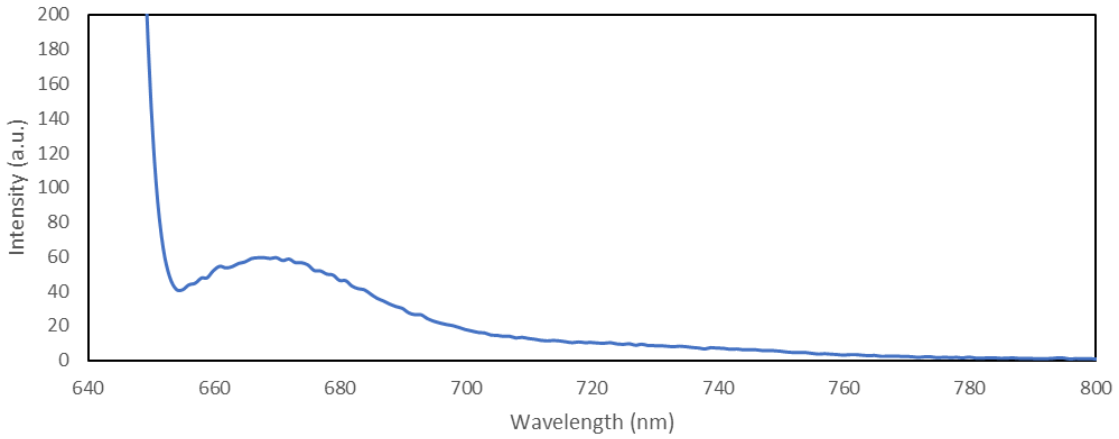

Figure 3. 16: Photoluminescence spectrum of Hybridized alphapi-DNA-functionalized SiO_2 Nanoparticles and Cy5-DNA

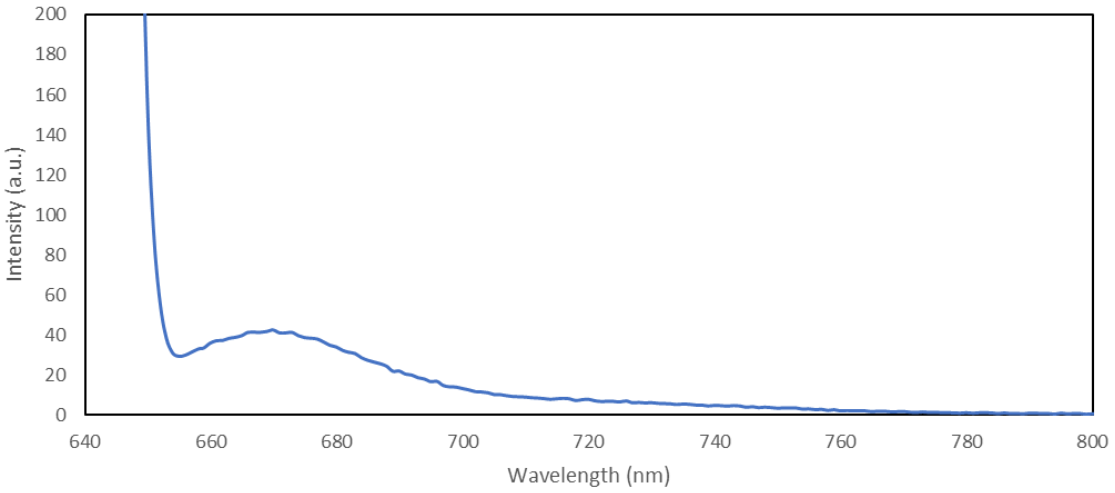

Figure 3. 17: Photoluminescence spectrum of Hybridized alpha-DNA-functionalized SiO_2 Nanoparticles and Cy5-DNA

The functionalisation of silica NPs was further confirmed with the help of FT-IR spectroscopy (Figure 3.18). An intense peak at 1100 cm^{-1} is the characteristic peak of Si-O-Si bond for SiO_2, after APTES functionalization, two absorption peaks at around 3400 and 1600 cm^{-1} were observed, which can be attributed to the N–H stretching vibration and NH_2 bending of the free NH_2 group in APTES which are attached to the surface of silica. After the interaction of glutaraldehyde with the amine groups of APTES, a peak at around 1600 cm^{-1} could be ascribed to C=N of imine [98].

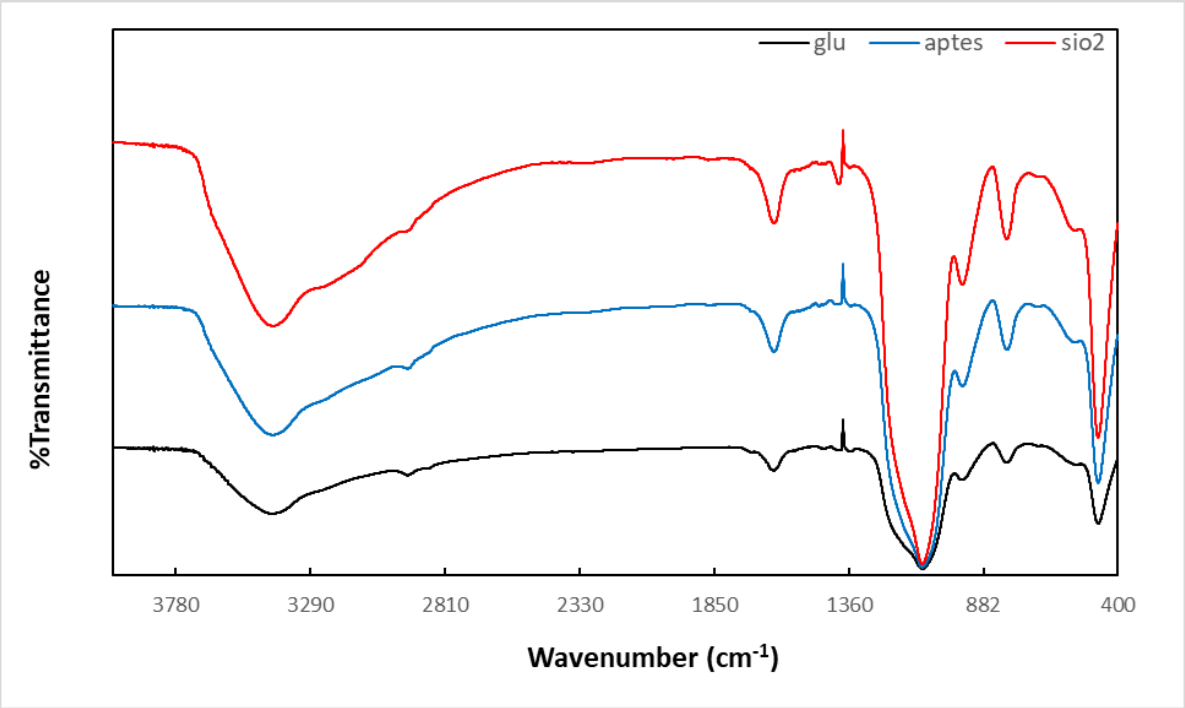

Figure 3. 18: FTIR spectra of SiO_2, APTES@SiO_2 and gluteraldehyde@APTES@SiO_2 NPs

3.2.3. DNA-Functionalization of Quantum Dots

In the present work, we attached amine-functionalized, single-stranded DNA molecules to the carboxyl-functionalized QDs by employing carbodiimide chemistry as described in Chapter 2. Further, to quantify the number of DNA conjugated per QD, we performed a fluorescence-based experiment with Cy5 DNA complementary to each QD-ssDNA conjugate, and we observed that as an average 23 DNAs were conjugated per QD (see Figure 3.19 for further details).

Below in Figure 3.19, we present the absorption spectra of the supernatant containing Cy5-DNAs as the strong peak at 680 nm. The peak at 260 nm belongs to the DNA molecules where the Cy5 dyes had been chemically attached to. These Cy5-DNAs are actually the molecules that did not hybridize with the complementary DNAs on the surface of the QDs. The ones that were connected to the DNAs on the surface of the QDs precipitated due to the relatively high salt concentration. Initially, we placed 10000 pmol of Cy5-DNAs to 400 pmol of the DNA-functionalized QD dispersion. The absorption spectrum measured presented in Figure 3.19 indicates that 988.2 pmol of the Cy5-functionalized DNAs were present in the supernatant, which was found by multiplying the volume of the supernatant, the absorbance and the extinction coefficient of the Cy5-dye at 680 nm. This calculation showed that 10000-988.2=9011.8 pmol of the Cy5-DNAs

were connected on the surface of the QDs possessing complementary DNAs. As a result, the average number of DNA molecules conjugated per quantum dot becomes 9011.8/400=23.

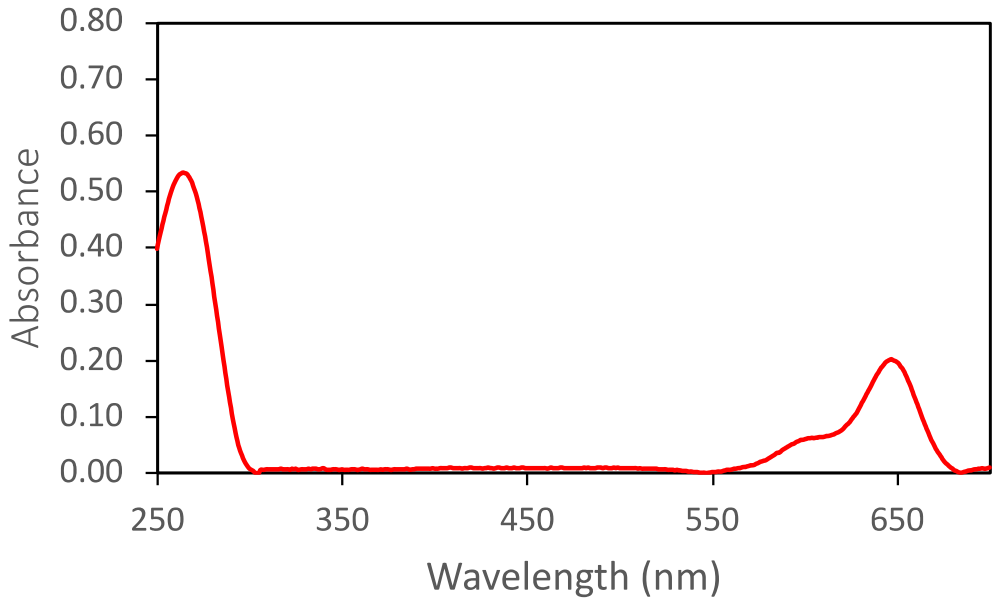

Figure 3. 19: Absorption spectrum of the supernatant containing not hybridized Cy5-DNA molecules.

3.3. Transmission Control of Gold Nanoparticle Network with Light

In this work, we investigate the effect of light on the DNA-driven self-assembly of nanoparticles and show the opportunities to manipulate the optical response of the nanoparticle network by light excitation. The temperature of the ambient medium is the main mechanism that tailors the binding and unbinding process of the nanoparticles that are connected to each other via complementary single-stranded DNA molecules. If the temperature is above a critical temperature called the melting temperature, the complementary ssDNAs remain separated leading to isolated nanoparticles within the aqueous medium. When the temperature decreases, the hydrogen bonds of the complementary DNAs on the nanoparticles will prevail and a network of nanoparticles will form. Here, we would like to use the light as a tool to control this process. The light that can be absorbed by the nanoparticles constituting the nanoparticle network will increase the temperature within their close proximity. As a result, the temperature will increase and dissolve the network of the nanoparticles if it rises above the melting temperature. Once the nanoparticle network dissolves, this should affect the intensity of

the scattered light leading to changes in the optical properties of the network. To test the applicability of this idea, we synthesized gold nanoparticles possessing a plasmon peak around 525 nm such that the light emitted by the commercially available, low-cost green lasers can be absorbed. Subsequently, we functionalized these nanoparticles with thiol-functionalized single-stranded DNAs. We then mixed the nanoparticles with complementary DNAs and formed a network utilizing DNA–DNA interactions. After heating the mixture above the melting temperature to dissolve the network, we quickly placed it between two microscope slides and sealed them with epoxy to avoid evaporation during the experiment. Before starting the optical experiments, we kept the mixture at a temperature below the melting temperature for a long time to guarantee the formation of the network. The scanning transmission electron microscope image in Fig. 3.20(a) shows this network of nanoparticles. We found the size of the nanoparticles to be 22.3 ± 4.6 nm using this electron microscopy image. Based on Haiss et al. [99] and the UV-Vis measurements, the concentration of the nanoparticles was found to be 0.81 nM.

In our first test, we measured the transmittance of a broadband white light through the sample while illuminating the sample with a green laser at an oblique angle as shown in Fig. 3.20(b). Our results in Fig. 3.20(c) show that the transmittance first decreases up to 60 min and subsequently increases upon continuous laser illumination. At 80 min of laser exposure, the transmittance reaches its maximum and afterward, we do not observe a significant variation in the transmittance levels. To make a better comparison, we analyzed the change in the intensity of the transmitted light by applying Eq. (3.2), where T(t,λ) stands for the measured transmittance as a function of the laser illumination duration (t) and the wavelength (λ),

$$\%\Delta T(t,\lambda) = 100 \times \frac{T(t,\lambda) - T(0,\lambda)}{T(0,\lambda)} \qquad \textbf{Eq. (3.2)}$$

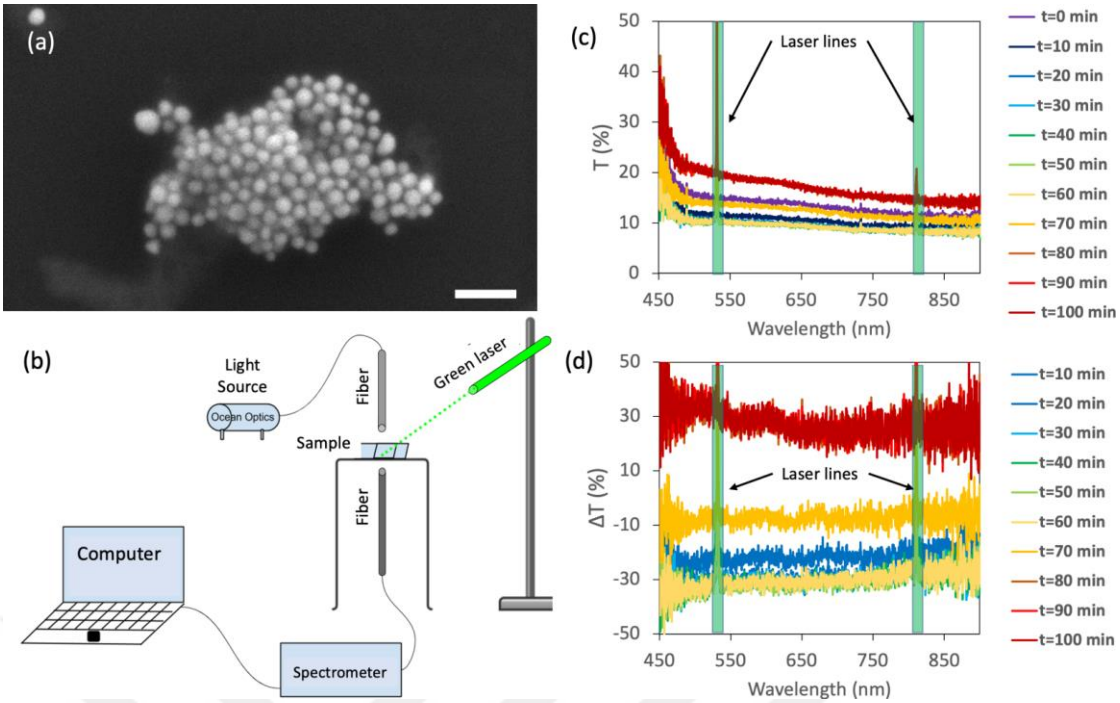

Figure 3. 20: (a) Scanning transmission electron microscope image of the network of gold nanoparticles functionalized with complementary single-stranded DNAs. Scale bar: 100 nm. (b) Illustration of the transmittance measurement setup. (c) Transmittance (T) spectra of the DNA-self-assembled network of gold nanoparticles as a function of laser irradiation duration (t). (d) Change in the transmittance (ΔT) of the self-assembled nanoparticle network as a function of laser irradiation duration with respect to the transmittance of the sample before the laser exposure.

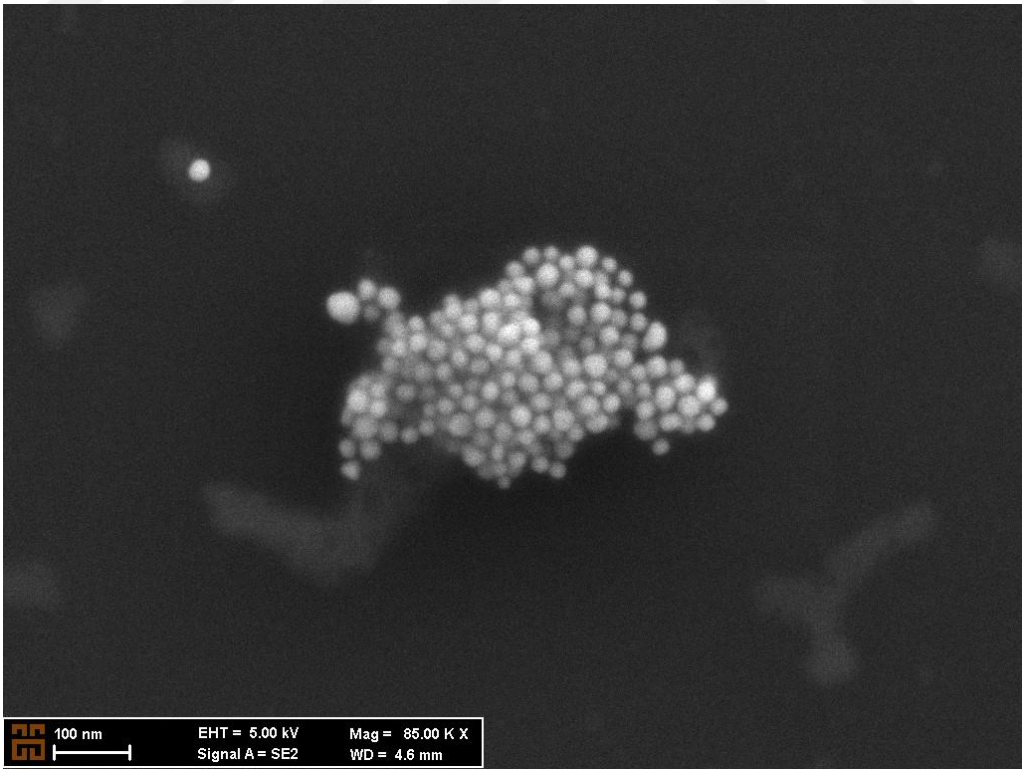

Figure 3.20 (a): Scanning transmission electron microscope image of the network of gold nanoparticles functionalized with complementary single-stranded DNAs

The transmittance data processed according to Eq. (3.2) are presented in Fig. 3.20(d). This analysis shows that the transmittance of the sample decreases within the first 60 min to about 65% of the initial transmittance value ($\Delta T \approx -35\%$). After 60 min, the transmittance starts to increase again at all the wavelengths of interest. After 70 min, the transmittance increases beyond its initial level, and at 80 min, it takes values ~30% higher than the level at $t = 0$ ($\Delta T \approx 30\%$) and remains unchanged until the end of the experiment. The decrease in transmittance within the first hour of laser exposure may be due to the large light-scattering clusters temporarily covering a larger area due to unbinding from larger features. Eventually, these large clusters disassociate into smaller clusters causing decreased scattering at longer laser exposures. Another point worth mentioning is that the variations in the transmittance occur over the whole spectral region of interest without distinct wavelength dependence except a slightly stronger increase in transmittance in the blue region.

At this stage of our study, we designed a control experiment using a single type of DNA-functionalized gold nanoparticles. The aim of this experiment was to understand whether the observed increase in the transmission occurs due to the structural changes in the material network or another unpredicted effect related to our experimental setup and gold nanoparticles. In our experiment, we placed these nanoparticles between microscope slides without hybridizing them with the nanoparticles functionalized with complementary DNAs. The measurements presented in Fig. 3.21 do not show any obvious changes in the transmission levels regardless of the time of laser exposure when the sample is illuminated with a green laser. This shows that the observed changes in Figs. 3.20(c) and 3.20(d) are directly related to the changes in the structure of the network.

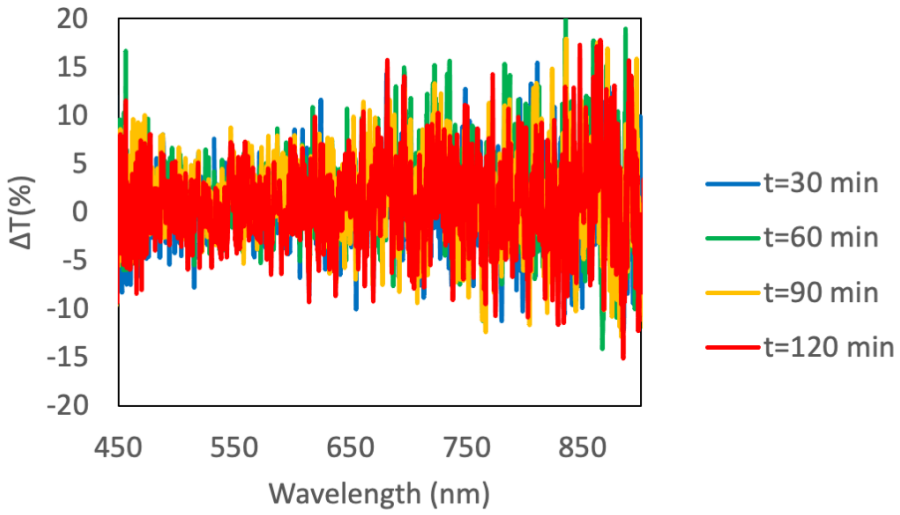

Figure 3. 21: Change in the transmittance (ΔT) of the gold nanoparticles functionalized with a single-type of single-stranded DNAs as a function of laser irradiation duration with respect to the transmittance of the sample before the laser exposure.

To gain further understanding on the process, we measured the melting temperature of the DNA-functionalized nanoparticle mixture to be 51 °C (Fig. 3.22). Using an infrared temperature, upon laser exposure for 2 h, we did not observe any increase beyond 32 °C in the temperature of the solution containing the nanoparticle mixture. The temperature remaining below the melting temperature suggests that no bulk heating in the sample occurs due to laser exposure. On the contrary, the laser light modifies the structure of the nanoparticle network owing to the laser light locally heating up the nanoparticles and their close proximity. Whether the separation of the nanoparticles is due to the separation of the connected DNA molecules on the nanoparticles or due to the disconnection of the ssDNAs from the nanoparticles is an important question. To test this, we exposed our sample with the laser at another time while measuring the transmittance (Fig. 3.23). Due to the reorganization of the nanoparticles, we observed different absolute transmittance values than that shown in Fig. 3.20. However, the variation in the transmittance (ΔT) shows that an increase in transmittance occurs similar to Fig. 3.20 at the end of the experiment. Reproduction of the increased transmittance of the same sample shows that the binding–unbinding process of the nanoparticles is a reversible process. This suggests that laser exposure causes the separation of DNA molecules connecting the nanoparticles together rather than separating the DNA molecules from the surface of the gold nanoparticles.

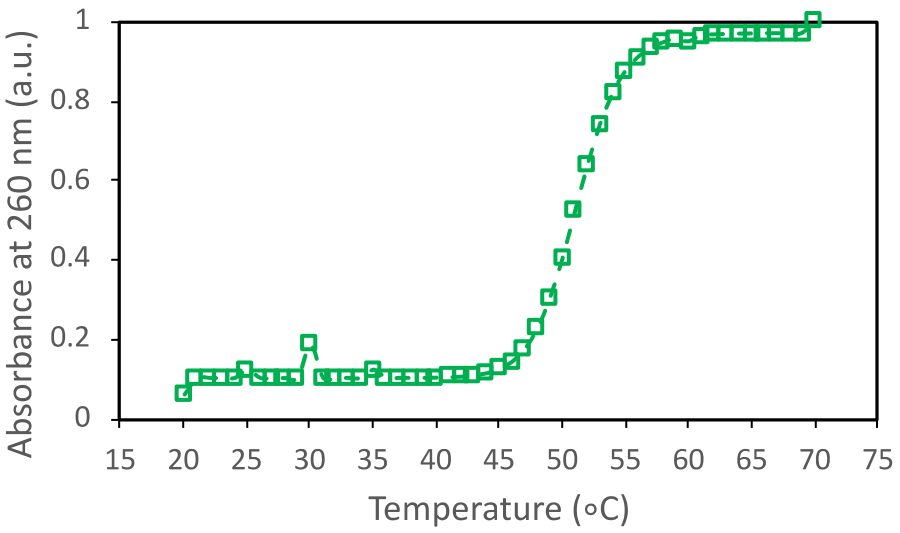

Figure 3. 22: Melting temperature measurement of complementary DNA-functionalized gold nanoparticles in phosphate buffer

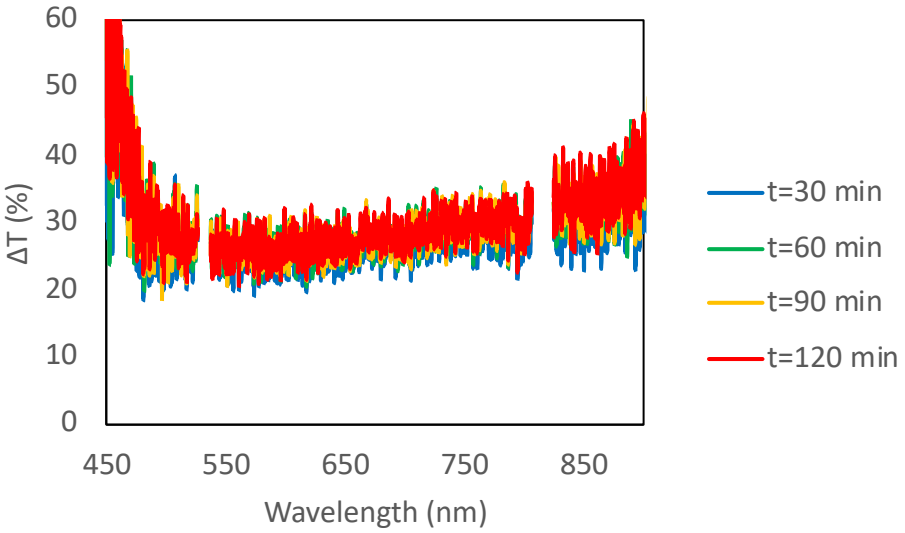

Figure 3. 23: Change in the transmittance (ΔT) of the self-assembled nanoparticle network as a function of laser irradiation duration with respect to the transmittance of the sample before the laser exposure. ΔT is calculated according to $\%\Delta T(t,\lambda) = 100 \times \frac{T(t,\lambda)-T(0,\lambda)}{T(0,\lambda)}$ **where** t **stands for the duration after the laser illumination starts and the** λ **is the wavelength.**

Despite its limitations on detecting the changes of the clusters with small sizes, the optical microscopy still provides valuable information on how the structure evolves over time upon laser irradiation (Fig. 3.24). Prior to laser irradiation, we see the broad dark regions inside the aqueous medium that indicates the clusters of gold nanoparticles. We did not observe any changes in the structures although we illuminate the nanoparticle network with white light. However, as shown in Fig. 3.24, upon laser illumination we observed the bright spots opening inside the dark features showing that the laser light

causes the nanoparticles to get separated from each other. To further evaluate whether the disassociation of the network is due to beam damage or due to unbinding of the nanoparticles owing to laser irradiation, we quickly cooled the sample at 4°C and observed the recovery of the network. The reversibility of the network shows that the laser beam does not cause damage on the nanoparticle surface but locally heats the nanoparticle surroundings leading to unbinding of the nanoparticles.

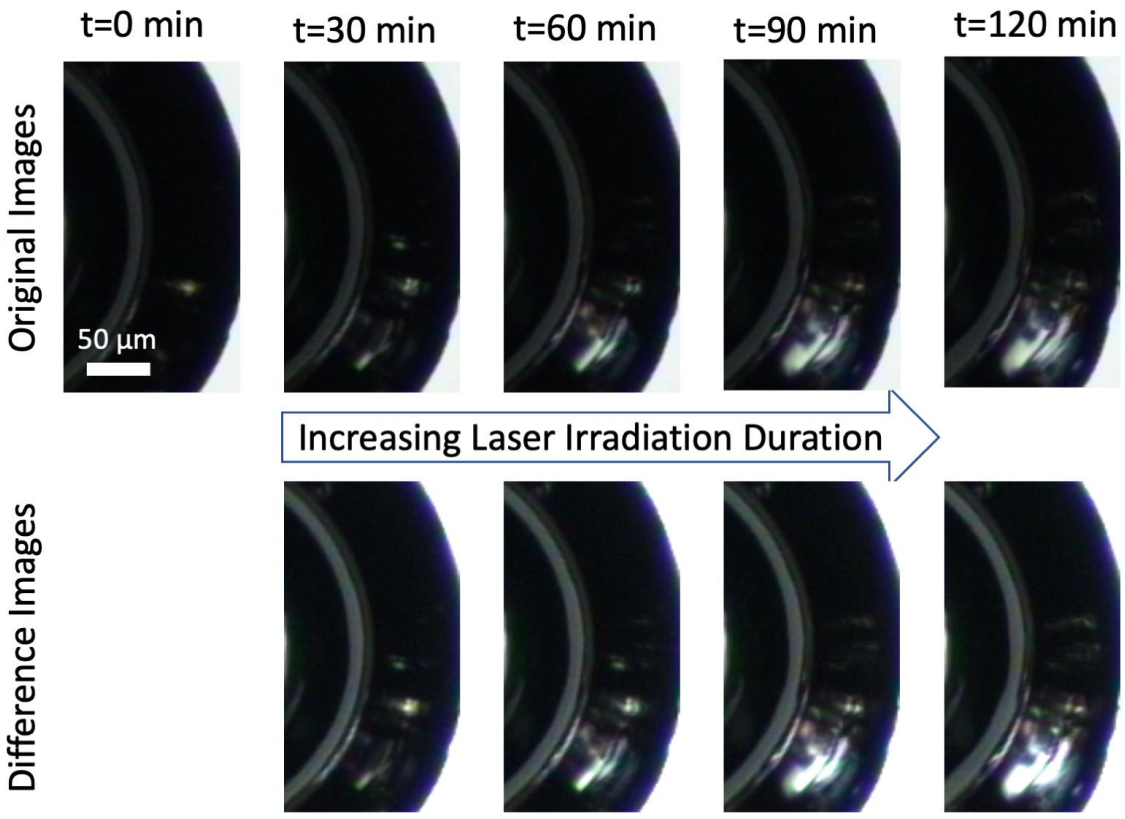

Figure 3. 24: Optical microscopy images of a cluster of nanoparticles functionalized with complementary DNAs. As the sample is exposed to green laser light, the cluster of nanoparticles is observed to disassociate. When the sample is cooled again at 4 °C (the right most image), we observe the disassociated region recovers indicating the reversibility of the process

To retrieve a quantitative information out of the microscope images, we calculated the area covered by the white areas on the microscope images that correspond to the areas not covered by the nanoparticle network. As shown in Fig. 3.25(a), we observe that the white areas on the image cover ~40% larger area at the end of the test compared to the initial white areas indicating that the nanoparticle network dissolves as a response to laser illumination. To compare this behavior with transmission measurements, we first integrated the transmittance presented in Fig. 3.20(c) over the whole spectrum and plotted the integrated transmittance variation relative to the integrated transmission before the

laser illumination starts [Fig. 3.25(b)]. This graph shows a qualitatively similar trend to Fig. 3.25(a), both of which indicate increased transmission owing to the disassociation of the nanoparticle network.

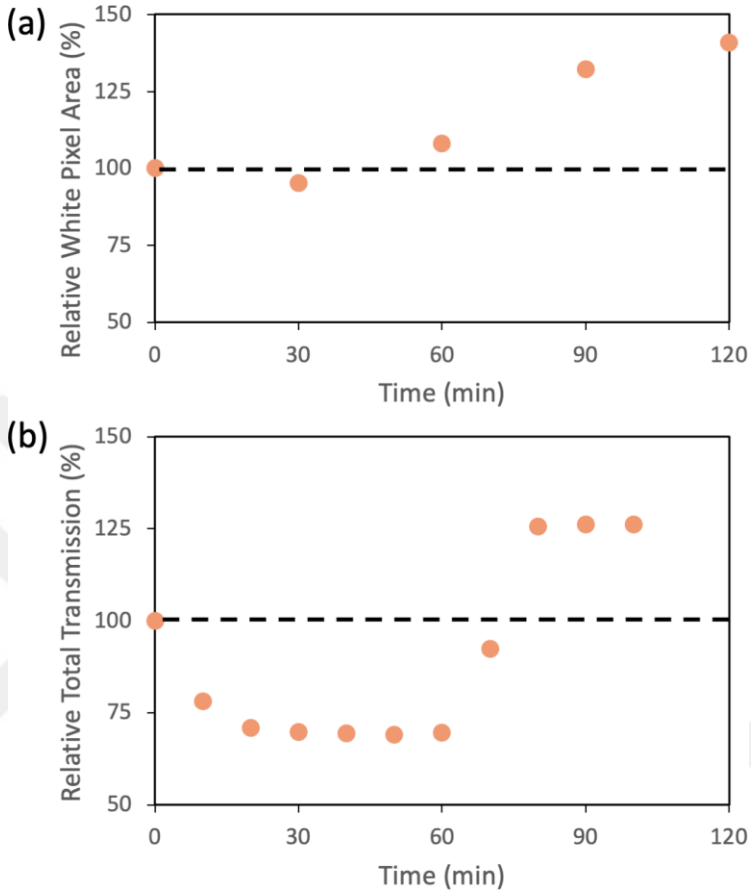

Figure 3. 25: Time evolution of the disassociation of the self-assembled nanoparticle networks as calculated using optical microscopy and transmission spectroscopy. (a) Relative change of the area covered by white pixels on the microscope images corresponding to the areas not covered by the large nanoparticle clusters blocking the light as calculated using the optical microscopy images in Fig. 3.16. The relative white areas at different time points are calculated with respect to the number of white pixels at t = 0. (b) The time-evolution of the relative area under the transmittance spectrum as a function of laser irradiation duration. The calculation is made using the transmittance information presented in Fig. 3.12 by calculating the area under the spectrum between 450 and 900 nm. The data at different time points are normalized in accordance with the integrated transmittance at t = 0.

3.4. Light-Controlled Self-Assembly of QDs on Glass Surface

An important target of our thesis has been the control of DNA-driven self-assembly of colloidal nanoparticles. We selected QDs as the candidate material since they act as the active medium of opto-electronic device. Owing to the local heating, we aimed tailoring the self-assembly with laser light. For this purpose, QD-ssDNA conjugates were dropped over the DNA-functionalized glass substrate possessing complementary bases to

the ones on the QD surface, and a specific area of the substrate was illuminated with a green laser emitting at 532 nm. Here, the QD-ssDNA conjugates can absorb the laser light as the absorption spectrum of the QDs indicates (Figure 3.10). During the laser irradiation, QD-ssDNA conjugates were added onto the NH_2-ssDNA-functionalized glass substrate.

The fluorescence microscopy image presented in Figure 3.26 clearly shows that the area of the substrate under the laser irradiation remained uncoated and appears as a dark spot while the QDs uniformly coated the not-illuminated area of the glass substrate. This obtained structure is even visible to the naked eye when the film is illuminated with a UV light (Figure 3.26(B)). As the fluorescence microscopy images also reveal, obtained feature extends to several 100s of micrometers (Figure 3.26(C)).

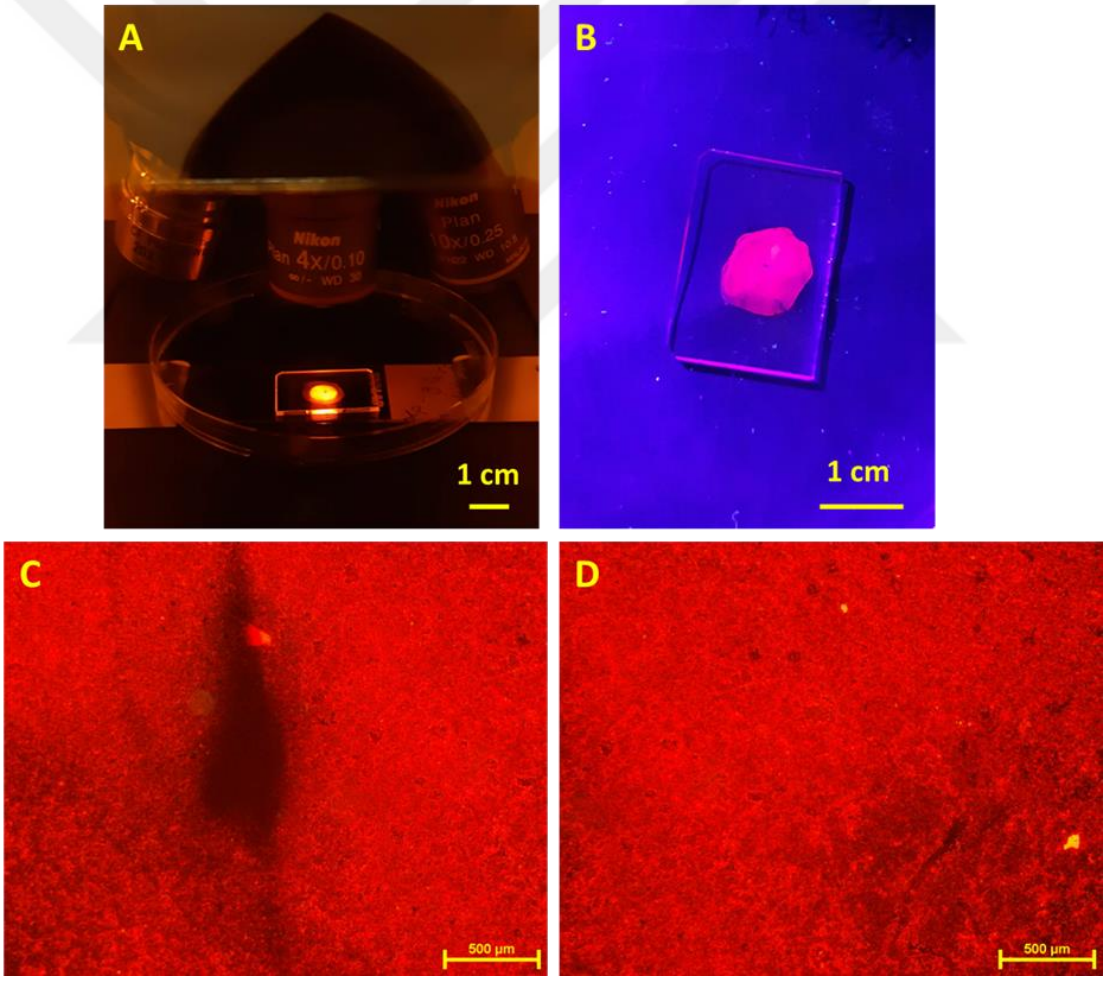

Figure 3. 26: (A) Photograph of the QD film during the fluorescence microscopy imaging using green light. (B) Photograph of the film taken under the excitation of UV light. This film was formed after applying green laser irradiation for 4 h on to the DNA-functionalized QDs. Obtained feature where the QDs are not coated are clearly visible in this photograph. (C) Fluorescence microscopy image of the same film taken from the centre of the illuminated area. (D) Fluorescence microscopy image of the same film taken from a region outside of the illuminated area.

It is possible that under prolonged laser irradiation, the QDs may experience photobleaching which may have caused the dark spots on the microscopy images. To reveal whether photobleaching was effective or not, we added the same DNA-functionalized red-emitting QDs onto the glass substrate functionalized with complementary DNAs. This time, we let the film dry prior to laser irradiation. After the film completely dried, we exposed the film to the green laser for 4 h. As shown in Figure 3.27, the QDs in the irradiated region were still as luminescent as the QDs in the region that was not irradiated with the laser light, ruling out the possibility of photobleaching as the cause of the dark spot formation. These results show that light irradiation can be used as an external tool to tailor binding and unbinding process between the DNA molecules attached to the QDs and the ones to the glass substrate.

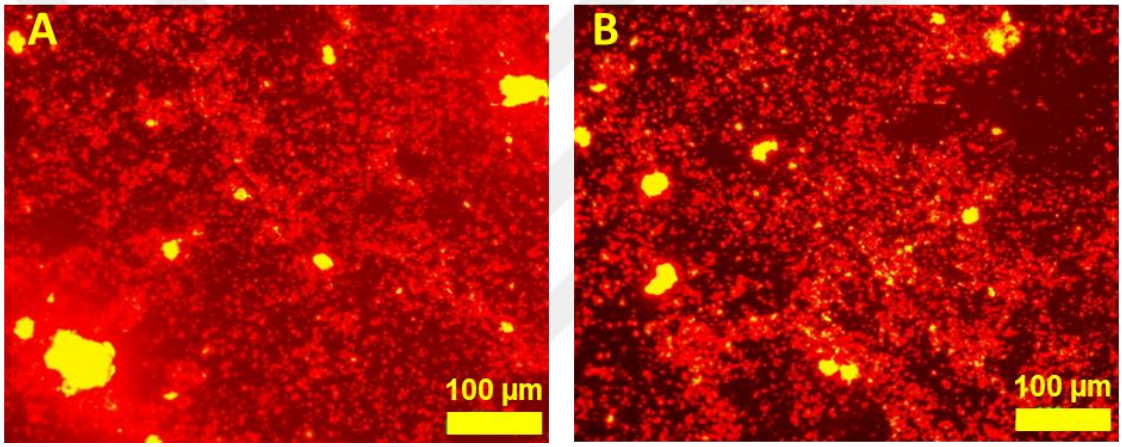

Figure 3. 27: Fluorescence microscopy image of DNA-functionalized glass surface coated with DNA-functionalized red-emitting QDs. The film was left to dry first and then exposed to green laser irradiation for 4 hours. (A) shows the fluorescence microscopy image taken from the irradiated area and (B) was taken from the nonirradiated area.

To analyse the effect of laser exposure time, we illuminated the DNA-functionalized glass with QD-ssDNA solution for 1, 2, 3, and 4 h. The laser exposure for 1 and 2 h was insufficient to produce a local heating effect, consequently there was no remarkable difference between the laser exposed and the unexposed area on the glass substrate (Figure 3.28-3.30). After 3 h laser irradiation, we observed a remarkable difference between the laser irradiated area (dark spot, Figure 3.31) and the non-irradiated region (red fluorescence area, Figure 3.31). Also Figure 3.26 shows the precise impact of laser irradiation after 4 h of exposure time. The laser used for the experiments had the power of 20 mW with an illumination area of 0.35 cm^2, so the effect of laser light on the self-

assembly could only be perceived after three hours when the area under illumination was exposed to laser light with an energy density of 617 J/cm^2.

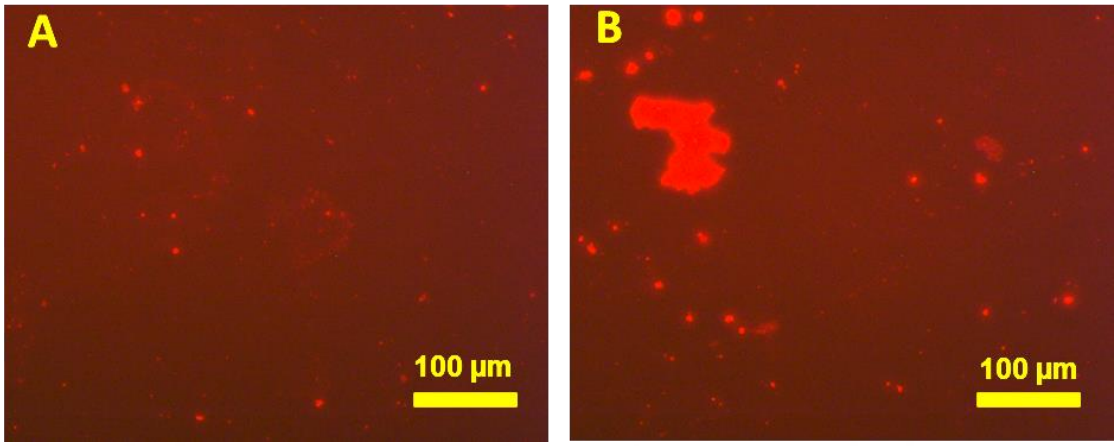

Figure 3. 28: Fluorescence microscopy image of DNA-functionalized glass surface and DNA functionalized QD after laser irradiation for 1 hour. (A) irradiated area and (B) nonirradiated area.

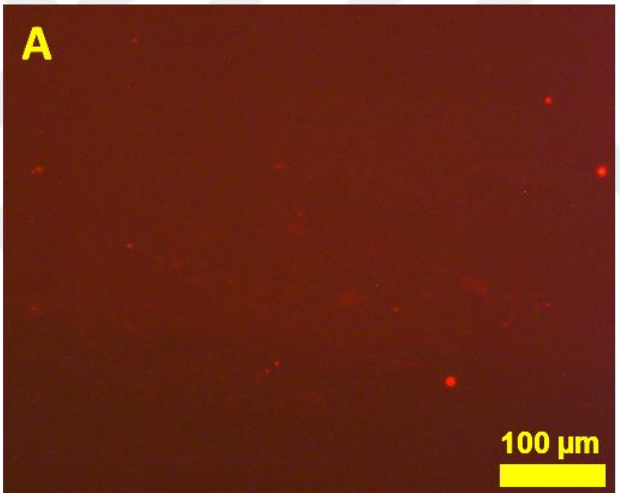

Figure 3. 29: Fluorescence microscopy image of DNA-functionalized glass surface and DNA functionalized QD after laser irradiation for 2 hours, irradiated area.

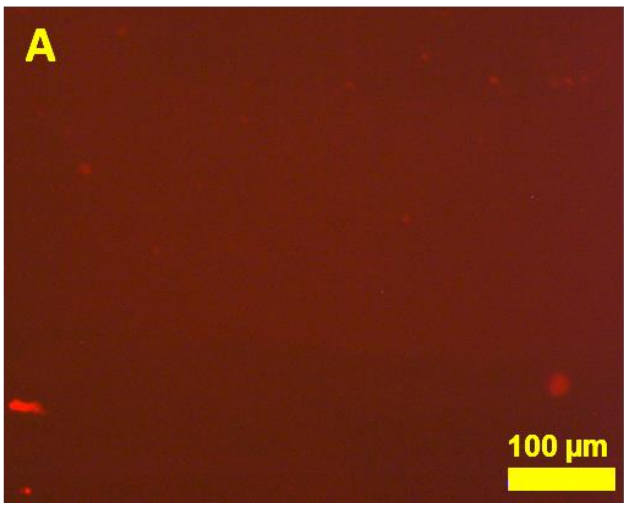

Figure 3. 30: Fluorescence microscopy image of DNA-functionalized glass surface and DNA functionalized QD after laser irradiation for 2 hours, nonirradiated area.

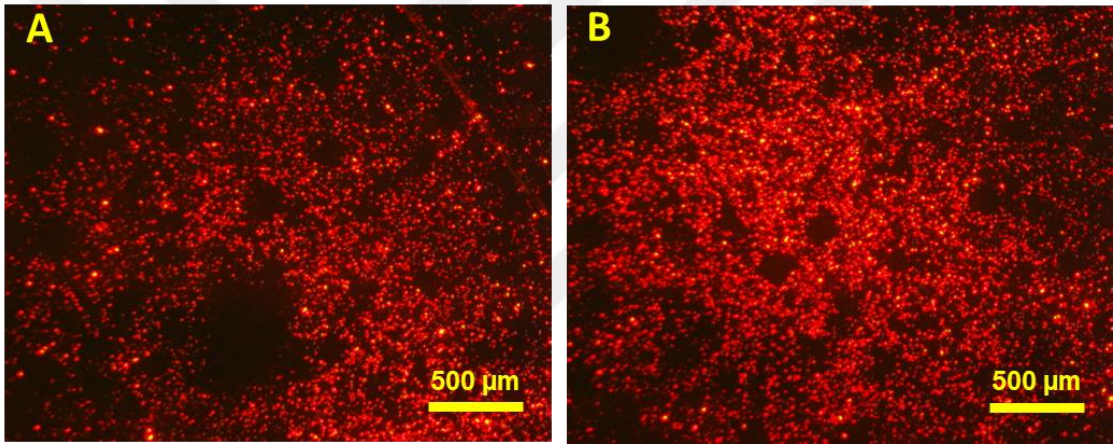

Figure 3. 31: Fluorescence microscope image of DNA-functionalized glass surface and DNA functionalized QD after laser irradiation for 3 hours. (A) irradiated area and (B) nonirradiated area.

The above concept of local heating via laser irradiation was applied to silica NPs possessing complimentary DNAs to ensure laser irradiation is responsible for the uncoating or dark spot. For this purpose, we coated the surface of a DNA-functionalized glass surface with DNA-functionalized silica NPs. As presented in the Methods Section, the DNAs on the glass surface and silica NP surface are complementary to each other. To test the effect of the laser light, we irradiated a portion of the surface during coating. Once the coating is done, we washed the surface, turned-off the laser irradiation, and then took optical microscopy images. As the silica NPs are not fluorescent, this time we analysed the coating using a bright-field optical microscopy in transmission mode. Since the silica NPs do not absorb the light at the laser irradiation wavelength (λ=532 nm), the light exposure was not expected to affect the nanoparticle coating on the glass surface. After four hours of laser irradiation, no difference was observed on the substrate (Figure 3.32).

These results support our hypothesis that the local heating of the QDs by the laser irradiation is responsible for controlling the self-assembly process.

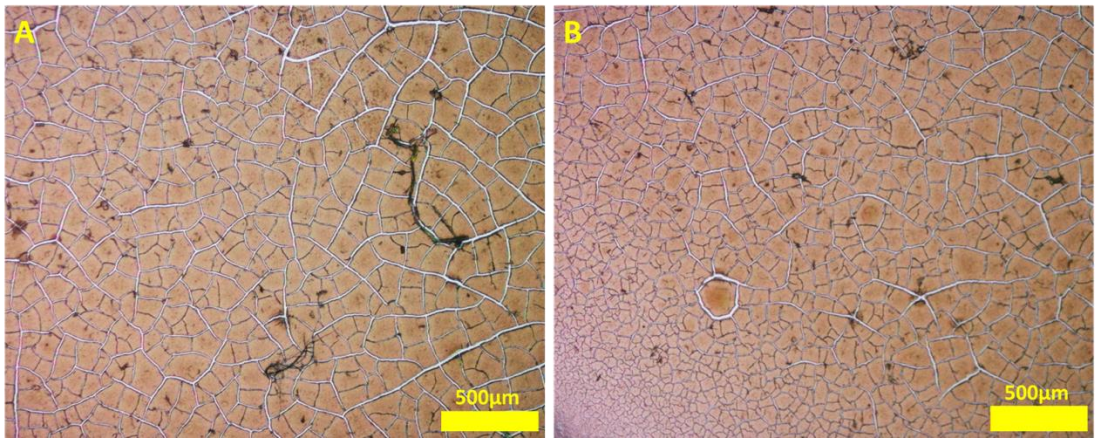

Figure 3. 32: Optical microscopy images of DNA-functionalized silica NP coated glass surface. During the coating process, the sample was irradiated for 4 hours. (A) was taken from the central region of the illuminated area whereas (B) was taken from a region outside of the illuminated area.

A similar, supporting control experiment was conducted using a red laser (λ=632 nm, 4.1 mW/cm^2) to test the effect of laser wavelength on the binding-unbinding process of QD-ssDNA on glass surface. Due to difference of intensities with the green laser, we exposed the surface to red laser for 42 h to achieve the same threshold energy density with the green laser (617 J/cm^2). At the end of the experiment, we observed that the QDs are coated without any major difference between irradiated and not irradiated areas (Figure 3.33). We attribute this difference to the fact that the DNA-functionalized QDs cannot absorb the light irradiated by a red laser. As a result, local heating of the QDs do not occur leading to the ineffectiveness of the red laser irradiation on coating. These results support our hypotheses that the coating of the DNA-functionalized QDs can be controlled by using a light source that the QDs can absorb enabling local heating.

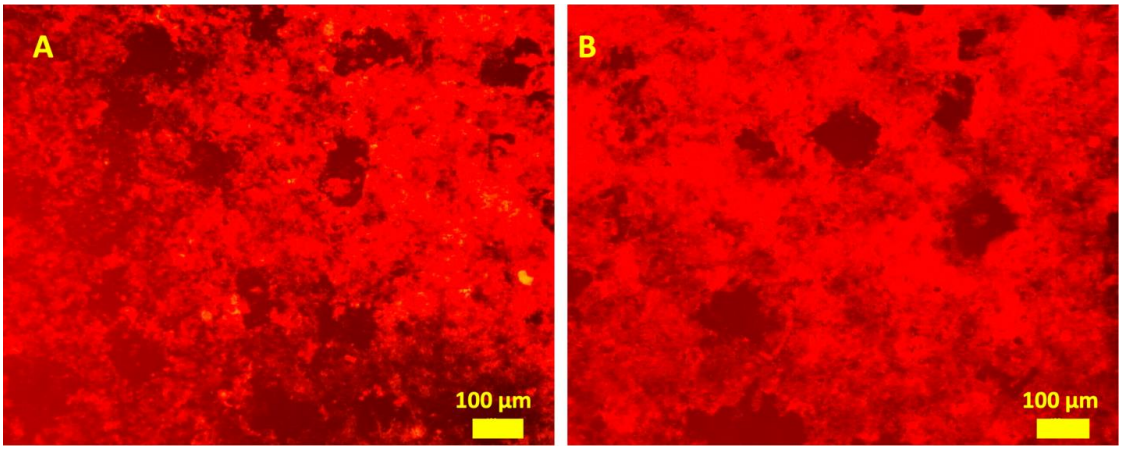

Figure 3. 33: Fluorescence microscopy images of the film where the DNA-functionalized QDs were added to DNA-functionalized glass possessing complementary bases while irradiating the sample with a red laser for 42 h. (A) shows the irradiated area and (B) shows not irradiated area on the same sample.

To demonstrate the capability of our method to self-assemble materials hierarchically, we dropped green-emitting QD-ssDNAs (Figure 3.35) and Cy3-ssDNAs (Figure 3.34) on the red-emitting QD-coated glass substrate that had already been structured with the laser light. Over time, the previously uncoated areas (dark spots) on the glass substrate were successfully coated with green-emitting QDs and Cy3-ssDNAs. These results prove that our proposed method can be utilized for designing complex architectures involving multiple DNA-functionalized materials.

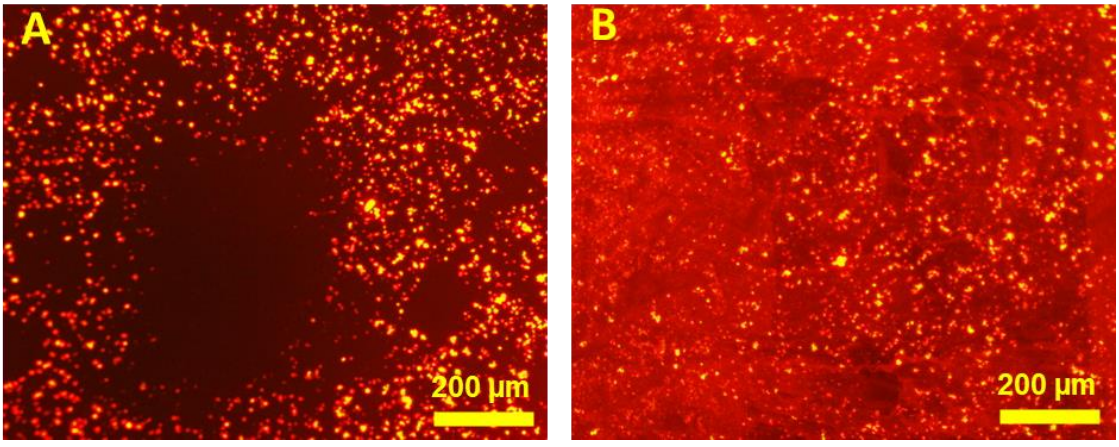

Figure 3. 34: Fluorescence microscopy images of (A) ssDNA-functionalized glass substrate and red-emitting QD-ssDNA with complementary bases after 3 hours laser treatment showing a dark spot and (B) after adding Cy-3 ssDNA on to the dark spot in(A).

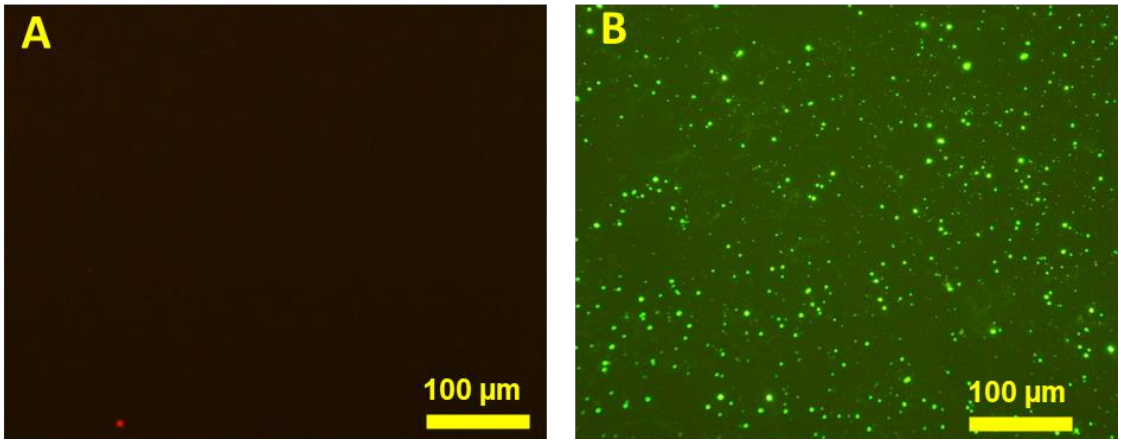

Figure 3. 35: Fluorescence microscopy image of DNA-functionalized glass surface and DNA functionalized red-emitting QD after focused blue laser irradiation for 4 hours under green-fluorescent light. Centre of the irradiated area (A) before and (B) after adding DNA functionalized green-emitting QDs.

3.5. Conductive Films Made of Self-Assembled AgNWs

For achieving fully self-assembled devices, obtaining patterned conductive surfaces is essential. In this thesis, we aimed to address this need by studying electrostatic self-assembly of AgNws.

Here we employed MPA-coated AgNWs. The average zeta potential of these NWs became around -20 mV which confirms the presence of carboxyl groups (–COOH) on the surface [11]. These results indicate a clear shift towards negative direction owing to COO^- ions on the surface of the NWs (Figure 3.36).

Results

		Mean (mV)	Area (%)	St Dev (mV)
Zeta Potential (mV):	-20,7	**Peak 1:** -22,0	92,3	6,56
Zeta Deviation (mV):	8,16	**Peak 2:** -1,97	7,7	3,35
Conductivity (mS/cm):	0,0161	**Peak 3:** 0,00	0,0	0,00
Result quality	Good			

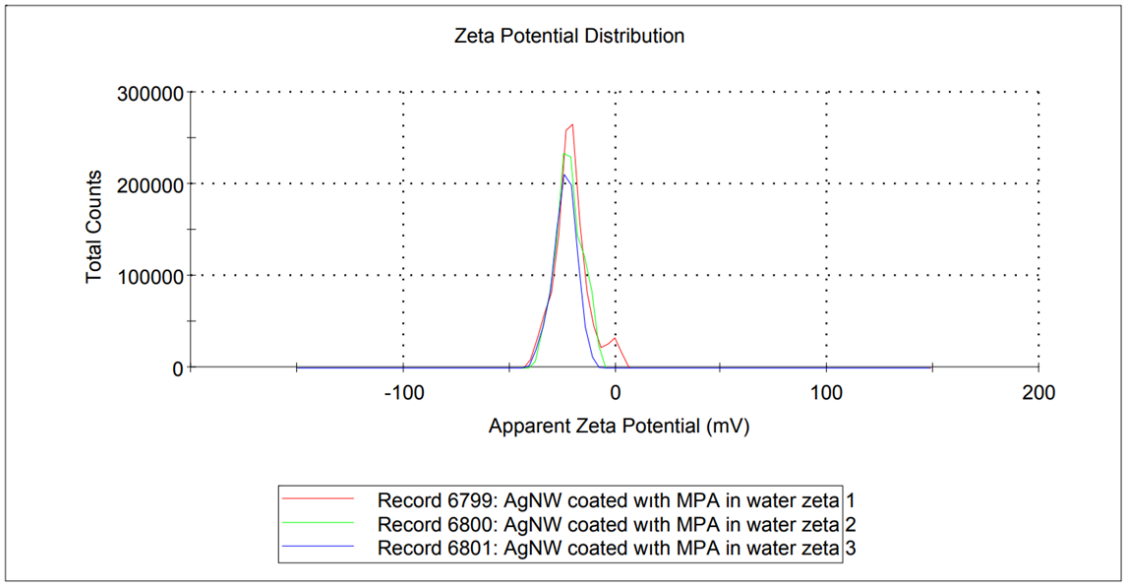

Figure 3. 36: Zeta potential of AgNW coated with MPA

As described in the Methods Chapter, we self-assembled AgNWs using charge-assisted coating method. We first coated a single layer of AgNWs by dipcoating the glass substrate for 5 min.

Optical microscopy image of the formed structure indicates that individual nanowires are scattered on the glass surface rather than forming a continuous film (Figure 3.37).

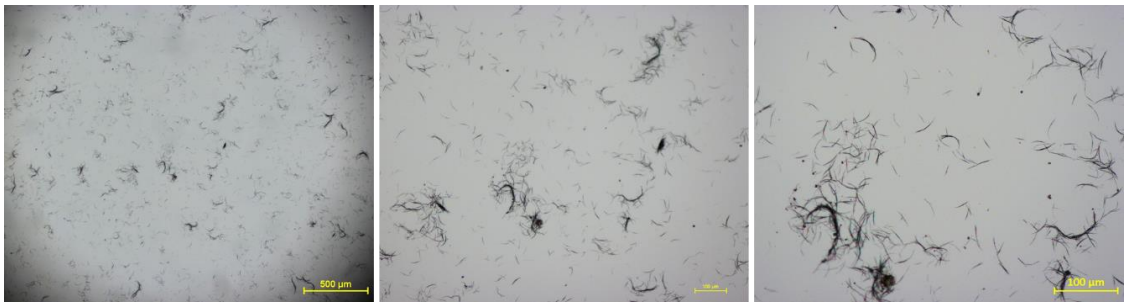

Figure 3. 37: Optical Microscopy Images of AgNWs coated glass, without laser light application

Next, we applied laser irradiation (λ=450 nm) for 10 min during the coating process (Figure 3.38).

We see that the laser irradiation did not significantly alter the NW coating on the glass.

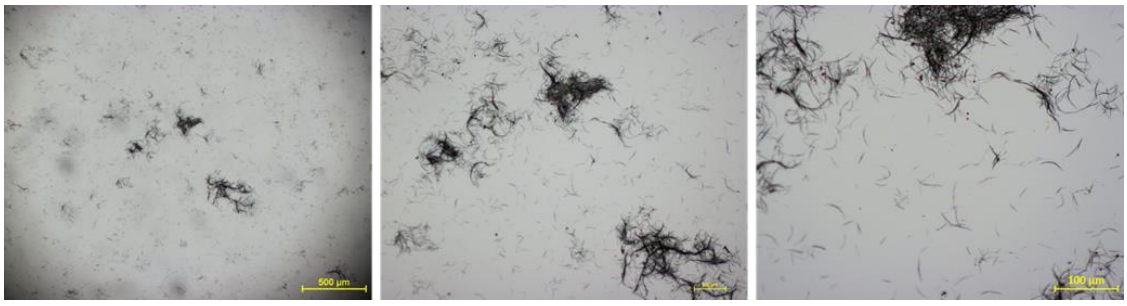

Figure 3. 38: Optical Microscopy Images of AgNWs coated glass, after application of blue laser light for 10 min

To find a remedy, we decided to increase the coating duration to 30 min, while keeping the laser irradiation on. Results presented in Figure 3.39 indicate that increasing the duration does not cause a significant difference (Figure 3.39).

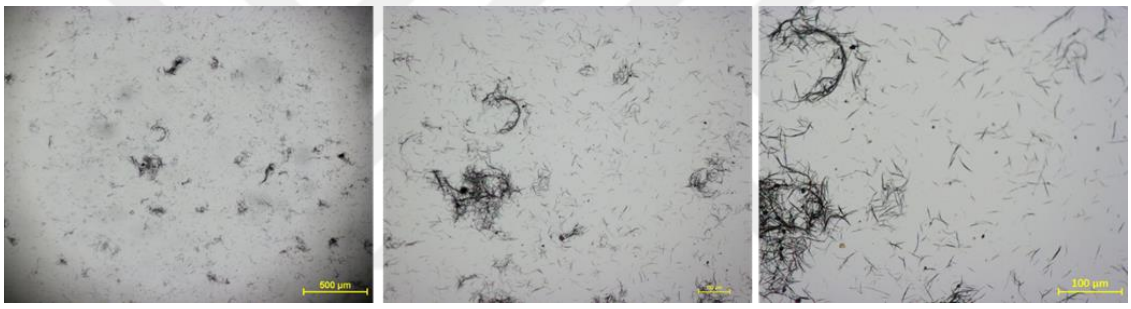

Figure 3. 39: Optical Microscopy Images of AgNWs coated glass, after application of focused blue laser light for 30 min

At this point, we decided to focus our attention first to form a continuous AgNW film. Therefore, we increased the AgNW concentration by three times and also increased the coating duration to 1.5 h. Result shown in Figure 3.40 indicates a better coating; however, the obtained film is still not a continuous one.

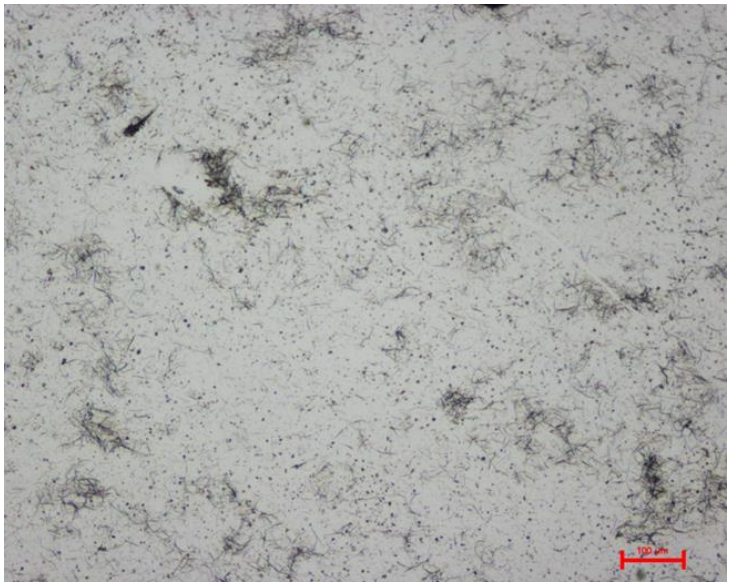

Figure 3. 40: Optical Microscopy Images of single layer AgNWs coated glass when the concentration is increased by three times and 1.5 hours waited inside AgNWs solution during stirring

Next, we increased the AgNW coating cycle from one to two, and we kept the film within a heated solution at ~100°C for 5 min. We realize that this approach improved the continuity of film significantly Figure 3.41. increasing the number of coatings to three further improved the coating quality Figure 3.42.

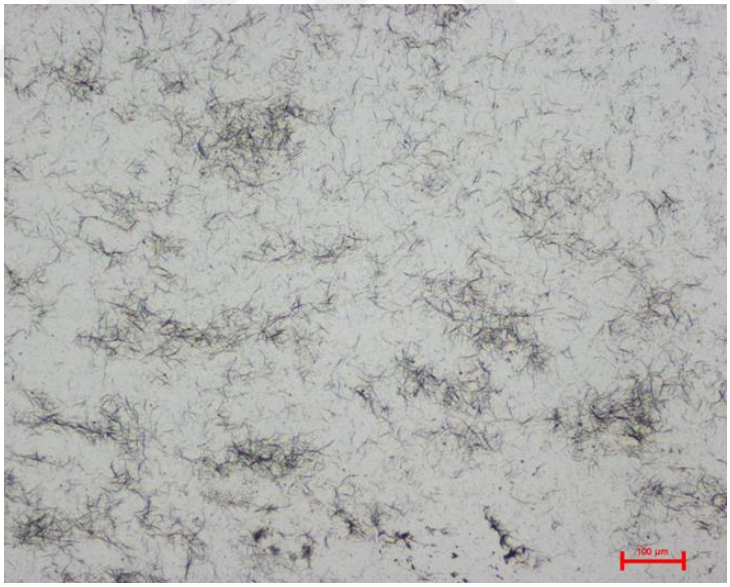

Figure 3. 41: Optical Microscopy Images of two-layer AgNWs coated glass when the concentration is increased by three times, waited inside heated solution of AgNWs for 5 min at 100°C by stirring

AgNWs solution concentration is increased three times more according to the procedure. Glass surface coated with three layers by dipped in AgNWs solution for each layer, 5 min waited stirred by magnetic stirrer after each layer of AgNW coating, surface heated at 100°C for 5 min.

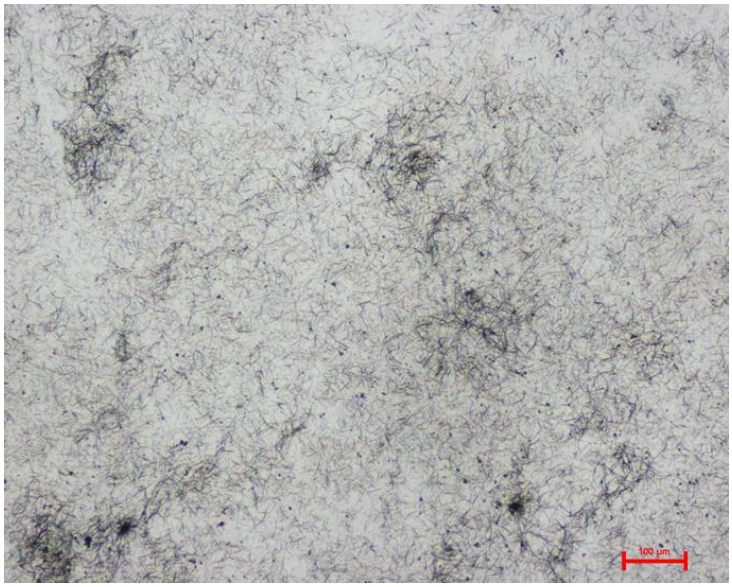

Figure 3. 42: Optical Microscopy Images of three-layer AgNWs coated glass when the concentration is increased by three times, waited inside AgNWs solution by stirring. After each coated AgNWs layers, surface heated at 100°C during 5 min.

AgNWs solution concentration is increased three times more according to the procedure. Glass surface coated with seven layers by dipping it into AgNWs solution for each layer, 5 min waited when stirring by magnetic stirrer after each layer of AgNW coating, surface heated at 100°C for 5 min. When each layer of AgNW coating process green/blue laser light applied. According to microscope images results, when we compare the Figure 3.43 and 3.44 (A-C) and (B-D), laser irradiated area seems less coated with AgNWs than nonirradiated area.

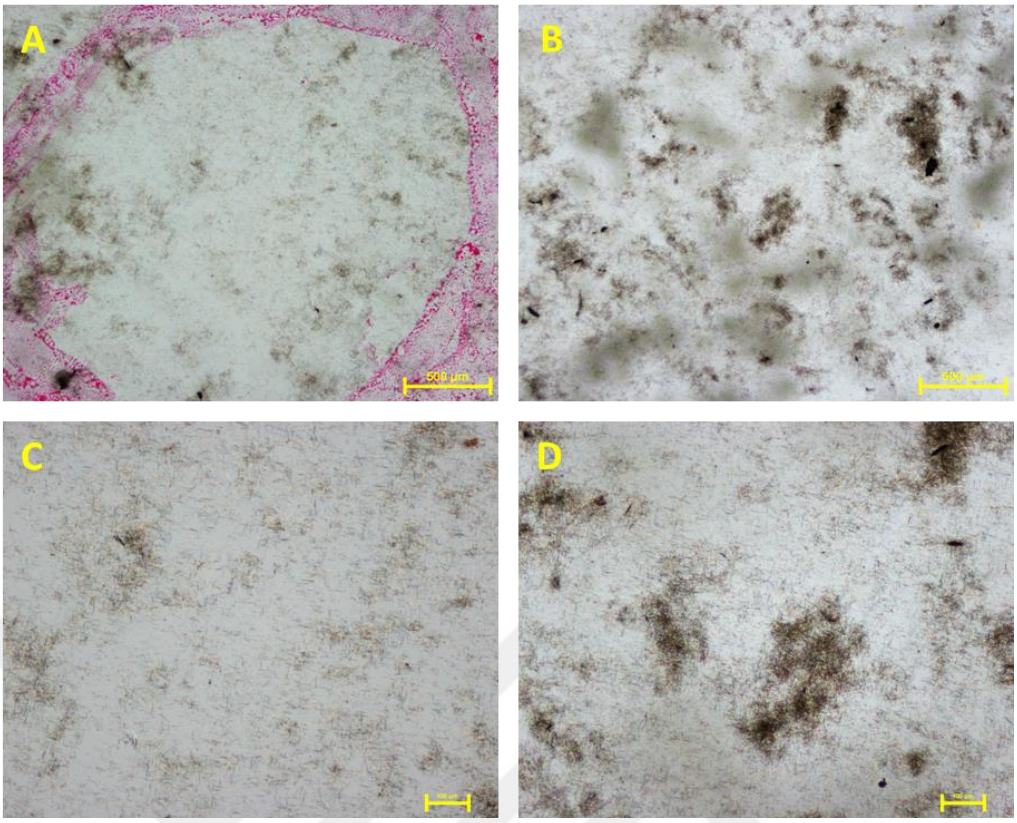

Figure 3. 43: Microscope image of complementary DNA-functionalized glass surface and AgNWs after laser irradiation. (A-C) irradiated area and (B-D) nonirradiated area with green laser.

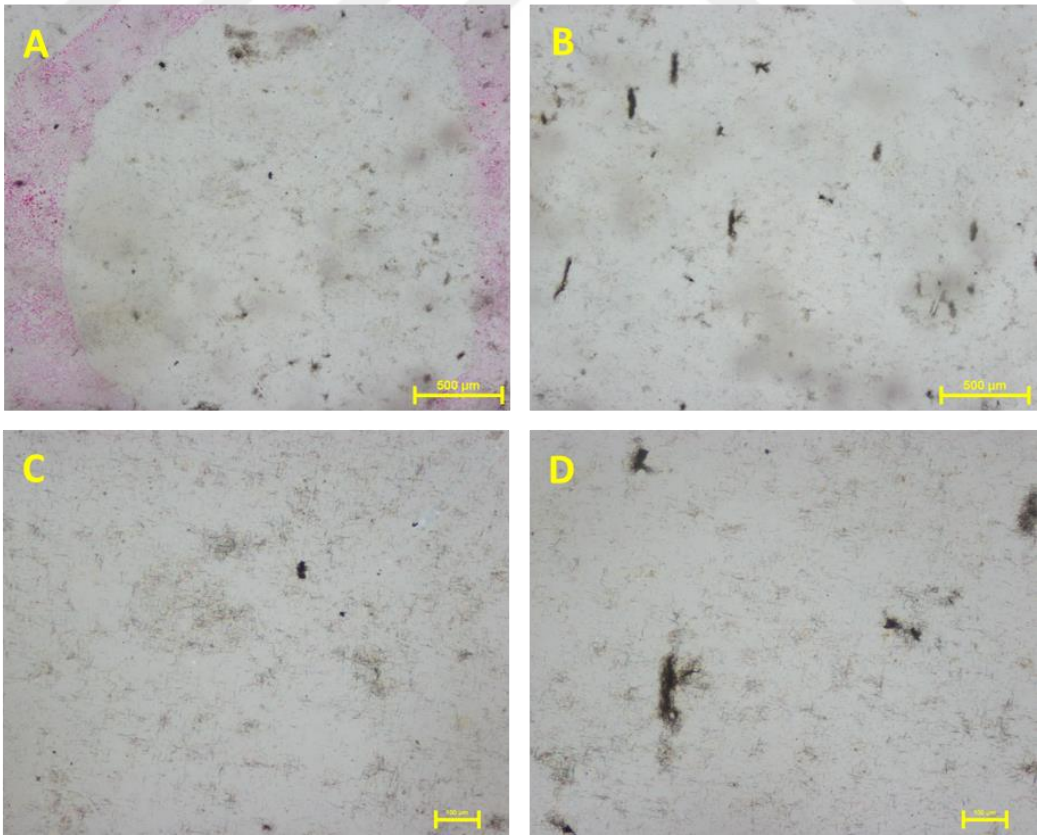

Figure 3. 44: Microscope image of complementary DNA-functionalized glass surface and AgNWs after laser irradiation for. (A-C) irradiated area and (B-D) nonirradiated area with blue laser.

Once we achieved acceptable levels of continuous film formation using AgNWs, we are ready to analyze the relation of AgNWs and sheet resistance. We started our tests with single layer AgNWs. In this sample the coating duration was 5 min. Sheet resistance measurements taken from six different locations on the glass substrate show an average sheet resistance of infinity Ω with a standard deviation of ~ 0 Ω. Then, we increased the duration of the glass staying inside the AgNWs solution to 1.5 hours. The average sheet resistance became infinity Ω with a standard deviation of ~ 0 Ω. After that we increased the number of coatings AgNWs to three layers while keeping the substrate in AgNWs for 5 min. The average sheet resistance became infinity Ω ($\pm$0 Ω). Later at the same time, we increased the concentration of AgNWs solution to double and number of coatings AgNWs to seven layers while keeping the substrate in the AgNWs solution for 5 min. The resulting sheet resistance became infinity Ω ($\pm$0 Ω). Finally, we increased the concentration of AgNWs solution three times and by keeping the glass in the AgNWs solution for 1.5 hours. The resulting sheet resistance was infinity Ω.

We observed first but very less conductivity for the sample coated by increased the concentration of AgNWs solution to (74.8 mg/ml) and increased number of coatings to three layers, by keeping the glass in the AgNWs solution for 5 min, for each cycle. Sheet resistance of coated glass sample was measured as 114kΩ ($\pm$55 kΩ).

To achieve a better conductivity, we increased the concentration of AgNWs solution to (112.2 mg/ml) and increased number of coatings to two layers by keeping the glass in AgNW solution having a temperature of 100°C. For each layer, the coating duration was 5 min. The measured sheet resistance became on average 31.6 MΩ with a standard deviation of ~77.5 MΩ.

Then, we observed another conductivity behaviour for the sample coated by increased the concentration of AgNWs solution to third times more (112.2 mg/ml) and increased number of coatings AgNWs to three layers for each layer waited inside the AgNWs solution for 5 min, stirred by magnetic stirrer. After each layer of AgNW coating, surface heated at 100°C for 5 min. The measured sheet resistance became on average 413.1 kΩ with a standard deviation of ~833.21 kΩ. Sheet resistance of coated glass sample measured to understand conductivity by four-probe.

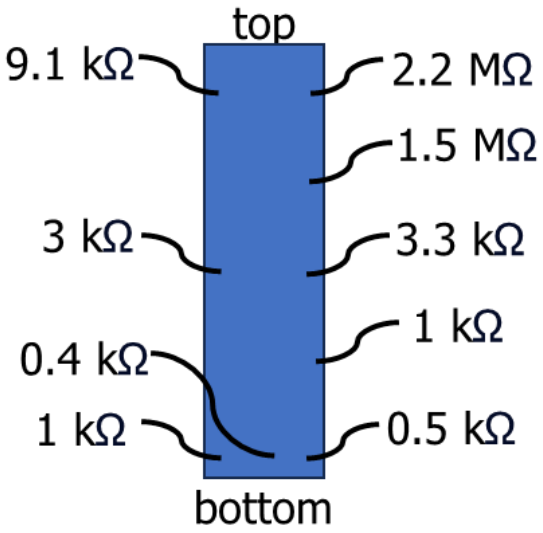

Figure 3. 45: Illustration of measured sheet resistance of three layers AgNWs coated glass / when the concentration is increased by three times, heated AgNWs solution at 100°C

We studied the development of conductive films whose morphology can be controlled externally via laser irradiation. While we have obtained some promising results concerning conductivity, further experimentation is necessary to fully understand and enhance the control over AgNWs deposition on surfaces.

Chapter 4

Conclusions and Future Prospects

4.1 Conclusions

This thesis elucidates the multifaceted capabilities of laser irradiation in arranging the assembly dynamics of DNA-functionalized nanoparticles (NPs) and quantum dots (QDs). In this study, we explore the utilization of laser irradiation to regulate the assembly and disassembly dynamics of DNA-functionalized nanoparticles (NPs) within a solution. Initially, we observe that the presence of complementary DNAs provides the formation of gold nanoparticle (AuNP) networks at lower temperatures, yet this network diminishes with increasing temperature of the medium. Through experimental investigation, we demonstrate that laser irradiation effectively modulate the binding and unbinding processes between DNA-functionalized AuNPs. The absorption of laser light by the nanoparticles induces localized heating, thereby causing the separation of complementary DNAs linking the colloidal particles. As a result, the network of the particles disassociates as a response to the applied light. Importantly, the reversible nature of this process underscores its reliance on localized heating rather than beam-induced nanoparticle damage. We clearly observed the structural changes on the particle clusters upon laser irradiation using optical microscopy images. Furthermore, we showed that using externally applied light the optical transmission can be tailored. Our results enable controlling the structure and the optical properties of particles that are self-assembled via DNA–DNA interactions locally, paving the way for defining the structures of the particle networks locally in three dimensions using an external effect. Our approach can also be used to externally control the near-field interactions between the DNA-functionalized nanoparticles.

Furthermore, our investigation extends to the application of laser-based self-assembly techniques to govern the coating patterns of DNA-functionalized quantum dots (QDs) on complementary DNA-functionalized substrates. Upon exposure to green laser irradiation, red-emitting QDs exhibit a propensity to avoid binding with DNA-functionalized glass

substrates, as evidenced by the emergence of dark spots under fluorescence microscopy. Notably, we ascertain that energy densities exceeding 617 J/cm^2 are required to evoke this effect. On the other hand, if the samples were irradiated with a red laser, the added QDs would not absorb the light and hence lead to a homogeneous coating on the glass substrate without any dark spot on the fluorescence microscope. Furthermore, when red-emitting QDs were replaced by dielectric particles that do not absorb the green laser light, these NPs were successfully coated onto the glass substrate. These results prove that local heating of QDs due to the absorption of light is responsible for breaking the hydrogen bonds of the DNA bases that connect two complementary DNAs on the substrate and the NPs. We anticipate that the outcomes of our investigation will underpin the development of a novel microfabrication paradigm predicated on the controlled self-assembly of nanoparticles driven by DNA interactions, offering a sustainable and cost-effective alternative to conventional micro/nano-fabrication methodologies. However, optimization efforts such as laser power, laser light's geometric distribution, pulsed vs. continuous laser use, laser pulse duration, coherent vs. incoherent sources, salt concentration, QD concentration, and temperature control of the surface during self-assembly are crucial to enhance patterns with a high resolution and broaden applicability across various domains, including electronics, optoelectronics, and photonics. Through ongoing refinement, we envision widespread adoption of our technique, empowering diverse applications requiring precise nanoparticle assembly control.

4.2 Societal Impact and Contribution to Global Sustainability

The utilization of laser irradiation-based methodologies for the precise control of nanoparticles and QDs assembly processes offers a transformative approach with significant potential for societal impact, directly contributing to several of the United Nations Sustainable Development Goals (SDGs). These techniques are particularly valuable for reducing energy consumption in manufacturing, aligning with Goal 7 (Affordable and Clean Energy) by promoting more sustainable and affordable energy sources. The energy efficiency of laser-based methods over traditional techniques highlights their importance in fostering more sustainable production processes. Furthermore, the ability to manipulate DNA-functionalized nanoparticles and QDs with laser irradiation supports Goal 9 (Industry, Innovation, and Infrastructure) by driving

technological innovation in micro and nanofabrication. This innovation is crucial for advancing industries toward more sophisticated and precise manufacturing capabilities. In addition to fostering innovation, integrating laser-based techniques into fabrication processes supports Goal 12 (Responsible Consumption and Production) by promoting resource-efficient and environmentally benign manufacturing practices. By minimizing material waste and reducing the use of hazardous chemicals, these methods offer a more responsible approach to production. Moreover, the selective detachment of QDs from DNA-functionalized substrates using laser irradiation presents a sustainable and cost-effective alternative to conventional, energy-intensive, and often environmentally harmful fabrication methods. This not only reduces the carbon footprint of manufacturing processes, supporting Goal 13 (Climate Action), but also contributes to the conservation of terrestrial ecosystems and biodiversity by minimizing waste through DNA self-assembly, compared to common microfabrication methods like lithography, aligning with Goal 15 (Life on Land). The emphasis on optimizing laser-based DNA self-assembly techniques further underscores the importance of collaboration and partnerships, aligning with Goal 17 (Partnerships for the Goals). Through these partnerships, knowledge sharing, and innovation are promoted, driving progress toward a more sustainable and equitable future. Overall, adopting laser irradiation-based methodologies for the self-assembly of nanoparticles, QDs, and surfaces fosters technological advancement and contributes to achieving multiple SDGs by promoting sustainable and responsible manufacturing practices, ultimately facilitating progress toward a more equitable and environmentally sustainable future.

4.3 Future Prospects

Looking ahead, the fusion of laser irradiation-based techniques with nanoparticle and quantum dot (QD) assembly processes holds promising future prospects for advancing various fields and addressing emerging challenges. The demonstrated capability to control the binding and unbinding dynamics of DNA-functionalized nanoparticles through laser irradiation offers avenues for tailored manipulation of particle structures at a local level, potentially revolutionizing the design and fabrication of advanced materials. By leveraging externally applied light to tailor optical transmission, this thesis approach not only enables precise control over particle structures but also opens doors to novel applications such as biosensing, microcameras, photocatalysis, phototransistors leading

to the implementation of our results in various fields including medicine, chemistry, electronics, photonics, optoelectronics, and beyond. Moreover, the investigation into laser irradiation-based self-assembly of DNA-functionalized QDs for substrate coating control lays the groundwork for developing innovative micro/ nano fabrication technologies. The potential to achieve homogeneous coatings through selective laser irradiation is promising for enhancing fabrication processes' efficiency and sustainability, offering a viable alternative to conventional methods. However, realizing these techniques' full potential requires further optimization, encompassing parameters such as laser power, distribution, pulse duration, and others. Addressing these optimization challenges is crucial for achieving sharp patterns with high resolution, thus unlocking the widespread adoption of laser-based assembly methodologies across diverse domains. Overall, the integration of laser irradiation-based techniques into nanoparticle and QD assembly processes heralds a future marked by enhanced precision, efficiency, and sustainability in materials fabrication, with far-reaching implications for technological innovation and societal advancement.

BIBLIOGRAPHY

[1] G. A. Mansoori and T. A. F. Soelaiman, 'Nanotechnology--An introduction for the standards community', *J ASTM Int*, vol. 2, no. 6, 2005, Accessed: May 14, 2024. [Online]. Available: https://www.researchgate.net/profile/G_Ali_Mansoori/publication/309901045_Nanotechnology-an_introduction_for_the_standards/links/5827cff008ae950ace6ce5f3/Nanotechnology-an-introduction-for-the-standards.pdf

[2] S. Bayda, M. Adeel, T. Tuccinardi, M. Cordani, F. Rizzolio, and A. Baeza, 'molecules The History of Nanoscience and Nanotechnology: From Chemical-Physical Applications to Nanomedicine', *Molecules*, vol. 25, p. 112, 2020, doi: 10.3390/molecules25010112.

[3] P. Iqbal, J. A. Preece, and P. M. Mendes, 'Nanotechnology: The "Top-Down" and "Bottom-Up" Approaches', *Supramol Chem*, Jan. 2012, doi: 10.1002/9780470661345.SMC195.

[4] Y. Wu *et al.*, 'Progress in the design, nanofabrication, and performance of metalenses', *iopscience.iop.orgZ Wang, Y Wu, D Qi, W Yu, H ZhengJournal of Optics, 2022•iopscience.iop.org*, vol. 24, p. 33001, 2021, doi: 10.1088/2040-8986/ac44d8.

[5] P. Beer, P. Gale, and D. Smith, 'Supramolecular chemistry', 1999, Accessed: May 10, 2024. [Online]. Available: https://eprints.soton.ac.uk/173903

[6] E. Kopperger and A. A. Rafat, 'AFM Studies and Surface Assisted Self-Assembly of DNA Nanostructures Fortgeschrittenenpraktikum für Physiker Experiment Guide', 2015.

[7] N. W. Alcock *et al.*, 'Red and blue luminescent metallo-supramolecular coordination polymers assembled through π-π interactions', *Journal of the Chemical Society, Dalton Transactions*, no. 9, pp. 1447–1461, 2000, doi: 10.1039/b000871k.

[8] A. Estève and C. Rossi, ' DNA Nanoengineering and DNA -Driven Nanoparticle Assembly ', in *Biological Soft Matter*, 2021. doi: 10.1002/9783527811014.ch1.

[9] C. K. Ullal, M. Maldovan, E. L. Thomas, G. Chen, Y. J. Han, and S. Yang, 'Photonic crystals through holographic lithography: Simple cubic, diamond-like,

and gyroid-like structures', *Appl Phys Lett*, vol. 84, no. 26, pp. 5434–5436, Jun. 2004, doi: 10.1063/1.1765734.

[10] K. G. Chiong, 'Contrast and sensitivity enhancement of resists for high-resolution lithography', *Journal of Vacuum Science & Technology B: Microelectronics and Nanometer Structures*, vol. 6, no. 6, p. 2238, Nov. 1988, doi: 10.1116/1.584089.

[11] J. Zhu *et al.*, 'Four-quadrant gratings moiré fringe alignment measurement in proximity lithography', *osapublishing.org*, Accessed: Jan. 10, 2020. [Online]. Available: https://www.osapublishing.org/abstract.cfm?uri=oe-21-3-3463

[12] K. Thorkelsson, P. Bai, and T. Xu, 'Self-assembly and applications of anisotropic nanomaterials: A review', 2015. doi: 10.1016/j.nantod.2014.12.005.

[13] M. Shimomura and T. Sawadaishi, 'Bottom-up strategy of materials fabrication: A new trend in nanotechnology of soft materials', 2001. doi: 10.1016/S1359-0294(00)00081-9.

[14] N. C. Seeman, 'DNA in a material world', 2003. doi: 10.1038/nature01406.

[15] S. H. Ko, M. Su, C. Zhang, A. E. Ribbe, W. Jiang, and C. Mao, 'Synergistic self-assembly of RNA and DNA molecules', *Nature Chemistry 2010 2:12*, vol. 2, no. 12, pp. 1050–1055, Oct. 2010, doi: 10.1038/nchem.890.

[16] N. P. King, Y.-T. Lai, F. Hollfelder, and S. Lutz, 'Practical approaches to designing novel protein assemblies', 2013, doi: 10.1016/j.sbi.2013.06.002.

[17] M. Antonietti and S. Förster, 'Vesicles and Liposomes: A Self-Assembly Principle Beyond Lipids', *Advanced Materials*, vol. 15, no. 16, pp. 1323–1333, Aug. 2003, doi: 10.1002/ADMA.200300010.

[18] S. Rinker, Y. Ke, Y. Liu, R. Chhabra, and H. Yan, 'Self-assembled DNA nanostructures for distance-dependent multivalent ligand-protein binding', 2008, doi: 10.1038/nnano.2008.164.

[19] K. Lund *et al.*, 'LETTERS Molecular robots guided by prescriptive landscapes', 2010, doi: 10.1038/nature09012.

[20] H. Li, J. D. Carter, and T. H. LaBean, 'Nanofabrication by DNA self-assembly', 2009. doi: 10.1016/S1369-7021(09)70157-9.

[21] H. John, A. Paulson, W. B. Rogers, W. M. Shih, and V. N. Manoharan, 'Using DNA to program the self-assembly of colloidal nanoparticles and microparticles', p. 16008, 2016, doi: 10.1038/natrevmats.2016.8.

[22] 'https://explorebiology.org/collections/genetics/the-structure-of-dnaHHMI'.

[23] J. D. Watson and F. H. C. Crick, ‘Molecular Structure of Nucleic Acids: A Structure for Deoxyribose Nucleic Acid’, *Nature 1953 171:4356*, vol. 171, no. 4356, pp. 737–738, Apr. 1953, doi: 10.1038/171737a0.

[24] A. Pinheiro, D. Han, W. Shih, H. Y.-N. nanotechnology, and undefined 2011, ‘Challenges and opportunities for structural DNA nanotechnology’, *nature.comAV Pinheiro, D Han, WM Shih, H YanNature nanotechnology, 2011•nature.com*, vol. 6, no. 12, pp. 763–772, 2011, doi: 10.1038/NNANO.2011.187.

[25] Z.-G. Wang and B. Ding, ‘DNA-Based Self-Assembly for Functional Nanomaterials’, 2013, doi: 10.1002/adma.201301450.

[26] F. A. Aldaye, A. L. Palmer, and H. F. Sleiman, ‘Assembling materials with DNA as the guide’, 2008. doi: 10.1126/science.1154533.

[27] N. Geerts and E. Eiser, ‘DNA-functionalized colloids: Physical properties and applications’, Oct. 07, 2010, *Royal Society of Chemistry*. doi: 10.1039/c001603a.

[28] N. L. Rosi and C. A. Mirkin, ‘Nanostructures in Biodiagnostics’, 2005, doi: 10.1021/cr030067f.

[29] S. Y. Park, A. K. R. Lytton-Jean, B. Lee, S. Weigand, G. C. Schatz, and C. A. Mirkin, ‘DNA-programmable nanoparticle crystallization’, *Nature*, vol. 451, no. 7178, pp. 553–556, Jan. 2008, doi: 10.1038/nature06508.

[30] D. Nykypanchuk, M. M. Maye, D. Van Der Lelie, and O. Gang, ‘DNA-guided crystallization of colloidal nanoparticles’, *Nature*, vol. 451, no. 7178, pp. 549–552, Jan. 2008, doi: 10.1038/nature06560.

[31] P. L. Biancaniello, A. J. Kim, and J. C. Crocker, ‘Colloidal interactions and self-assembly using DNA hybridization’, *Phys Rev Lett*, vol. 94, no. 5, p. 058302, Feb. 2005, doi: 10.1103/PhysRevLett.94.058302.

[32] M. R. Jones, N. C. Seeman, and C. A. Mirkin, ‘Programmable materials and the nature of the DNA bond’, 2015. doi: 10.1126/science.1260901.

[33] C. A. Laramy, C. R., O’Brien, M. N., & Mirkin, ‘Crystal engineering with DNA’, Nature Reviews Materials, 4(3), 201-224. Accessed: Nov. 07, 2020. [Online]. Available: https://www.nature.com/articles/s41578-019-0087-2.pdf?origin=ppub

[34] D. Joshi *et al.*, ‘Kinetic control of the coverage of oil droplets by DNA-functionalized colloids’, *science.orgD Joshi, D Bargteil, A Caciagli, J Burelbach, Z Xing, AS Nunes, DEP Pinto, NAM AraújoScience advances, 2016•science.org*, vol. 2, no. 8, Aug. 2016, doi: 10.1126/sciadv.1600881.

[35] L. Di Michele, F. Varrato, J. Kotar, S. H. Nathan, G. Foffi, and E. Eiser, 'Multistep kinetic self-assembly of DNA-coated colloids', *nature.com*, 2013, doi: 10.1038/ncomms3007.

[36] J. Moon, I. Jo, E. Ducrot, J. Oh, D. P.-M. Research, and undefined 2018, 'DNA-coated microspheres and their colloidal superstructures', *SpringerJ Moon, IS Jo, E Ducrot, JS Oh, DJ Pine, GR YiMacromolecular Research, 2018•Springer*, vol. 26, no. 12, pp. 1085–1094, Dec. 2018, doi: 10.1007/s13233-018-6151-8.

[37] Z. Li, Q. Fan, and Y. Yin, 'Colloidal Self-Assembly Approaches to Smart Nanostructured Materials', *Chem Rev*, vol. 122, no. 5, pp. 4976–5067, Mar. 2022, doi: 10.1021/ACS.CHEMREV.1C00482.

[38] G. P. Mitchell, C. A. Mirkin, and R. L. Letsinger, 'Programmed assembly of DNA functionalized quantum dots [10]', *J Am Chem Soc*, vol. 121, no. 35, pp. 8122–8123, Sep. 1999, doi: 10.1021/JA991662V/SUPPL_FILE/JA991662V_S.PDF.

[39] M. Han, X. Gao, J. Z. Su, and S. Nie, 'Quantum-dot-tagged microbeads for multiplexed optical coding of biomolecules', *Nature Biotechnology 2001 19:7*, vol. 19, no. 7, pp. 631–635, 2001, doi: 10.1038/90228.

[40] Z. M. Ruff, 'Towards Colloidal Self-Assembly for Functional Materials', 2018, Accessed: May 14, 2024. [Online]. Available: https://www.repository.cam.ac.uk/items/dde6b04f-28af-4079-9eaa-e3ba526509ba

[41] N. Mueller, Y. Okamura, B. Vieira, S. J.- Nature, and undefined 2020, 'Deep strong light–matter coupling in plasmonic nanoparticle crystals', *nature.comNS Mueller, Y Okamura, BGM Vieira, S Juergensen, H Lange, EB Barros, F Schulz, S ReichNature, 2020•nature.com*, Accessed: May 14, 2024. [Online]. Available: https://idp.nature.com/authorize/casa?redirect_uri=https://www.nature.com/articles/s41586-020-2508-1&casa_token=D_eSWw4e8XQAAAAA:O_Yj5-o4b58KlH6-WaogmKijCtzXKaz0UaBqgsp6EBm35x5LssBGyXB7tbImVrkDFUGPWhe8uKozRFx7

[42] J. Wang *et al.*, 'Structural color of colloidal clusters as a tool to investigate structure and dynamics', *Wiley Online LibraryJ Wang, U Sultan, ESA Goerlitzer, CF Mbah, M Engel, N VogelAdvanced Functional Materials, 2020•Wiley Online Library*, vol. 30, no. 26, Jun. 2019, doi: 10.1002/adfm.201907730.

[43] S. Wang *et al.*, ‘Colloidal crystal engineering with metal–organic framework nanoparticles and DNA’, *nature.comS Wang, SS Park, CT Buru, H Lin, PC Chen, EW Roth, OK Farha, CA MirkinNature communications, 2020•nature.com*, doi: 10.1038/s41467-020-16339-w.

[44] R. Elghanian, J. J. Storhoff, R. C. Mucic, R. L. Letsinger, and C. A. Mirkin, ‘Selective colorimetric detection of polynucleotides based on the distance-dependent optical properties of gold nanoparticles’, *Science (1979)*, vol. 277, no. 5329, pp. 1078–1081, Aug. 1997, doi: 10.1126/SCIENCE.277.5329.1078.

[45] C. A. Mirkin, R. L. Letsinger, R. C. Mucic, and J. J. Storhoff, ‘A DNA-based method for rationally assembling nanoparticles into macroscopic materials’, *Nature*, vol. 382, no. 6592, pp. 607–609, Aug. 1996, doi: 10.1038/382607a0.

[46] A. P. Alivisatos *et al.*, ‘Organization of “nanocrystal molecules” using DNA’, *Nature*, vol. 382, no. 6592, pp. 609–611, Aug. 1996, doi: 10.1038/382609a0.

[47] W. Liu *et al.*, ‘Diamond family of nanoparticle superlattices’, *Science*, vol. 351, no. 6273, pp. 582–586, Feb. 2016, doi: 10.1126/SCIENCE.AAD2080.

[48] M. Y. Ben Zion, X. He, C. C. Maass, R. Sha, N. C. Seeman, and P. M. Chaikin, ‘Self-assembled three-dimensional chiral colloidal architecture’, *Science*, vol. 358, no. 6363, pp. 633–636, Nov. 2017, doi: 10.1126/SCIENCE.AAN5404.

[49] R. J. Macfarlane, B. Lee, M. R. Jones, N. Harris, G. C. Schatz, and C. A. Mirkin, ‘Nanoparticle superlattice engineering with DNA’, *Science (1979)*, vol. 334, no. 6053, pp. 204–208, Oct. 2011, doi: 10.1126/science.1210493.

[50] Y. Zhang, F. Lu, and O. Gang, ‘A general strategy for the DNA-mediated self-assembly of functional nanoparticles into heterogeneous systems’, 2013, doi: 10.1038/nnano.2013.209.

[51] K. V. Gothelf and T. H. Labean, ‘DNA-programmed assembly of nanostructures’, *Org Biomol Chem*, vol. 3, no. 22, 2005, doi: 10.1039/b510551j.

[52] N. C. Seeman, ‘An Overview of Structural DNA Nanotechnology’, 2007. doi: 10.1007/s12033-007-0059-4.

[53] T. H. LaBean and H. Li, ‘Constructing novel materials with DNA’, *Nano Today*, vol. 2, no. 2, 2007, doi: 10.1016/S1748-0132(07)70056-7.

[54] Y. Zhang, F. Lu, K. G. Yager, D. Van Der Lelie, and O. Gang, ‘A general strategy for the DNA-mediated self-assembly of functional nanoparticles into heterogeneous systems’, *NATURE NANOTECHNOLOGY* |, vol. 8, 2013, doi: 10.1038/NNANO.2013.209.

[55] L. Sun, H. Lin, K. L. Kohlstedt, G. C. Schatz, and C. A. Mirkin, 'Design principles for photonic crystals based on plasmonic nanoparticle superlattices', doi: 10.1073/pnas.1800106115.

[56] D. B. Litt *et al.*, 'Hybrid Lithographic and DNA-Directed Assembly of a Configurable Plasmonic Metamaterial That Exhibits Electromagnetically Induced Transparency', *Nano Lett*, vol. 18, no. 2, pp. 859–864, Feb. 2018, doi: 10.1021/acs.nanolett.7b04116.

[57] Q. Y. Lin *et al.*, 'Building superlattices from individual nanoparticles via template-confined DNA-mediated assembly', *Science (1979)*, vol. 359, no. 6376, pp. 669–672, Feb. 2018, doi: 10.1126/science.aaq0591.

[58] S. Simoncelli, Y. Li, E. Cortés, and S. A. Maier, 'Nanoscale Control of Molecular Self-Assembly Induced by Plasmonic Hot-Electron Dynamics', *ACS Nano*, vol. 12, no. 3, pp. 2184–2192, Mar. 2018, doi: 10.1021/acsnano.7b08563.

[59] A. M. Goodman, N. J. Hogan, S. Gottheim, C. Li, S. E. Clare, and N. J. Halas, 'Understanding Resonant Light-Triggered DNA Release from Plasmonic Nanoparticles', *ACS Nano*, vol. 11, pp. 171–179, 2017, doi: 10.1021/acsnano.6b06510.

[60] L. Z. Zornberg, P. A. Gabrys, and R. J. MacFarlane, 'Optical Processing of DNA-Programmed Nanoparticle Superlattices', *Nano Lett*, vol. 19, no. 11, pp. 8074–8081, Nov. 2019, doi: 10.1021/ACS.NANOLETT.9B03258/ASSET/IMAGES/LARGE/NL9B03258_0005.JPEG.

[61] A. F. De Fazio *et al.*, 'Light-Induced Reversible DNA Ligation of Gold Nanoparticle Superlattices', *ACS Nano*, vol. 13, no. 5, 2019, doi: 10.1021/acsnano.9b01294.

[62] N. Kanayama, S. Kishi, T. Takarada, and M. Maeda, 'Photo-switching of blunt-end stacking between DNA strands immobilized on gold nanoparticles', *Chemical Communications*, vol. 56, no. 93, 2020, doi: 10.1039/d0cc05085g.

[63] J. Zhu *et al.*, 'Light-Responsive Colloidal Crystals Engineered with DNA', *Advanced Materials*, vol. 32, no. 8, 2020, doi: 10.1002/adma.201906600.

[64] M. You *et al.*, 'Ultrafast Photonic PCR Based on Photothermal Nanomaterials', 2020. doi: 10.1016/j.tibtech.2019.12.006.

[65] J. H. Lee *et al.*, 'Plasmonic Photothermal Gold Bipyramid Nanoreactors for Ultrafast Real-Time Bioassays', *J Am Chem Soc*, vol. 139, no. 24, 2017, doi: 10.1021/jacs.7b01779.

[66] J. Song *et al.*, 'Light-responsible DNA hydrogel-gold nanoparticle assembly for synergistic cancer therapy', *J Mater Chem B*, vol. 3, no. 8, 2015, doi: 10.1039/c4tb01519c.

[67] Z. Şenel, K. İçöz, and T. Erdem, 'Tuning optical properties of self-assembled nanoparticle network with external optical excitation', *J Appl Phys*, vol. 129, no. 15, 2021, doi: 10.1063/5.0036737.

[68] D. Jaque *et al.*, 'Nanoparticles for photothermal therapies', *Nanoscale*, vol. 6, no. 16, pp. 9494–9530, Aug. 2014, doi: 10.1039/C4NR00708E.

[69] B. del Rosal, E. Carrasco, … F. R.-A. F., and undefined 2016, 'Infrared-emitting QDs for Thermal therapy with real-time subcutaneous temperature feedback', *Wiley Online LibraryB del Rosal, E Carrasco, F Ren, A Benayas, F Vetrone, F Sanz-Rodríguez, D Ma, Á JuarranzAdvanced Functional Materials, 2016•Wiley Online Library*, vol. 26, no. 33, pp. 6060–6068, Sep. 2016, doi: 10.1002/adfm.201601953.

[70] M. Chu, X. Pan, D. Zhang, Q. Wu, J. Peng, and W. Hai, 'The therapeutic efficacy of CdTe and CdSe quantum dots for photothermal cancer therapy', *Biomaterials*, vol. 33, no. 29, pp. 7071–7083, Oct. 2012, doi: 10.1016/J.BIOMATERIALS.2012.06.062.

[71] D. A. Hanifi *et al.*, 'Redefining near-unity luminescence in quantum dots with photothermal threshold quantum yield', *Science (1979)*, vol. 363, no. 6432, pp. 1199–1202, 2019, doi: 10.1126/SCIENCE.AAT3803.

[72] Z. Senel, R. Phul, A. Faruk Yazıcı, E. Taze, and T. Erdem, 'Light-assisted hierarchical fabrication of two-dimensional surfaces using DNA-functionalized semiconductor nanocrystal quantum dots'.

[73] G. FRENS, 'Controlled Nucleation for the Regulation of the Particle Size in Monodisperse Gold Suspensions', *Nature Physical Science*, vol. 241, no. 105, pp. 20–22, Jan. 1973, doi: 10.1038/physci241020a0.

[74] T. Kim, A. Canlier, G. Hong Kim, J. Choi, M. Park, and S. Min Han, 'Electrostatic Spray Deposition of Highly Transparent Silver Nanowire Electrode on Flexible Substrate', 2012, doi: 10.1021/am3023543.

[75] M. Özkutlu Demirel, M. B. Öztürkmen, M. Savaş, E. Mutlugün, T. Erdem, and Y. Öz, 'Effects of silver nanowires and their surface modification on electromagnetic interference, transport and mechanical properties of an aerospace grade epoxy', *J Compos Mater*, Mar. 2024, doi: 10.1177/00219983241238057/ASSET/IMAGES/LARGE/10.1177_00219983241238057-FIG10.JPEG.

[76] Q. Yang, M. H. De Vries, F. Picchioni, and K. Loos, 'A novel method of preparing metallic Janus silica particles using supercritical carbon dioxide', *Nanoscale*, vol. 5, no. 21, 2013, doi: 10.1039/c3nr81280d.

[77] W. K. Bae, K. Char, H. Hur, and S. Lee, 'Single-step synthesis of quantum dots with chemical composition gradients', *Chemistry of Materials*, vol. 20, no. 2, 2008, doi: 10.1021/cm070754d.

[78] J. Lim, S. Jun, E. Jang, H. Baik, H. Kim, and J. Cho, 'Preparation of highly luminescent nanocrystals and their application to light-emitting diodes', *Advanced Materials*, vol. 19, no. 15, 2007, doi: 10.1002/adma.200602642.

[79] S. Akhavan, A. F. Cihan, B. Bozok, and H. V. Demir, 'Nanocrystal Skins with Exciton Funneling for Photosensing', 2014, doi: 10.1002/smll.201303808.

[80] D. Lee and T. Cui, 'pH-dependent conductance behaviors of layer-by-layer self-assembled carboxylated carbon nanotube multilayer thin-film sensors', *Journal of Vacuum Science & Technology B: Microelectronics and Nanometer Structures Processing, Measurement, and Phenomena*, vol. 27, no. 2, pp. 842–848, Mar. 2009, doi: 10.1116/1.3002386.

[81] Y. Noh, H. Jeong, J. Park, and D. Lee, 'Charge-assisted coating of silver nanowire transparent conductive layer and application to flexible heater', 2022, doi: 10.1016/j.surfin.2022.102105.

[82] S. J. Hurst, A. K. R. Lytton-Jean, and C. A. Mirkin, 'Maximizing DNA loading on a range of gold nanoparticle sizes', *Anal Chem*, vol. 78, no. 24, pp. 8313–8318, Dec. 2006, doi: 10.1021/ac0613582.

[83] L. M. Demers *et al.*, 'A fluorescence-based method for determining the surface coverage and hybridization efficiency of thiol-capped oligonucleotides bound to gold thin films and nanoparticles', *Anal Chem*, vol. 72, no. 22, pp. 5535–5541, Nov. 2000, doi: 10.1021/ac0006627.

[84] J. J. Storhoff, A. A. Lazarides, R. C. Mucic, C. A. Mirkin, R. L. Letsinger, and G. C. Schatz, 'What controls the optical properties of DNA-linked gold nanoparticle

assemblies?', *J Am Chem Soc*, vol. 122, no. 19, pp. 4640–4650, May 2000, doi: 10.1021/ja993825l.

[85] R. Jin, G. Wu, Z. Li, C. A. Mirkin, and G. C. Schatz, 'What controls the melting properties of DNA-linked gold nanoparticle assemblies?', *J Am Chem Soc*, vol. 125, no. 6, pp. 1643–1654, Feb. 2003, doi: 10.1021/ja021096v.

[86] S. H. Han and J. S. Lee, 'Synthesis of length-controlled polyvalent silver nanowire-DNA conjugates for sensitive and selective detection of DNA targets', *Langmuir*, vol. 28, no. 1, pp. 828–832, Jan. 2012, doi: 10.1021/LA203423N/SUPPL_FILE/LA203423N_SI_001.PDF.

[87] J. M. Nam, K. J. Jang, and J. T. Groves, 'Detection of proteins using a colorimetric bio-barcode assay', *Nat Protoc*, vol. 2, no. 6, 2007, doi: 10.1038/nprot.2007.201.

[88] M. Q. Dai and L. Y. L. Yung, 'Ethylenediamine-assisted ligand exchange and phase transfer of oleophilic quantum dots: Stripping of original ligands and preservation of photoluminescence', *Chemistry of Materials*, vol. 25, no. 11, 2013, doi: 10.1021/cm304136a.

[89] D. Sun and O. Gang, 'DNA-functionalized quantum dots: Fabrication, structural, and physicochemical properties', *Langmuir*, vol. 29, no. 23, 2013, doi: 10.1021/la4000186.

[90] N. Zammatteo *et al.*, 'Comparison between different strategies of covalent attachment of DNA to glass surfaces to build DNA microarrays', *Anal Biochem*, vol. 280, no. 1, 2000, doi: 10.1006/abio.2000.4515.

[91] M. Sun, S. Zhang, J. Wang, Z. Jia, X. Lv, and X. Huang, 'Enhanced Biosensor Based on Assembled Porous Silicon Microcavities Using CdSe/ZnS Quantum Dots', *IEEE Photonics J*, vol. 13, no. 4, 2021, doi: 10.1109/JPHOT.2021.3101656.

[92] Ł. Syga, D. Spakman, C. M. Punter, and B. Poolman, 'Method for immobilization of living and synthetic cells for high-resolution imaging and single-particle tracking', *Sci Rep*, vol. 8, no. 1, 2018, doi: 10.1038/s41598-018-32166-y.

[93] G. Festag, A. Steinbrück, A. Wolff, A. Csaki, R. Möller, and W. Fritzsche, 'Optimization of gold nanoparticle-based DNA detection for microarrays', *J Fluoresc*, vol. 15, no. 2, 2005, doi: 10.1007/s10895-005-2524-4.

[94] Y. S.- Nanoscale and undefined 2010, 'Silver nanowires–unique templates for functional nanostructures', *pubs.rsc.orgY SunNanoscale, 2010•pubs.rsc.org*, Accessed: Sep. 11, 2024. [Online]. Available: https://pubs.rsc.org/en/content/articlehtml/2010/nr/c0nr00258e

[95] P. Ramasamy, D. Seo, S. Kim, J. K.-J. of M. Chemistry, and undefined 2012, 'Effects of TiO 2 shells on optical and thermal properties of silver nanowires', *pubs.rsc.orgP Ramasamy, DM Seo, SH Kim, J KimJournal of Materials Chemistry, 2012•pubs.rsc.org*, doi: 10.1039/c2jm00010e.

[96] M. V Kovalenko, M. I. Bodnarchuk, J. Zaumseil, J.-S. Lee, and D. V Talapin, 'Expanding the Chemical Versatility of Colloidal Nanocrystals Capped with Molecular Metal Chalcogenide Ligands', doi: 10.1021/ja1024832.

[97] T. D. Corrigan, S. Guo, R. J. Phaneuf, and H. Szmacinski, 'Enhanced fluorescence from periodic arrays of silver nanoparticles', *J Fluoresc*, vol. 15, no. 5, 2005, doi: 10.1007/s10895-005-2987-3.

[98] L. Alizadeh, E. Alizadeh, A. Zarebkohan, E. Ahmadi, M. Rahmati-Yamchi, and R. Salehi, 'AS1411 aptamer-functionalized chitosan-silica nanoparticles for targeted delivery of epigallocatechin gallate to the SKOV-3 ovarian cancer cell lines', *Journal of Nanoparticle Research*, vol. 22, no. 1, 2020, doi: 10.1007/s11051-019-4735-7.

[99] W. Haiss, N. T. K. Thanh, J. Aveyard, and D. G. Fernig, 'Determination of size and concentration of gold nanoparticles from UV-Vis spectra', *Anal Chem*, vol. 79, no. 11, pp. 4215–4221, Jun. 2007, doi: 10.1021/AC0702084/SUPPL_FILE/AC0702084SI20070321_014144.PDF.

CURRICULUM VITAE

2011-2015 B.Sc., Biomedical Engineering, Erciyes University, Kayseri, TURKEY

2016 – 2018 M.Sc., Electric and Computer Engineering, Abdullah Gül University, Kayseri, TURKEY

2018 – 2024 Ph.D., Electrical and Computer Engineering, Abdullah Gül University, Kayseri, TURKEY

SCI Journal Publications:

1) Z. Şenel, K. İçöz, and T. Erdem, 'Tuning optical properties of self-assembled nanoparticle network with external optical excitation', *J Appl Phys*, vol. 129, no. 15, 2021, doi: 10.1063/5.0036737
2) Z. Senel, R. Phul, A. Faruk Yazıcı, E. Taze, and T. Erdem, 'Light-assisted hierarchical fabrication of two-dimensional surfaces using DNA-functionalized semiconductor nanocrystal quantum dots'. Submitted.

International Conferences:

1) Z. Senel, R. Phul, A. Faruk Yazıcı, E. Taze, E. Mutlugün, and T. Erdem, 'Optical control of hierarchical DNA-functionalized nanoparticle self-assembly on 2D surfaces', 11th EOSAM, 11-15 September 2023, doi: 10.1051/epjconf/202328705004.

National Conferences:

1) Z. Senel, K. İçöz, and T. Erdem, 'Light-assisted Control of Optical Transparency in Smart Self-Assembled Nanoparticle Network', 23. Ulusal Optik, Elektro-Optik ve Fotonik Çalıştayı, FOTONİK 2022, 9 September 2022, Bilkent University

Scholarships:

- The Higher Education Council (HEC) of Turkey YÖK-100/2000 Ph.D. Scholarship Program
- 2211-A National Ph.D. Scholarship Program
- This work has been conducted with support from Tübitak 2247-A Program (Grant no. 120C124)